4-2-2015

Advanced Oxidation Processes of Problematic Toxin and Water Contaminants: Cylindrospermopsin, Iopamidol, 4-methylcyclohexane Methanol and Propylene Glycol Phenyl Ether

Cen Zhao
Florida International University, czhao001@fiu.edu

DOI: 10.25148/etd.FIDC000064

FLORIDA INTERNATIONAL UNIVERSITY

Miami, Florida

ADVANCED OXIDATION PROCESSES OF PROBLEMATIC TOXIN AND WATER CONTAMINANTS: CYLINDROSPERMOPSIN, IOPAMIDOL, 4-METHYL CYCLOHEXANE METHANOL AND PROPYLENE GLYCOL PHENYL ETHER

A dissertation submitted in partial fulfillment of

the requirements for the degree of

DOCTOR OF PHILOSOPHY

in

CHEMISTRY

by

Cen Zhao

2015

To: Dean Michael R. Heithaus
College of Arts and Sciences

This dissertation, written by Cen Zhao, and entitled Advanced Oxidation Processes of Problematic Toxin and Water Contaminants: Cylindrospermopsin, Iopamidol, 4-Methyl Cyclohexane Methanol and Propylene Glycol Phenyl Ether, having been approved in respect to style and intellectual content, is referred to you for judgment.

We have read this dissertation and recommend that it be approved.

_____
Wenzhi Li

_____
Bruce McCord

_____
Jaroslava Miksovska

_____
Stanislaw Wnuk

_____
Kevin E. O'Shea, Major Professor

Date of Defense: April 2, 2015

The dissertation of Cen Zhao is approved.

_____
Dean Michael R. Heithaus
College of Arts and Sciences

_____
Dean Lakshmi N. Reddi
University Graduate School

Florida International University, 2015

DEDICATION

I would like to dedicate this dissertation to my family. Without their invaluable knowledge, unconditional love and support in my life, this work would not have been completed.

ACKNOWLEDGMENTS

First of all, I would like to thank my advisor, Dr. Kevin O'Shea, for providing me the opportunity to join his research group and for his support and encouragement. I will always be grateful for his mentorship.

I would extend my appreciation to my committee, Dr. Stanislaw Wnuk, Dr. Bruce McCord, Dr. Jaroslava Miksovska, and Dr. Wenzhi Li, for their advice on my research projects.

I gratefully acknowledge the faculty and staff in the Department of Chemistry & Biochemistry at FIU. Special thanks to Dr. Anthony DeCaprio and Dr. Luis Arroyo-Mora.

I am also thankful to Dr. Prashant V. Kamat from University of Notre Dame, Dr. Julie Peller from Valparaiso University, Dr. Stephen Mezyk from California State University, Long beach for their generous help in instrumentation and research guidance.

I would like to thank all the previous and current members of Dr. O'Shea research group. Also, I would like to thank my husband for his encouragement and support during my PhD study at FIU, and my family and friends in China, who gave me love, support, and power.

Dissertation Year Fellowship (DYF) and Doctoral Evidence Acquisition (DEA) Fellowship were supported by University Graduate School. Graduate teaching assistant was supported by University Graduate School and Department of Chemistry. Conference travel funding was provided by College of Arts & Sciences and Graduate and Professional Student Committee (GPSC).

ABSTRACT OF THE DISSERTATION

ADVANCED OXIDATION PROCESSES OF PROBLEMATIC TOXIN AND WATER CONTAMINANTS: CYLINDROSPERMOPSIN, IOPAMIDOL, 4-METHYL CYCLOHEXANE METHANOL AND PROPYLENE GLYCOL PHENYL ETHER

By

Cen Zhao

Florida International University, 2015

Miami, Florida

Professor Kevin E. O'Shea, Major Professor

The occurrences of cyanotoxin and organic contaminants threaten drinking water sources and are a serious human health and environmental concern. The control and remediation of the potent contaminants are critical for ensuring safe drinking water to significant populations. Advanced oxidation processes (AOPs) have received considerable attention as a potential water treatment for various pollutants. In this dissertation, advanced oxidative degradation of four problematic water toxic contaminants (cylindrospermopsin, iopamidol, 4-methylcyclohexanemethanol and propylene glycol phenyl ether) were studied to develop the fundamental understanding required to assess AOPs as a potential water treatment process.

UV and visible light activated (VLA) TiO_2 photocatalysis using nitrogen and fluorine-TiO_2 (NF-TiO_2), phosphorus and fluorine-TiO_2 (PF-TiO_2) and sulfur-TiO_2 (S-TiO_2) were employed for the degradation of 6-hydroxymethyl uracil (6-HOMU), a model compound for the potent cyanotoxin cylindrospermopsin (CYN). NF-TiO_2 is the most photoactive, followed by marginally active PF-TiO_2 and inactive S-TiO_2 under visible

light irradiation. Our results indicate that $O_2^{-\bullet}$ plays an important role in VLA TiO_2 photocatalysis.

Fe (VI), an environmentally friendly oxidant, was employed for the degradation of CYN and 6-HOMU over a range of solution pH (7 ~ 9.5). The second order rate constants for the reaction of Fe (VI) with CYN decrease from 38.8 ± 0.1 $M^{-1}s^{-1}$ at pH 7 to 5.0 ± 0.1 $M^{-1}s^{-1}$ at pH 9.5. Fe (VI) mediated reactions primarily occur via oxidation of the uracil ring in CYN. ELISA results demonstrate that Fe (VI) oxidation process leads to a significant decrease in the bioactivity of CYN as a function of treatment time.

Fe (III)-oxalate/H_2O_2 process was employed for the remediation of iopamidol, a model for ICM, to determine the formation rates and steady concentrations of •OH and $O_2^{-\bullet}$ under UV and visible light irradiation. Reduction by $CO_2^{-\bullet}$ and oxidation by •OH contribute to the degradation pathways.

Pulse and gamma radiolysis of 4-methylcyclohexanemethanol (MCHM) and propylene glycol phenyl ether (PPh) were studied to determine the hydroxyl radical bimolecular rate constants and reaction pathways. •OH addition to *ortho* and *para* positions in PPh are the predominant reaction pathways; H-abstraction are the primary reaction mechanisms for •OH mediated oxidation of MCHM.

TABLE OF CONTENTS

LIST OF TABLES

TABLES PAGE

LIST OF FIGURES

FIGURES PAGE

LIST OF SCHEMES

SCHEMES PAGE

CHAPTER 1

General Introduction

1.1 Toxic water contaminants

The World Health Organization reports that one out of every five children and more than one billion people have not access to clean drinking water. With the increasing world population, the demand for clean water continues to increase while industrialization of developing countries decreases the clean water supplies because of the associated pollution. Water contamination also occurs during Harmful Algae Blooms (HABs), which have increased in recent years because of global warming and increased eutrophication of natural water systems. Seventy percent of HABs produce potent natural cyanotoxins (Codd 1995, Ho et al. 2006), which can lead to serious health problems, even death, and have forced the closure of large drinking water sources. The need for effective economical environmentally friendly water treatment is critical to Earth's sustainability and is also a global challenge.

1.1.1 Cyanotoxin cylindrospermopsin

Cyanobacteria known as blue-green algae commonly exists in drinking water sources and can lead to harmful algae blooms (HABs). Seventy percent of HABs produce potent toxins (Codd 1995, Ho et al. 2006), which pose a tremendous risk to humans and the environment. Ingestion of water contaminated by cyanotoxins can lead to serious health problems, including acute gastro-intestinal disorders, acute skin eruptions (Stewart et al. 2006), inhalational problems (Codd et al. 1999, Turner et al. 1990) and even death in humans and animals.

Cyanbacteria can produce a range of cyanotoxins (**Fig 1.1**) from relatively simple structures, such as domoic acid, a glutamate antagonist, to microcystin heptapeptides that inhibit protein phosphatase. The proposed study focuses on cylindrospermopsin (CYN),

an alkaloid toxin with a tricyclic guanidine group and uracil ring (Fig 1). CYN was first isolated and identified in 1992 (Ohtani et al. 1992). At ambient temperature and the pH of natural water, cylindrospermopsin is zwitterionic, water-soluble and stable (Chiswell et al. 1999). Cyanobacteria, *Cylindrospermopsis, Anabaena, Umezakia and Aphanizomenon*, are known to produce CYN (Falconer 2005). The occurrence of CYN has been reported in tropical and subtropical areas of Australia, Israel, New Zealand, Brazil and Florida, USA (de la Cruz et al. 2013). While the presence of CYN has been primarily limited to warm regions, recent reports confirm that occurrences of CYN extend to more temperate regions in Europe, such as Italy, Germany and France.

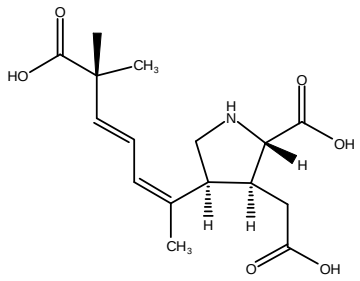

Domoic acid

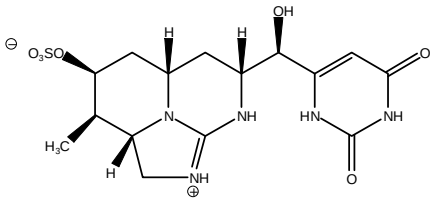

Cylindrospermopsin

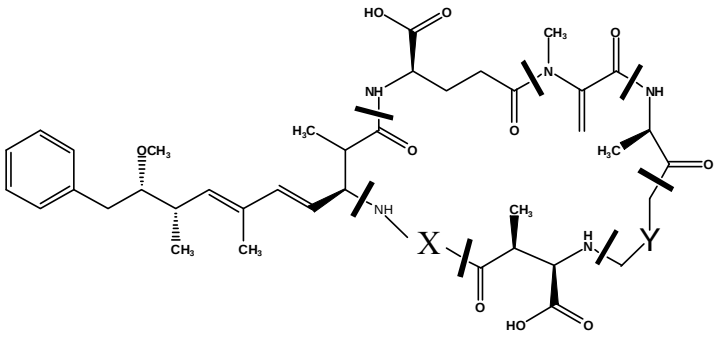

Microcystin

Fig.1.1 The structures of domoic acid, cylindrospermopsin and microcystins.

Human exposure to CYN occurs through ingestion of CYN contaminated food or water, or during recreational activities during HABs in lakes and fresh water ways. CYN has been showed to be genotoxic (Humpage et al. 2000), and carcinogenic (Falconer and Humpage 2001). The toxic activity of CYN partly results from the uracil moiety which inhibits protein translation or it bands to DNA to cause strand breakage (Banker et al. 2001). The most notable incident of CYN on human health was discovered on Palm Island, Australia in 1979, which led to hepatoenteritis in 138 children and 10 adults (Griffiths and Saker 2003). "The Palm Island Mystery" was the result of an outbreak of algae blooms in Solomon Dam, the source of local drinking water. Upon treatment with copper sulphate, the algae died leading to the rapid release of the toxin into water (Bourke et al. 1983). Exposure to CYN from the Palm Island incident led to severe damage in the kidneys and gastrointestinal lining, and bloody urine resulting in fluid and electrolyte loss in the patients. There were the most typical acute clinical symptoms of CYN exposure (Bourke et al. 1986, Falconer 1998).

CYN also has a pronounced biological impact on wild and domestic animals. CYN poisoning of livestock from drinking *C. raciborskii*-contaminated water in northwest Queensland, resulted in deaths of a significant number of cattle. Histopathological examination of the livers of deceased cattle revealed pale and swollen tissues with extensive bile duct proliferation. Extensive epicardial hemorrhaging was discovered in the heart and subserosal hemorrhaging was observed in the small intestine and omentum (Saker et al. 1999, Thomas et al. 1998).

1.1.2 Pharmaceutical and personal care products (PPCPs)

The widespread releases of organic contaminants from pharmaceutical and personal care products (PPCPs) and manufacturing waste chemicals to the water bodies have received increasing attention. PPCPs include a variety of regularly used chemicals, such as fragrances, cosmetics and drugs. Numerous PPCPs and drugs after ingestion, external application and /or disposal have been detected in the environment and surface water across the world (Kolpin et al. 2002). PPCPs are consumed by humans and animals and may be released into the environmental water bodies via direct (disposal from external application) (Halling-Sorensen et al. 1998) and indirect (excretion, washing) routes (Zhao et al. 2014a). Some PPCPs are persistent in the natural water and resistant to natural degradation, which can lead to environmental impacts and potential adverse effects on human health.

Iodinated x-ray contrast media (ICM), one of the most prevalent PPCPs, are widely used to enhance the imaging of organs or blood vessels during diagnostic tests (Zhao et al. 2014a). Approximately 3.5×10^6 kg per year of ICM are consumed worldwide (Perez and Barcelo 2007). ICM is administered in high daily doses (up to 200 g/day) and excreted primarily non-metabolized (> 95 %) (Mutschler 1996). ICM is frequently detected in wastewater, groundwater, rivers, creeks and even drinking water supplies at elevated concentrations (at μg/L levels for wastewater and surface water) (Schulz et al. 2008, Ternes and Hirsch 2000). The presence of ICM is responsible for the high concentration of adsorbable organic halogen material (AOX) present in hospital wastewater (Kummerer et al. 1998) with the potential for adverse health impacts on humans. Iopamidol, the focus of this dissertation, is the most frequently detected ICM in

aqueous environments (Duirk et al. 2011, Tian et al. 2014). Shown in **Fig. 1.2**, iopamidol has a molecular weight of 777 and the structure features commonly associated contrast agents, i.e., a central *iodo* substituted aromatic ring. The aromatic ring is substituted with alkyl side chains labeled A and B, which are coupled to the aromatic ring through amide linkages. The chains contain hydroxyl and amide functionalities, which make the compound more water soluble.

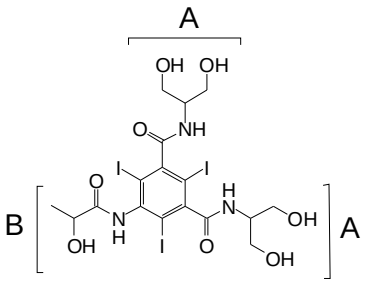

Fig. 1.2 The structure of iopamidol

1.1.3. Chemical spills and leaking

The organic chemical spills and leaking associated with underground water have been studied by the EPA since mid-1983. An estimated 3.5 million underground tanks are used for storage of petroleum products, hazardous waste and other chemicals. Approximately 10 ~ 30 % of the tanks leak to the surrounding environment, such as soil, surface water and air. For example, 261 cases of petroleum leaking contaminants incidents were reported between 1972 and 1984 in New Mexico. The detailed documentary reported that almost 40,000 gallons of petroleum products leaked from an underground storage to the local soil and water systems in Albuquerque, New Mexico over a three-month period in 1981, which threatened the nearby residences due to the explosive level of gasoline vapors (Jercinovic 1985).

A serious chemical leak occurred on Jan 9, 2014: an estimated 10,000 gallons of crude 4-methyl cyclohexane methanol (MCHM) leaked from freedom industries facility into the Elk River near Charleston, West Virginia and contaminated the local drinking water, which threatened the health of 300,000 residents within nine counties in the Charleston (Tullo et al. 2014). According to the freedom industries, they reported that the leaking tank contained 88.5 % crude MCHM, 7.3 % proprietary mixture and 4.2 % water by weight (Tullo et al. 2014). The proprietary mixture primarily consisted of propylene glycol phenyl ether (PPh) and dipropylene glycol phenyl ether (DiPPh). Crude MCHM and PPh are the chemical foaming agents used to wash coal and remove impurities that contribute to pollution during combustion (**Fig. 1.3**). Following this spill, the concentrations of MCHM from initial water testing were determined to be 1.04 ~ 3.35 ppm at the West Virginia American Water intake on the Elk River and 1.02 ~ 1.56 ppm in the treated drinking water (Tullo et al. 2014). The Center for Disease Control & Prevention (CDC) has set a screening level of 1 ppm for MCHM (2014a) and 1.2 ppm for PPh (2014b) in drinking water.

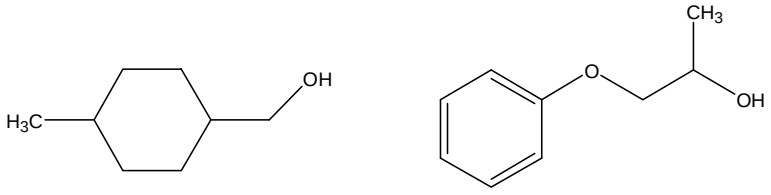

4-methylcyclohexanemethanol
MCHM

Propylene glycol phenyl ether
PPh

Fig. 1.3 The structure of MCHM and PPh

1.2 Advanced oxidation processes (AOPs) for the remediation of water contaminants

Advanced oxidation processes (AOPs) have received considerable attention for the treatment of water contaminated with a wide variety of toxins and pollutants. AOPs employ hydroxyl radical as the primary oxidant in the oxidative remediation of toxins in drinking water. Hydroxyl radical (HO•) is a powerful oxidant (**Table 1.1**) that can react rapidly with nearly all organic compounds (**Table 1.2**) due to its strong oxidation potential. Hydroxyl radical typically attacks organic compounds by radical addition, hydrogen abstraction and/or electron transfer. The oxidation potential of several chemicals for water treatment and disinfection are list in **Table 1.1**. Among these chemical oxidants, hydroxyl radical is the most powerful with an electrochemical oxidation potential of 2.8V. Ozone is currently used for drinking water treatment in a number of countries, but cost is the primary concern and bromate formation is also a serious problem. Hydroxyl radical has much higher reaction rates than ozone for a wide range of organic pollutants and toxins as presented in **Table 1.2**.

Table 1.1: Oxidizing potential for oxidation regents

Oxidizing agent (ADEL AL-KDASI 2004)	Hydroxyl radical (HO•)	Ozone (O_3)	Hydrogen peroxide (H_2O_2)	Hypochlorite (ClO^-)	Chlorine (Cl_2)	Chlorine dioxide (ClO_2)
Electronchemical oxidation potential (EOP),V	2.80	2.08	1.78	1.49	1.36	1.27

Table 1.2: Reaction rate constants (k, $M^{-1}s^{-1}$) of ozone vs. hydroxyl radical (Munter 2001)

Compounds	Chlorinated alkenes	Phenols	N-containing organics	Aromatics	Ketones	Alcohols
O_3 (k, $M^{-1}s^{-1}$)	10^3-10^4	1000	10-100	1-100	1	0.01-1
HO• (k, $M^{-1}s^{-1}$)	10^9-10^{11}	10^9-10^{10}	10^8-10^{10}	10^8-10^{10}	10^9-10^{10}	10^8-10^9

1.2.1 TiO_2 photocatalysis

TiO_2 photocatalysis is effective for the destruction of an extensive number of toxins and organic contaminants in the wastewater and drinking water (Tong et al. 2012, Zhao et al. 2014b). TiO_2 is a cheap, readily available, non-toxic semiconductor for photochemical applications. Upon UV photoexcitation electron/hole pairs are generated with the potential to reduce molecular dioxygen forming superoxide anion radical and oxidize water to hydroperoxide radicals. While a number of subsequent processes can lead to the degradation of target compounds, hydroxyl radical (HO•) is generally considered to be the primary oxidant in the UV TiO_2 photocatalysis processes. Extensive studies on the UV TiO_2 photocatalysis have demonstrated that hundreds of pollutants can be transformed into harmless compounds such as CO_2 and H_2O (Chatterjee and Dasgupta 2005).

Pathways of photocatalytic degradation of organic pollutants (P) by TiO_2 photocataysis is represented in **Fig 1.4**. The process is initiated when the TiO_2 semiconductor absorbs light energy equal to or greater than its band-gap between the conduction and valence bands, promoting an electron to the conduction band (e^-_{cb}) and leaving a "hole" in valence band (h^+_{vb}). Molecular oxygen is used to scavenge the e^-_{cb} at the TiO_2 surface yielding superoxide radical anions ($O_2^{-\bullet}$). The pKa of superoxide radical anions occurs at the pH=4.6, thus hydroperoxide radical ($HO_2^\bullet$) is formed under more acidic conditions; and subsequent disproportionation results in the formation of hydrogen peroxide (H_2O_2). The h^+_{vb} produced during UV TiO_2 photocataysis has the potential to oxidize surface absorbed H_2O or hydroxyl groups to generate hydroxyl radical. However,

the produced HO• in VLA NF-TiO_2 likely results from the reduction of H_2O_2 rather than oxidizing surface absorbed H_2O by h^+_{vb} (Zhao et al. 2014b).

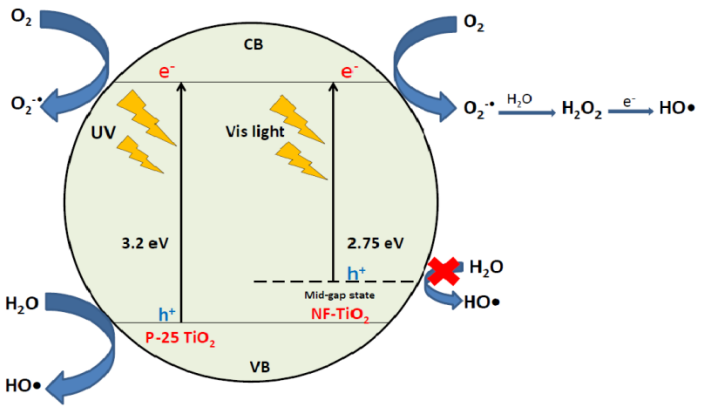

Fig. 1.4 Oxidation of pollutants by UV and VLA TiO_2 photocatalysis.

1.2.2 Radiolysis

The radiolysis technique, an advanced oxidation process, has been widely used for treatment of PPCPs (Abdelmelek et al. 2011, Santoke et al. 2012), pesticides (Song et al. 2009a) and cyanotoxins (Song et al. 2009b, Song et al. 2012) contaminated water supplies. The high energy electron beam from an accelerator or gamma ray can be absorbed by water, leading to bond breakage and the formation of several primary reactive species, such as hydroxyl radical (·OH), hydrated electron (e_{aq}^-) and hydrogen atom (·H) shown in **Eq. 1.1**, which can react with cyanotoxins for the removal from the drinking water. The radiolysis method has a great advantage over other methods for generating reaction species which is the fact that the amount of energy absorbed by water solution is proportional to its electron fraction so that the yield of primary reaction species are well known (Buxton et al. 1988).

$$H_2O \text{ /\/\/\} \rightarrow e_{aq}^- (0.27) + \cdot H (0.06) + \cdot OH (0.28) + H_2 (0.05) + H_2O_2 (0.07) + H_3O^+ (0.27) \qquad (1.1)$$

(where the numbers in brackets are the radiation chemical yields of these species (G-values) per 100 eV absorbed energy).

$$e_{aq}^- + N_2O + H_2O \rightarrow N_2 + {}^-OH + {}^{\cdot}OH \qquad k_1 = 9.1\times 10^9\ M^{-1}s^{-1} \qquad (1.2)$$

$$^{\cdot}H + N_2O \rightarrow {}^{\cdot}OH + N_2 \qquad k_3 = 2.1\times 10^6\ M^{-1}s^{-1} \qquad (1.3)$$

$$(CH_3)_2CHOH + {}^{\cdot}OH \rightarrow (CH_3)_2C^{\cdot}OH + H_2O \qquad k_4 = 1.9\times 10^9\ M^{-1}s^{-1} \qquad (1.4)$$

$$(CH_3)_2CHOH + {}^{\cdot}H \rightarrow (CH_3)_2C^{\cdot}OH + H_2 \qquad k_5 = 1.9\times 10^9\ M^{-1}s^{-1} \qquad (1.5)$$

The high yield product ·OH is generated during this process which can rapidly react with nearly all organic compounds due to its strong oxidation potential (+2.80V) (Thakur et al. 2010). Besides the formation of ·OH, hydrated electron (e_{aq}^-) and hydrogen atom (·H) are also generated with relatively high yield. To study the reactions with ·OH, the solutions are saturated with nitrous oxide (N_2O), which quantitatively converts hydrated electron (e_{aq}^-) and hydrogen atom (·H) to ·OH (**Eq. 1.1 and 1.2**). To promote the reactions of hydrated electron (e_{aq}^-) and organic pollutants, the solution is saturated in N_2 containing isopropanol to scavenger ·OH and hydrogen atom (·H) (**Eq. 1.3 and 1.4**). These reactive species produced during radiolysis of water have been reported for the application of the remediation of the problematic cyanotoxins and contaminants in drinking water (Abdelmelek et al. 2011, Song et al. 2012).

1.2.3 Iron-oxalate Photochemical system

Advanced oxidation processes (AOPs) such as photo-Fenton or photo-Fenton-like processes have been widely reported to efficiently degrade organic pollutants from wastewater (Tao et al. 2005). These processes involve the generation of hydroxyl radical

(•OH) as the primary oxidant. A variety of iron species and a number of carboxylic acids are abundant in natural environments, their coexistence can establish homogenous photo-Fenton type conditions with the potential to produce reactive species leading to the degradation of organic pollutants under solar irradiation. Oxalic acid, a simple abundant naturally occurring dicarboxylic acid, effectively initiates the degradation of the problematic pollutants, biphenol A and 4-chlorophenol (4-CP), under photo-Fenton conditions (Li et al. 2006). The photochemical Fe(III)-oxalate system can be more efficient and catalytic in degrading organic pollutants then Fenton reactions (Fe(III) or Fe(II)/ H_2O_2) because of the rapid redox cycling of iron and faster production of •OH (Jeong and Yoon 2005).

The Fe(III)- oxalate complex exhibits strong ligand-to-metal charge absorption bands in the near UV and visible regions. UV and visible light photoexcitation of Fe(III)-oxalate complex leads to events and species capable of degrading a variety of pollutants as summarized in reactions 1.6 through 1.17 (below). Initial photoexcitation leads to an Fe(II)-oxalate excited complex or Fe(II) ion and the oxalate radical anion ($C_2O_4^{-\bullet}$) illustrated by reaction (1.6). The majority of $C_2O_4^{-\bullet}$ readily decomposes to carbon dioxide (CO_2) and the carbon dioxide radical anion ($CO_2^{-\bullet}$) via rapid decarboxylation (Mulazzani et al. 1986). $CO_2^{-\bullet}$ has a high reduction potential and reacts with dissolved oxygen to form the superoxide anion radical ($O_2^{-\bullet}$) at a near diffusion rate which subsequently forms hydroperoxyl radical ($HO_2\bullet$) in acid media (reactions 1.7 and 1.8). $O_2^{-\bullet}$ and $HO_2\bullet$ react with Fe(III) ion or Fe(III)-oxalate complex to generate Fe(II) ions (reactions 1.10 and 1.11) or Fe(II)-oxalate complex (reactions 1.12 and 1.13). Subsequent reactions of Fe(II) with $O_2^{-\bullet}$/ $HO_2\bullet$ can lead to hydrogen peroxide (H_2O_2) (reactions 1.14 and 1.15). The

reaction of H_2O_2 and Fe(II) by the Fenton reaction produces the •OH (reactions 1.16 and 1.17). The ROS (•OH, $O_2^{-\bullet}$, $HO_2\bullet$, H_2O_2) produced in Fe(III)-oxalate photochemical system can oxidize organic contaminants in the aqueous media.

$$Fe(III)(C_2O_4)_n^{(3-2n)} + h\nu \rightarrow Fe(II)(C_2O_4)_{n-1}^{(4-2n)} + C_2O_4^{-\bullet} \quad (1.6)$$

$$C_2O_4^{-\bullet} \rightarrow CO_2 + CO_2^{-\bullet} \quad (1.7)$$

$$CO_2^{-\bullet} + O_2 \rightarrow CO_2 + O_2^{-\bullet} \quad (1.8)$$

$$HO_2\bullet \leftrightarrow O_2^{-\bullet} + H^+ \quad (1.9)$$

$$Fe(III) + O_2^{-\bullet} \rightarrow Fe(II) + O_2 \quad (1.10)$$

$$Fe(III) + HO_2\bullet \rightarrow Fe(II) + O_2 + H^+ \quad (1.11)$$

$$Fe(III)(C_2O_4)_n^{(3-2n)} + O_2^{-\bullet} \rightarrow Fe(II))(C_2O_4)_n^{(2-2n)} + O_2 \quad (1.12)$$

$$Fe(III)(C_2O_4)_n^{(3-2n)} + HO_2\bullet \rightarrow Fe(II)(C_2O_4)_n^{(2-2n)} + O_2 + H^+ \quad (1.13)$$

$$Fe(II) + O_2^{-\bullet} \rightarrow Fe(III) + H_2O_2 + OH^- \quad (1.14)$$

$$Fe(II) + HO_2\bullet \rightarrow Fe(III) + H_2O_2 + OH^- \quad (1.15)$$

$$Fe(II) + H_2O_2 \rightarrow Fe(III) + \bullet OH + OH^- \quad (1.16)$$

$$Fe(II)(C_2O_4) + H_2O_2 \rightarrow Fe(III)(C_2O_4)^+ + \bullet OH + OH^- \quad (1.17)$$

1.2.4 Ferrate (VI) oxidation treatment

Ferrate (Fe (VI) iron in + 6 oxidation state) has received increasing attention as an environmentally friendly oxidant in water and wastewater treatment due to its dual functions of an oxidant and a subsequent coagulant as ferric hydroxide ($Fe(III)(OH)_3$) (Ma and Liu 2002). Alkaline solutions of Fe(VI) exhibit a maximum absorption at 510 nm ($\varepsilon = 1150 \pm 25\ M^{-1}cm^{-1}$) by UV/Vis spectroscopy. The species of Fe(VI) as a function

of pH are shown in **Fig. 1.5** (Sharma 2011, 2013). Fe(VI) has triprotonated, diprotonated, monoprotonated and deprotonated species present in the acidic to basic pH range.

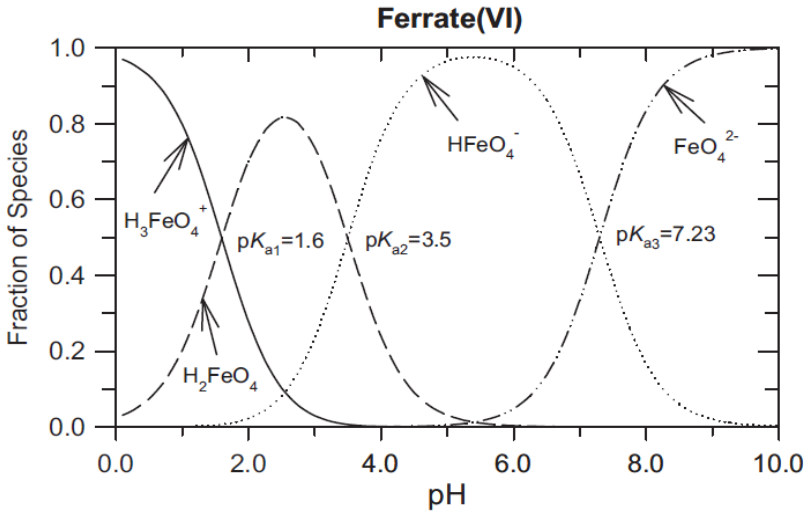

Fig. 1.5 Speciation of Fe(VI) as a function of pH. Source: Adapted from (Sharma 2011) with the permission of Elsevier Inc.

Fe(VI) is a selective oxidant which has a tendency to react with electron-rich organic moieties, such as amines, oldfin and aniline (Yang et al. 2012). Therefore, electron-rich organic moieties containing compounds can be potentially transformed during Fe(VI) oxidation. The reaction mechanisms of Fe(VI) with substrates can undergo 1) a one electron transfer step from Fe(VI) to Fe(V) and then followed by a two electron transfer step to Fe(III) as the final product; 2) a two electron transfer step following Fe(VI) → Fe(IV) → Fe(II) (Sharma 2013).

1.3. General objectives of dissertation

My dissertation project is to explore novel solar activated photocatalysts and advanced oxidation processes (AOPs) for the destruction of four target problematic toxins and pollutants: cylindrospermopsin (CYN), a potent cyanotoxin produced by

cyanobacteria in fresh water systems; iopamidol, widely employed as iodinated X-ray contrast media (ICM), and 4-methylcyclohexanemethanol (MCHM) and propylene glycol phenyl ether (PPh) related to the contamination of local drinking water in Charleston, West Virginia, on Jan 9 2014. In the present study, UV and visible light active TiO_2 photocatalysis, Fe(III)-oxalate photochemical systems, radiolysis technique and ferrate (VI) oxidation process were studied for the degradation of CYN, iopamidol, MCHM and PPh to develop the fundamental understanding required to assess AOPs as a potential water treatment process.

CHAPTER 2

UV and Visible Light Activated TiO_2 Photocatalysis of 6-hydroxymethyl uracil, a model compound for the potent cyanotoxin cylindrospermopsin

2.1 Abstract

TiO_2 photocatalyses of 6-hydroxymethyl uracil (6-HOMU) a model compound for the potent cyanotoxin, cylindrospermopsin (CYN), were carried out employing visible and UV irradiation using different non-metal doped TiO_2 materials, nitrogen and fluorine-TiO_2 (NF-TiO_2), phosphorus and fluorine-TiO_2 (PF-TiO_2) and sulfur-TiO_2 (S-TiO_2). The model compound was readily degraded under UV TiO_2 photocatalysis with pseudo-first-order rate constants (k) of 2.1, 1.0, and 0.44 h^{-1} for NF-TiO_2, PF-TiO_2 and S-TiO_2, respectively. Under visible light activated (VLA), NF-TiO_2 was the most active photocatalyst, PF-TiO_2 was marginally active and S-TiO_2 inactive. VLA NF-TiO_2 was effective and increased the k with increasing pH from 3 to 9. The presence of humic acid (HA), Fe^{3+} and Cu^{2+} can enhance the degradation. However, at 20 ppm HA significant inhibition was observed, likely due to shadowing of the catalyst, quenching of ROS or blocking active sites of TiO_2. We probed the roles of different reactive oxygen species (ROS) using specific scavengers and the results indicate that $O_2^{-\bullet}$ plays an important role in VLA TiO_2 photocatalysis. Our results demonstrate that NF-TiO_2 photocatalysis is effective under UV and visible irradiation and over a range of water qualities. VLA NF-TiO_2 photocatalysis is an attractive alternative technology for the CYN contaminated water treatment.

2.2 Introduction

Cyanobacteria commonly exist in drinking water sources and can lead to harmful algae blooms (HABs). Seventy percent of HABs can produce potent toxins (Codd 1995, Ho et al. 2006) and thus pose a tremendous risk to humans and the environment. One of the more problematic cyanotoxins is cylindrospermopsin (CYN), an alkaloid with a

tricyclic guanidine group and uracil ring. CYN has been showed to be genotoxic (Humpage et al. 2000) and carcinogenic (Falconer and Humpage 2001). The main target organs of CYN include the liver, kidney, thymus, lungs and adrenal glands. Human exposure to cylindrospermopsin occurs through ingestion of CYN contaminated food or water, or during recreational activities during HABs in lakes and fresh water systems. The most notable incident of CYN on human health occurred on Palm Island, Australia in 1979, which led to hepatoenteritis in 138 children and 10 adults (Griffiths and Saker 2003). Despite this notorious incident, CYN was not isolated and identified until 1992 (Ohtani et al. 1992). CYN is also responsible for the poisoning of livestock (Saker et al. 1999).

The occurrences and volumes of toxic cyanobacterial blooms have increased significantly in recent years due to climate change and increasing eutrophication. With the increasing pressure and global need for clean water, it is desirable to identify a sustainable treatment process for the elimination of naturally occurring cyanotoxins from drinking water. Conventional water treatment methods such as coagulation, flocculation, sedimentation and filtration are often not viable for removing cyanotoxins (Chow et al. 1999, Newcombe and Nicholson 2004). Although activated carbon may be effective to remove cyanotoxins in the laboratory, treatments of large volumes of contaminated water are often not economically practical. The high levels of natural organic material (NOM) associated with HABs can have a pronounced negative impact on the effectiveness of the activated carbon process (Newcombe et al. 2002). Chlorine and ozone based treatments have been studied for removal of cyanotoxins, however, by products like trihalomethanes

(THMs) (by chlorination) and bromate (by ozonation) are a concern because of associated health consequences (Rodríguez et al. 2007a, Rodríguez et al. 2007b).

Advanced oxidation processes (AOPs) have received considerable attention for the treatment of water contaminated with a wide variety of toxins and pollutants. AOPs employ the hydroxyl radical (HO•) as the primary oxidant in the oxidative remediation of toxins in drinking water. HO• is a very powerful oxidant, which can react rapidly with nearly all organic compounds due to its strong oxidation potential (+2.80V) (Thakur et al. 2010). UV TiO_2 photocatalysis is effective for the destruction of an extensive number of toxins and organic contaminants in the wastewater and drinking water (Tong et al. 2012). Conventional UV TiO_2 photocatalysis can produce a number of reactive oxygen species (ROS), however HO• is generally associated with the effective destruction of organic compounds. UV photoexcitation of TiO_2 produces electron/hole (e^-_{cb} / h^+_{vb}) pairs as illustrated by **Eq. (2.1)**. The e^-_{cb} can reduce molecular oxygen yielding superoxide anion radical ($O_2^{-\bullet}$), **Eq. (2.2)** and the h^+_{vb} has the potential to oxidize surface absorbed H_2O or hydroxyl groups to generate HO•, **Eq. (2.3)**. Another source of HO• can occur via disproportionation of $O_2^{-\bullet}$, yielding H_2O_2, **Eq. (2.4)**, which can be reduced to HO• **Eq. (2.5)**.

$$TiO_2 + h\nu \rightarrow e^-_{cb} + h^+_{vb} \quad (2.1)$$

$$e^-_{cb} + O_2 \rightarrow O_2^{-\bullet} \quad (2.2)$$

$$h^+_{vb} + H_2O \rightarrow H^+ + HO\bullet \quad (2.3)$$

$$2O_2^{-\bullet} + 2H_2O \rightarrow H_2O_2 + 2OH^- + O_2 \quad (2.4)$$

$$H_2O_2 + e^-_{cb} \rightarrow OH^- + HO\bullet \quad (2.5)$$

Limitations effecting the broad application of UV TiO_2 photocatalysis include the requirement of costly UV light (< 387 nm) and the rapid recombination of e^-_{cb} / h^+_{vb} pairs, leading to low quantum yields. The wavelengths of solar irradiation that reach the surface of the earth are mostly in the visible region (40%) with a small fraction (5%) in UV region. Hence, photocatalysts activated by visible light or by a broad spectrum of wavelengths (solar) have significant economic advantages. Doping of TiO_2 (NF-TiO_2, PF-TiO_2 and S-TiO_2) can result in a decrease in band gap such that longer wavelength light (visible and solar light) becomes applicable (Han et al. 2011, Pelaez et al. 2009). In addition, doped TiO_2 can inhibit e^-_{cb} / h^+_{vb} pairs recombination through trapping of charge carriers. VLA photocatalysis employing TiO_2 based materials has received significant attention recently and also been reviewed by the research groups of Zhao (Zhao et al. 2005) and Dionysiou (Pelaez et al. 2012b). UV and VLA TiO_2 photocatalysis are effective for treatment of microcystin cyanotoxins (MC), however only a limited number of reports have appeared on the photocatalysis of CYN (Pelaez et al. 2012a). The high cost of CYN limited our ability to conduct detailed studies to optimize the reaction conditions for the TiO_2 photocatalytic destruction of CYN. The uracil moiety in CYN is critical to the toxicity of CYN. HO• reacts primarily (84%) at the uracil ring of CYN (Song et al. 2012). With this in mind, 6-hydroxymethyl uracil (6-HOMU) (**Fig. 2.1**) was synthesized and used as a model compound for the UV and VLA photocatalysis of CYN. We report herein the photocatalytic activity of different non-metal doped TiO_2 materials, NF-TiO_2, PF-TiO_2 and S-TiO_2 under 350, 420 and 450 nm irradiation. Among these photocatalysts, NF-TiO_2 was the most UV and visible light active for the degradation of the CYN model compound. The treatment is effective over a range of pH, and in the

presence of ions and HA. $O_2^{-\bullet}$ appears to play the predominant role in the VLA photocatalytic degradation process. Our results demonstrate NF-TiO_2 can be used for the UV and visible light photocatalytic destruction of uracil based compounds under a variety of conditions.

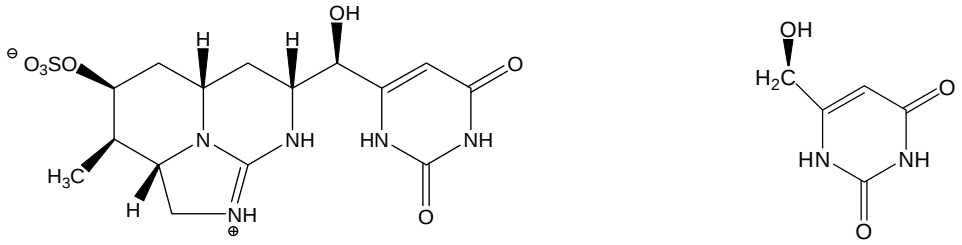

Fig. 2.1 Structure of cylindrospermopsin (CYN) and the model compound 6-hydroxymethyl uracil (6-HOMU)

2.3 Materials and methods

2.3.1 Materials

$FeCl_3 \cdot 6H_2O$, $CuCl_2 \cdot 2H_2O$, $CaCl_2 \cdot 2H_2O$, $MgCl_2$ as the sources of common ions, acetic acid, sodium bisulfite and HPLC grade methanol were purchased from Fisher Scientific. The humic acid was obtained from Fluka. 6-methyl uracil and selenium dioxide were purchased from Sigma Aldrich. Sodium borohydride was obtained from Acros organics. All reagents were used as received. The synthesis and characterization of the doped-TiO_2 materials (NF-TiO_2, PF-TiO_2, and S-TiO_2) are reported elsewhere (Pelaez et al. 2012a). The model compound (6-hydroxymethyl uracil) was synthesized according to standard organic functional group transformations. All aqueous solutions were prepared with Millipore filtered water.

2.3.2 Sample preparation

The loading of doped-TiO_2 materials employed for UV photocatalysis experiments was 0.05 g/L with the initial model compound concentration of 5 ppm unless otherwise stated. VLA TiO_2 photocatalysis of model compound was conducted with 0.1 g/L NF-TiO_2 and 1 ppm initial concentration of model compound. The reaction solution was transferred to a pyrex cylindrical reactor (12 × 1 in., 150 ml capacity, with a vented Teflon screw top) and magnetically stirred in the dark and purged with oxygen for 15 mins prior to irradiation and during irradiation. A Rayonet photochemical reactor (Southern New England Ultra Violet Company, www.rayonet.org, model RPR-100) was used for all experiments, equipped with a cooling fan and 15 phosphor-coated inter changeable lamps at λ= 350, 420 and 450 nm. Aliquots (1 ml) were collected at given time intervals and filtered through a 0.45 μm filter prior to high-performance liquid chromatography (HPLC) analysis.

2.3.3 Preparation of model compound

The synthesis of 6-HOMU includes two steps **(Fig. 2.2)**: synthesis of orotaldehyde and reduction of orotaldehyde to 6-HOMU. The orotaldehyde was prepared by Kwang-Yuen's method (Zee-Chen and Cheng 1967). Briefly, 6-methyl uracil (2.54 g) was refluxed in acetic acid (60 mLs) with selenium dioxide (2.66 g) for 6 hrs. The hot reaction mixture was filtered and the yellow filtrate collected and solvent evaporated. The crude orotaldehyde was then dissolved in hot water (24 mLs) and 5 % sodium bisulfite was added dropwise into the stirred mixture. The solution was boiled with active carbon for 10 mins and then gravity filtered to remove the carbon. The filtrate was acidified to pH 1 using concentrated HCl. Upon cooling, pure orotaldehyde was obtained as a

precipitate from the solution. A mixture of pure orotaldehyde (0.14 g) and sodium borohydride (0.076 g) was refluxed in 95 % methanol for 4 hrs. The resulting solution was filtered and the solvent was evaporated yielding the pure 6-HOMU with the purity of 98 %. ^{1}H NMR spectrum (400 Hz, D_2O): δ 4.234 (2H, s, CH_2), 5.679 (1H, s, H5). ^{13}C NMR (400 Hz, D_2O): δ 62.18 (CH_2), 98.76 (C5), 160.19 (C2), 167.86 (C6), 170.63 (C4). Mass spectrum (ESI): m/z 141.1 (M-1).

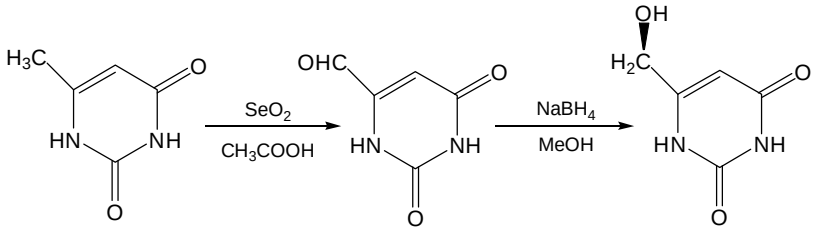

Fig. 2.2 Synthesis of 6-hydroxymethyl uracil.

2.3.4 Analysis

The concentration of the model compound was monitored by HPLC, Varian ProStar equipped with a ProStar 410 autosampler and a ProStar 335 photodiode array detector under the following conditions: a Luna RP C18 column (5 μm, 250 × 4.6 mm); 30 μl injection volume and 1 ml/min flow rate; The mobile phase was consisted of a linear gradient starting at 5 % methanol, 95 % water increased to 30 % methanol in 5 min and then held constant for an additional 5 min; the detection wavelength was at 260 nm.

2.4 Results and discussion

2.4.1 TiO_2 photocatalysis of 6-hydroxymethyl uracil

TiO_2 photocatalysis experiments were carried out with 6-HOMU under 350, 420 and 450 nm irradiation varying only the catalysts, NF-TiO_2, PF-TiO_2 and S-TiO_2, to evaluate the relative photocatalytic activity of these non-metal doped TiO_2 materials.

The concentration of 6-HOMU was monitored by HPLC as a function of irradiation time (**Fig. 2.3**). Under UV irradiation (350 nm), the degradation follows the order of NF-TiO_2 > PF-TiO_2 > S-TiO_2. The percent removal of 6-HOMU was 100, 86 and 59 % for NF-TiO_2, PF-TiO_2 and S-TiO_2, respectively after 120 mins of UV irradiation. The observed pseudo-first-order rate constants (k) were 2.1 h^{-1} for NF-TiO_2, 1.0 h^{-1} for PF-TiO_2, and 0.44 h^{-1} for S-TiO_2. VLA NF-TiO_2 photocatalysis (at 420 and 450 nm) leads to the degradation of 6-HOMU but at a slower rate than under UV irradiation (**Fig. 2.3**). 6-HOMU was slightly degraded by PF-TiO_2 under 420 nm irradiation and no degradation was observed employing S-TiO_2 under our VLA (450 nm) conditions. The photocatalytic activity of these materials is dependent on the recombination e^-_{cb} / h^+_{vb} pairs, the band gap energies and structural properties (Pelaez et al. 2009). The band gaps of NF-TiO_2, PF-TiO_2 and S-TiO_2 and the corresponding photoexcitation wavelengths are presented in **Table 2.1**.

Table 2.1 Doped TiO_2 band gaps and corresponding photoexcited wavelengths

Doped TiO_2	Band-gap (eV)	Wavelength λ (nm)
S-TiO_2	2.94	422
NF-TiO_2	2.75	451
PF-TiO_2	2.68	463

PF-TiO_2 has the smallest band gap and should be activated by wavelengths of ≤ 463 nm. However, no degradation was observed at 450 nm during VLA PF-TiO_2 under our conditions, indicating that PF-TiO_2 has the poor photocatalytic activity likely due to faster recombination e^-_{cb} / h^+_{vb} pairs and poor structural properties. While the band gap energy of S-TiO_2 (~ 422 nm) matches well with the light source of 420 nm, no detectable

degradation of 6-HOMU was observed under 420 nm irradiation after 4 hrs. VLA S-TiO_2 photocatalysis was reported to be effective for the destruction of microcystin-LR (MC-LR) (Han et al. 2011). The differences in the structures of the MC-LR and 6-HOMU will influence the adsorption and hence degradation of these compounds. MC-LR has more functional groups (carboxylic acid, amide, amine) than 6-HOMU, which will enhance the adsorption and subsequent degradation of MC-LR by the surface initiated processes involved in heterogeneous photocatalysis. NF-TiO_2 leads to the effective degradation of 6-HOMU under UV and visible light irradiation indicating the recombination of e^-_{cb} / h^+_{vb} pairs in NF-TiO_2 with a band gap of 2.75 ev is slow enough to allow the production of ROS. VLA TiO_2 photocatalysis using NF-TiO_2 is reported to be effective for a number of compounds including acetic acid (Wu et al. 2010) and 4-chlorophenol (Li et al. 2011). Our results indicate that NF-TiO_2 should be an effective visible light driven photocatalyst for the destruction of the CYN.

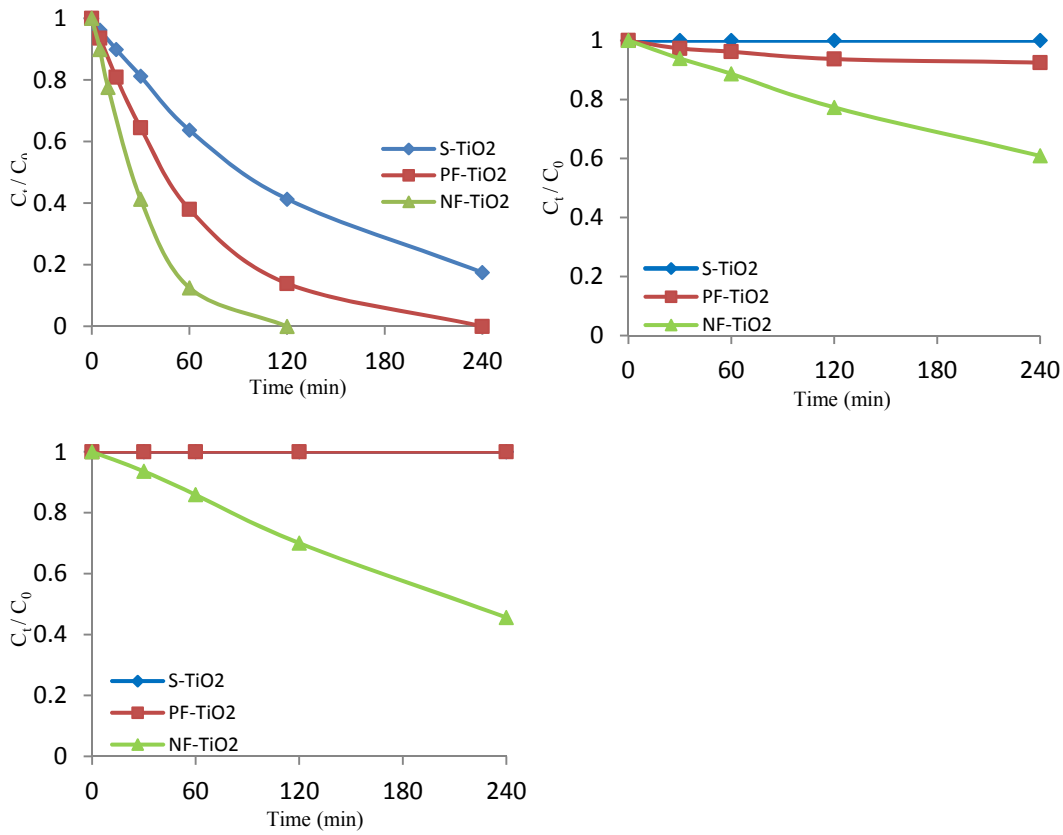

Fig. 2.3. TiO_2 photocatalysis of 6-HOMU under 350, 420 and 450 nm. [6-HOMU]$_0$=5ppm, [TiO_2] =0.05g/L. The reproducibility is within ± 10 % on the basis of triplicate runs.

2.4.2 Degradation Kinetics

The TiO_2 photocatalytic degradation kinetics of 6-HOMU were evaluated under 350, 420 and 450 nm irradiation for each catalyst. While TiO_2 photocatalysis is a heterogeneous process, the initial degradation kinetics often follow pseudo-first-order type kinetics (Xu et al. 2007). The concentration of 6-HOMU was monitored by HPLC as a function of irradiation time. The plots of ln (C_o/C) as a function of treatment time exhibit linear relationships and the pseudo-first order rate constants were determined from the slope of the line. The results are summarized in **Table 2.2**.

Table 2.2 Pseudo-first-order rate constants (*k*) of 6-HOMU under 350, 420 and 450 nm

Photocatalysts	k (h^{-1}) (R^2)		
	350 nm	420 nm	450 nm
S-TiO_2	0.44 (0.999)	0.0 (1.00)	0.0 (1.00)
PF-TiO_2	1.0 (0.999)	0.03 (0.915)	0.0 (1.00)
NF-TiO_2	2.1 (0.994)	0.12 (0.994)	0.20 (0.996)

2.4.3 Heterogeneous kinetics

Evaluation of reaction kinetics can provide useful mechanistic information and important parameters for the assessment and modeling of TiO_2 photocatalytic treatment. TiO_2 photocatalysis involves the generation of ROS and their subsequent reactions with the adsorbed target compounds at the TiO_2 surface. In these heterogeneous processes, both adsorption and reactivity play critical roles in governing the degradation. To assess the adsorption and reactivity parameters for heterogeneous TiO_2 photocatalysis, the Langmuir-Hinshelwood (L-H) kinetic model was employed **Eq. (2.6**). The L-H model has been widely used for assessment of TiO_2 photocatalysis at the liquid-solid interfaces (Ollis 2005, Xu et al. 2007). This model assumes limited surface adsorption sites, no interaction between adsorbed species on the surface and reversible adsorption reaction (Fox and Dulay 1993).

$$1/ r_0 = 1/ k_r K C_o + 1/ k_r \quad (2.6)$$

Where r_0 is the initial rate, C_0 is the initial 6-HOMU concentration, k_r is a reactivity coefficient related to oxidation reactions, and K is the equilibrium constant related to surface adsorption. The L-H model applied to TiO_2 photocatalysis yields apparent kinetic

parameters. The L-H experiments were conducted over a range of initial concentrations (3.52-35.2 μM) and a constant NF-TiO_2 concentration (0.1g/L) under visible light (450 nm) irradiation **(Fig. 2.4)**. The L-H kinetic parameters k_r and K were determined from the slope and intercept of the linear fit of the $1/r_0$ vs. $1/C_0$, which shows that k_r is 0.304 μM/L·min and K is 0.016 L/μM under our experimental conditions. L-H kinetic parameters for phenylarsonic acid (PA) with P-25 TiO_2 using the same reaction vessels and photochemical reactor under 350 nm irradiation has been reported with k_r 2.8 μM/L·min and K 0.034 L/μM (Zheng et al. 2010). The L-H parameters for PA under UV TiO_2 photocatalysis may imply stronger adsorption and a more reactive system than 6-HOMU treatment by VLA NF-TiO_2 photocatalysis. The degradations at different initial concentrations follow pseudo-first-order kinetic model (insert table in Fig. 4). The apparent kinetic parameters obtained from our results are useful for modeling and predicting specific treatment objectives.

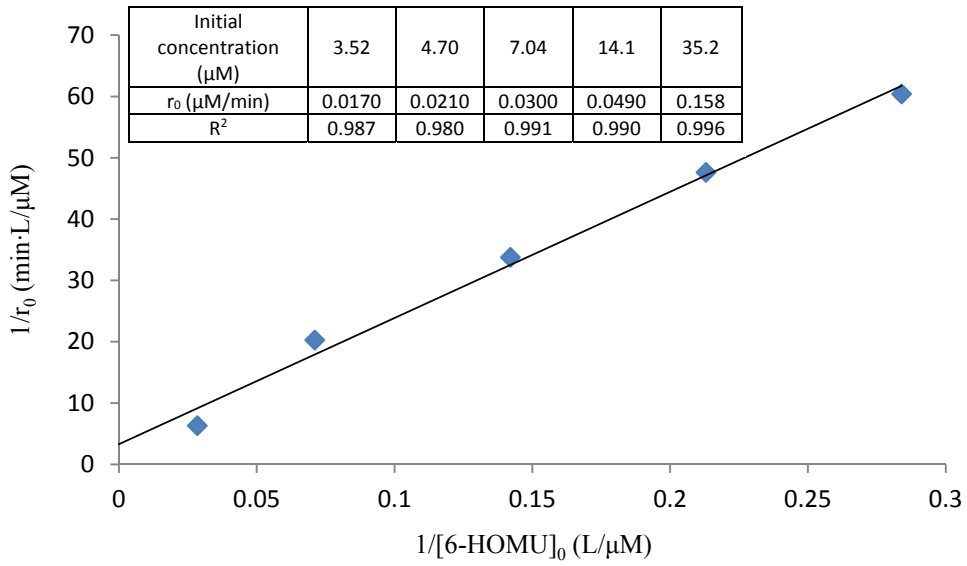

Fig. 2.4. L-H plot of TiO_2 photocatalysis of 6-HOMU under visible light (450 nm). The insert table is the initial rates at different concentration of 6-HOMU. [NF-TiO_2]=0.1 g/L. The reproducibility is within ± 5 % on the basis of triplicate runs.

2.4.4 Environmental factors on VLA TiO_2 photocatalysis

2.4.4.1 pH effects

VLA TiO_2 photocatalyses of 6-HOMU were performed under acidic, neutral, and basic conditions (pH 3, 5, 7 and 9). The concentrations of 6-HOMU as a function of irradiation time at different pH values are illustrated in **Fig. 2.5**. The degradation of 6-HOMU was fastest at pH 7 and 9 with overall degradation of 62 ± 3 %, decreasing to 40 % at pH 5 and to 23 % at pH 3 after 4 hrs of treatment. The decrease in degradation with decreasing pH is rationalized based on electrostatic repulsion between positively charged 6-HOMU and the NF-TiO_2 surface. The point of zero charge (PZC) for NF-TiO_2 is 6.4. Under acidic conditions, the surface of NF-TiO_2 is protonated (TiO_2H^+) and possesses an overall positive charge. While the pK_a value for 6-HOMU is not reported, we assume the

pK_a of 6-HOMU is similar to 5-HOMU (pK_a= 9.27) (Privat and Sowers 1996) and thus positively charged in the pH range of this study. The neutral and negative charges on the surface of the catalyst under neutral and basic conditions lead to stronger adsorption of the positively charged 6-HOMU and thus faster degradation. As the pH decreases the overall positive charge on the surface increases along with the electrostatic repulsion with positively charged 6-HOMU inhibiting adsorption resulting in slower degradation at under acidic conditions.

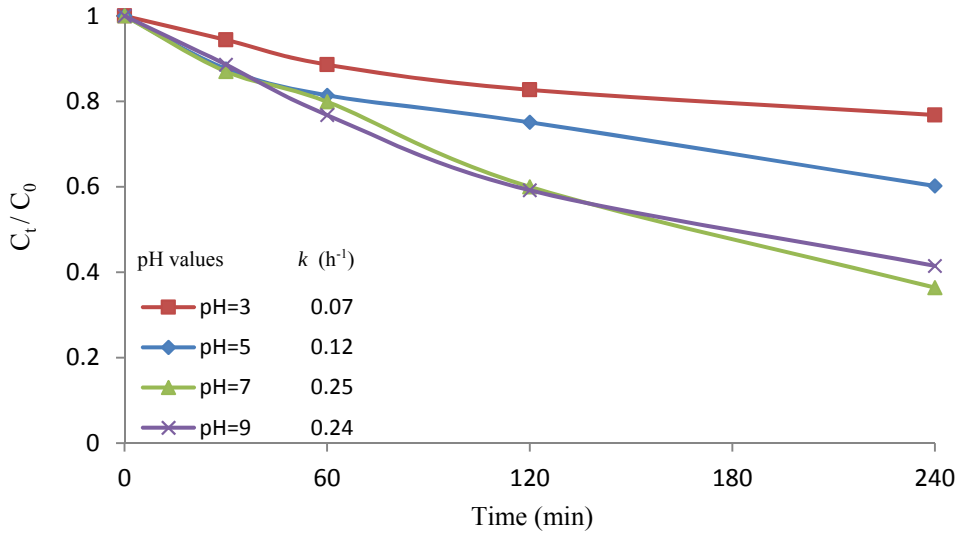

Fig. 2.5. TiO_2 photocatalysis of 6-HOMU at pH 3, 5, 7 and 9. The insert table is the 1st order rate constants at different solution pH. $[6\text{-HOMU}]_0$=1 ppm, $[NF\text{-}TiO_2]$=0.1 g/L, λ=450 nm. The reproducibility is within ± 5 % on the basis of triplicate runs.

2.4.4.2 Dissolved metal ions effects

Dissolved ions can influence the overall efficiency of TiO_2 photocatalysis of organic compounds. In order to investigate the influence of dissolved ions on VLA TiO_2 photocatalysis, Ca^{2+}, Mg^{2+}, Fe^{3+} and Cu^{2+} ions were added to the reaction solutions in the range of 0.2~8 ppm. The effects of Ca^{2+} and Mg^{2+} ions on photocatalysis of 6-HOMU are

negligible under our experimental conditions. The pseudo-first-order rate constants (k) of 6-HOMU photodegradation with Ca^{2+}, Mg^{2+} and without the ions are identical (0.25 ± 0.01 h^{-1}). The addition of Fe^{3+} and Cu^{2+} ions enhanced the VLA TiO_2 photocatalysis of 6-HOMU. In the presence of Fe^{3+} ions, the degradation rate constant increased by ~ 2.5 times at a concentration of 8 ppm with pseudo-first-order rate constant (k) of 0.61 h^{-1}. The NF-TiO_2 photocatalysis process of 6-HOMU was also promoted by adding Cu^{2+} ions in the range of 0.2~2 ppm. The presence of Fe^{3+}/Fe^{2+} and Cu^{2+} ions can promote photo-Fenton/Fenton type reactions **Eq. (2.7, 2.8)** to produce HO• which may be responsible for the observed enhancement in the degradation of 6-HOMU.

$$Fe^{3+} / Cu^{2+} + e^- \rightarrow Fe^{2+} / Cu^+ \quad (2.7)$$

$$Fe^{2+} / Cu^+ + H_2O_2 \rightarrow Fe^{3+} / Cu^{2+} + HO\bullet + HO^- \quad (2.8)$$

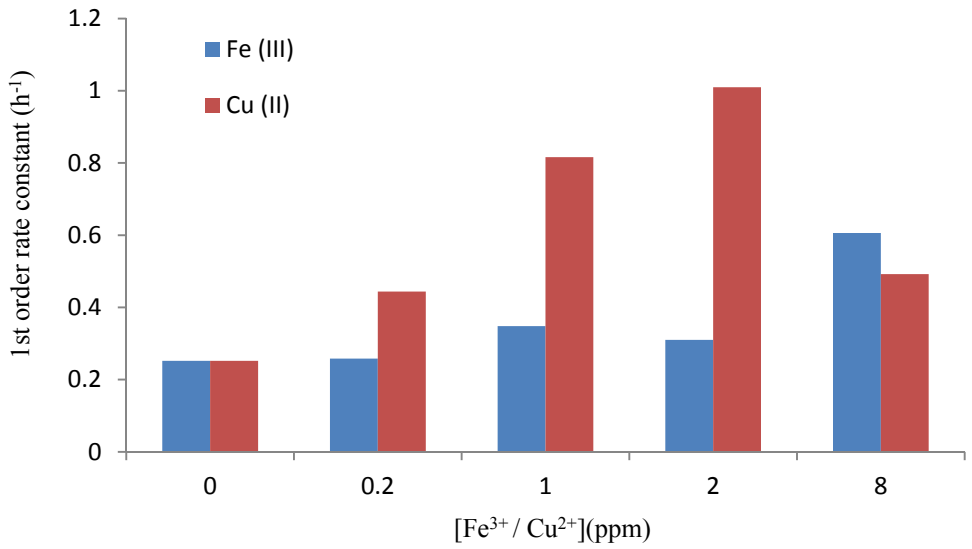

Fig. 2.6. The effects of Fe^{3+} and Cu^{2+} ion on TiO_2 photocatalysis of 6-HOMU. [6-HOMU]$_0$=1 ppm, [NF-TiO_2]=0.1g/L, λ=450 nm. The reproducibility is within ± 2 % on the basis of triplicate runs.

Fe^{3+}/Cu^{2+} ions can also scavenge the e^{-}_{cb} during TiO_2 photocatalysis, converting to Fe^{2+}/Cu^{+} ions, while inhibiting e^{-}_{cb} / h^{+}_{vb} pairs recombination to indirectly increase the HO• production. The decrease in the degradation rate constant at higher Cu^{2+} ion concentrations may be the result of Cu^{2+} ions acting as the primary e^{-}_{cb} scavenger at the expense of dissolve oxygen, inhibiting the formation of $O_2^{-\bullet}$ and thus reducing the levels of $O_2^{-\bullet}$ and indirectly reducing the production of HO•. Under our experimental conditions, inhibition however was not observed in the case of Fe^{3+} which may be a result of stronger adsorption of Cu^{2+} at the TiO_2 surface leading to more effective competition for e^{-}_{cb}.

2.4.4.3 Dissolved Organic Matter (DOM) effects

The presence of dissolved organic matter (DOM) can have a pronounced effect on photochemical based water treatment processes. DOM derived from decomposed biomass is composed of large carbon based structures with a number of light absorbing chromophores. Upon light absorption DOM can lead to an excited state (DOM*) **Eq. (2.9)**. The DOM* can undergo energy or electron transfer pathways with molecular oxygen to generate $^1O_2$ or $O_2^{-\bullet}$ **Eq. (2.10)**. These ROS can initiate the degradation of 6-HOMU, **Eq. (2.11)**. The DOM* can also sensitize TiO_2 **Eq. (2.12)** leading to charge carriers with the potential to initiate degradation processes **Eq. (2.13)**.

$$DOM + h\nu \rightarrow DOM^* \quad (2.9)$$

$$DOM^* + O_2 \rightarrow {}^1O_2\ (O_2^{-\bullet}) \quad (2.10)$$

$$^1O_2\ (O_2^{-\bullet}) + \text{6-HOMU} \rightarrow \text{6-HOMU}_{[OX]} \quad (2.11)$$

$$DOM^* + TiO_2 \rightarrow TiO_2^* \quad (2.12)$$

$$TiO_2^* \rightarrow e^{-}_{cb} + h^{+}_{vb} \rightarrow ROS + \text{6-HOMU} \rightarrow \text{6-HOMU}_{[OX]} \quad (2.13)$$

The influence of DOM on the solar photolysis of organic contaminants has been widely studied (Chen et al. 2009, Guerard et al. 2009). We used HA to assess the role of DOM* initiated degradation of 6-HOMU under 450 nm irradiation in the absence of NF-TiO_2 as a control experiment. The photolysis of 6-HOMU was also carried out in the presence of HA under 450 nm irradiation for 240 mins. The concentration of 6-HOMU was monitored as a function irradiation time under different experimental conditions, shown in (**Fig. 2.7**). DOM alone did not lead to the photo-transformation 6-HOMU under our experimental conditions.

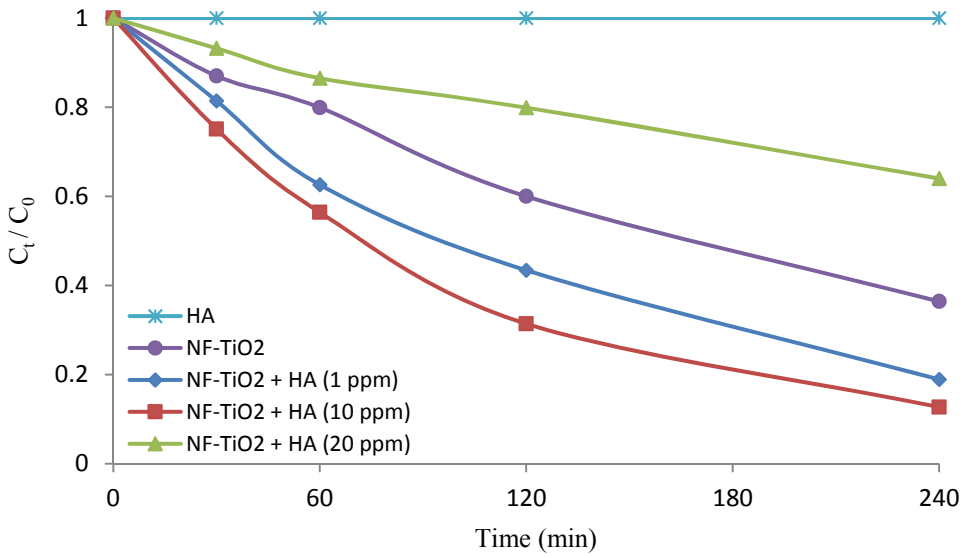

Fig. 2.7. The effects of HA on photo-transformation and TiO_2 photocatalysis of 6-HOMU. $[6\text{-HOMU}]_0$=1 ppm, $[\text{NF-TiO}_2]$=0.1 g/L, λ=450 nm. The reproducibility is within ± 5 % on the basis of triplicate runs.

The concentrations of HA were varied from 1~20 ppm while holding the catalyst loading and 6-HOMU constant. The observed pseudo-first-order rate constants (*k*) of degradation in the absence and presence of different HA concentrations are illustrated in

Fig. 2.7. An enhanced degradation was observed for HA concentrations between 1 and 10 ppm. This enhancement was attributed to HA photosensitized processes, in which ROS can be formed to accelerate the overall photodegradation. However, the degradation process was strongly inhibited by the increased HA because at higher concentrations, HA can act as a light filter and attenuate the photochemically active processes (Canonica et al. 2011), as well as scavenge ROS leading to the reduced degradation of 6-HOMU.

2.4.5 The role of reactive oxygen species in VLA TiO_2 photocatalysis

UV TiO_2 photocatalysis leads to a number of ROS, among them HO• produced by h^+_{vb} oxidation of adsorbed hydroxyl groups is generally considered responsible for the degradation of organic pollutants and toxins. While the effectiveness of UV TiO_2 photocatalysis is often correlated to the production of HO•, during VLA doped-TiO_2 photocatalysis the direct formation of HO• from h^+_{vb} is not thermodynamically plausible. VLA doped-TiO_2 photocatalysis can however lead to the formation of HO• indirectly from $O_2^{-\bullet}$. $O_2^{-\bullet}$ can also lose an electron to produce $^1O_2$ which can contribute to the oxidation of organic compounds. In an attempt to better understand the formation and roles of different ROS during VLA NF-TiO_2 photocatalysis, specific scavengers were employed during the treatment of 6-HOMU. The degradation of 6-HOMU was carried out in the absence and presence of various quenchers and scavengers as outlined in **Table 2.3**. Molecular oxygen was used as the e^-_{cb} scavenger, t-BuOH was added as a HO• scavenger, furfuryl alcohol was used to probe the role of $^1O_2$, formic acid was used to quench oxidative processes, and superoxide dismutase employed to quench $O_2^{-\bullet}$.

Table 2.3 Scavengers effects on TiO_2 photodegradation

Reactive species	Scavengers	Mechanisms
e^-_{cb} (electron)	O_2	$e^-_{cb} + O_2 \rightarrow O_2^{-\bullet}$ $k = 7.6 \times 10^7\ M^{-1}s^{-1}$ (Xu et al. 2008)
HO• (hydroxyl radical)	*t*-BuOH (*tert*-Butyl alcohol)	HO• + *t*-BuOH → H_2O + $\bullet CH_2C(CH_3)_2OH$ $k = 5.0 \times 10^8\ M^{-1}s^{-1}$ (Xu et al. 2008)
$^1O_2$ (singlet oxygen)	Furfuryl alcohol (FFA)	FFA + $^1O_2 \rightarrow FFA_{ox}$ $k = 1.2 \times 10^8\ M^{-1}s^{-1}$ (Haag et al. 1984)
h^+_{vb} (hole)	HCO_2H (formic acid)	$2\ h^+_{vb} + 2HCO_2^- \rightarrow CO_2 + 2H^+$
$O_2^{-\bullet}$ (superoxide anion radical)	SOD_{red} (superoxide dismutase)	$SOD_{red} + O_2^{-\bullet} + 2H^+ \rightarrow SOD + H_2O_2$ $k = 2.0 \times 10^9\ M^{-1}s^{-1}$ (Xu et al. 2008)

(Argon saturated conditions) no detectable degradation of 6-HOMU was observed during VLA NF-TiO_2 photocatalysis illustrating molecular oxygen is required for the degradation as an e^-_{cb} trap and/or in the production of $O_2^{-\bullet}$. The presence of *t*-BuOH, a HO• scavenger, significantly reduced the observed degradation of 6-HOMU. While hydroxyl radicals do not form directly via the h^+_{vb} oxidation of surface hydroxyl groups during VLA NF-TiO_2 photocatalysis, the formation of HO• can occur indirectly via reduction of H_2O_2 the product of $O_2^{-\bullet}$ disproportion.

Furfuryl alcohol (FFA) is commonly used as a scavenger for $^1O_2$, but also readily reacts with HO• (Albinet et al. 2010) and thus can function as a scavenger for both $^1O_2$ and HO•. The decreases in degradation of 6-HOMU were similar in the presence of FFA and *t*-BuOH, a selective HO• scavenger. Since FFA quenches $^1O_2$ and *t*-BuOH does not, the similar decrease in the presence of FFA or *t*-BuOH indicates $^1O_2$ plays a minimal role in the degradation process. To further test the role of $^1O_2$ in VLA NF-TiO_2 photocatalysis,

the degradation of 6-HOMU was performed in D_2O. The lifetime of $^1O_2$ in D_2O is longer than that in H_2O and thus singlet oxygen mediated processes are enhanced in D_2O. The degradations in solution of H_2O and D_2O were similar indicating $^1O_2$ does not play an important role under our experimental conditions.

VLA NF-TiO_2 photocatalysis of 6-HOMU was not affected by the presence of formic acid. While formic acid has been used to quench the h^+_{vb} mediated processes during UV TiO_2 photocatalysis, our observations are consistent with previous reports that h^+_{vb} trapped in the region of inter-valence band does not possess the redox potential to efficiently oxidize formic acid (Beranek et al. 2007). Therefore, the produced HO• in VLA NF-TiO_2 likely results from the reduction of H_2O_2 rather than oxidizing surface absorbed H_2O by h^+_{vb}. Our results indicate the photogenerated h^+_{vb} in VLA NF-TiO_2 photocatalysis does not play a significant role in the observed degradation process.

In TiO_2 photocatalysis, dissolved oxygen serves as an electron trap and leads to the formation of $O_2^{-\bullet}$ which can proportionate or produce to $^1O_2$ with loss of an electron. In the presence of superoxide dismutase, an effective quencher of $O_2^{-\bullet}$, the degradation of 6-HOMU was completely inhibited indicating that $O_2^{-\bullet}$ is critical in the VLA NF-TiO_2 photocatalytic degradation process. $O_2^{-\bullet}$ has been implicated in the destruction of a strongly visible light absorbing dye during VLA TiO_2 photocatalysis (Stylidi et al. 2004). The previous study is complicated by potential self-sensitized degradation pathways. Our model compound does not absorb visible-light and thus contributions from self-sensitized reaction pathways can be ruled out. Therefore, according to these findings, $O_2^{-\bullet}$ plays a critical role in VLA TiO_2 photocatalytic processes.

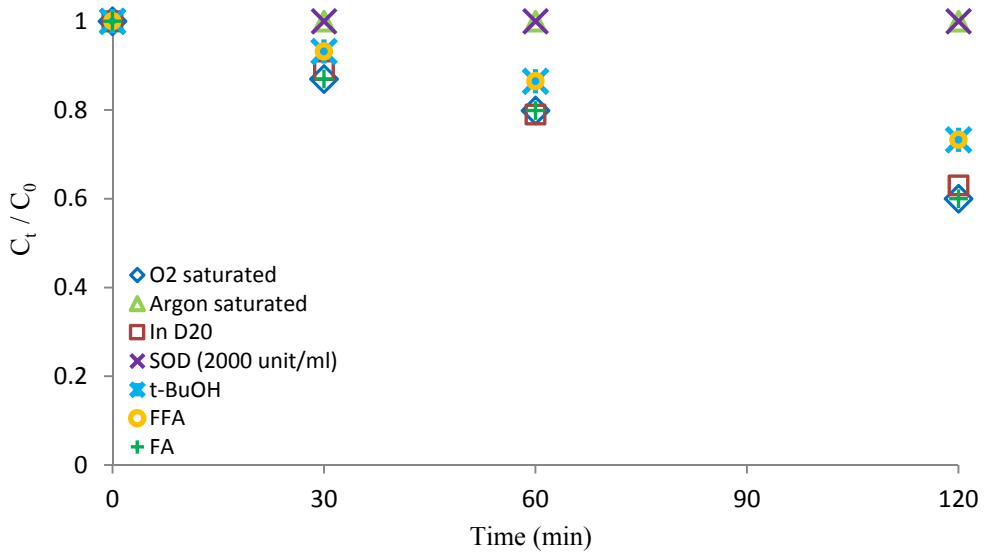

Fig. 2.8. The contribution of ROS to VLA TiO_2 photocatalysis. $[6\text{-HOMU}]_0$=1 ppm, [NF-TiO_2]=0.1 g/L, λ=450 nm. The reproducibility is within ± 5 % on the basis of triplicate runs.

2.5 Conclusions

S-TiO_2, PF-TiO_2 and NF-TiO_2 are photoactive under UV irradiation and the degradation of 6-HOMU follows a pseudo-first-order kinetic model. Among non-metal doped TiO_2 materials, our results indicate that NF-TiO_2 exhibits the best performance to destroy the model compound of CYN due to its high photocatalytic activity. The kinetics is accurately modeled and degradation is effective over a range of pH. A synergetic effect is observed in photodegradation of 6-HOMU in the presence of Fe^{3+}, Cu^{2+}ions and HA due to more production of HO• or ROS in the photooxidation process. Experiments performed in the presence of scavengers for $O_2^{-\bullet}$, $^1O_2$, HO• and h^+_{vb} indicate that $O_2^{-\bullet}$ is the predominant species leading to the VLA TiO_2 photocatalytic destruction of 6-HOMU. Our results provide a better fundamental understanding of the different roles of ROS

during VLA TiO_2 photocatalysis and demonstrate VLA TiO_2 photocatalysis has potential for water treatment for cyanotoxins.

CHAPTER 3

Reductive and oxidative degradation of iopamidol, iodinated X-ray contrast media, by Fe(III)-oxalate under UV and visible light treatment

3.1 Abstract

Iopamidol, widely employed as iodinated X-ray contrast media (ICM), is readily degraded in a Fe(III)-oxalate photochemical system under UV (350 nm) and visible light (450 nm) irradiation. The degradation is nicely modeled by pseudo first order kinetics. The rates of hydroxyl radical (•OH) production for Fe(III)-oxalate/H_2O_2/UV (350 nm) and Fe(III)-oxalate/H_2O_2/visible (450 nm) systems were 1.19 ± 0.12 and 0.30 ± 0.01 μM/min, respectively. The steady-state concentration of hydroxyl radical (•OH) for the Fe(III)-oxalate/H_2O_2/UV (350 nm) conditions was 10.88 ± 1.13 × 10^{-14} M and 2.7 ± 0.1 × 10^{-14} M for the Fe(III)-oxalate/H_2O_2/visible (450 nm). The rate of superoxide anion radical ($O_2^{-\bullet}$) production under Fe(III)-oxalate/H_2O_2/UV (350 nm) was 0.19 ± 0.02 μM/min with a steady-state concentration of 5.43 ± 0.473 × 10^{-10} M. Detailed product studies using liquid chromatography coupled to Q-TOF/MS demonstrate both reduction (multiple dehalogenations) and oxidation (aromatic ring and side chains) contribute to the degradation pathways. The reduction processes appear to be initiated by the carbon dioxide anion radical ($CO_2^{-\bullet}$) while oxidation processes are consistent with •OH initiated reaction pathways. Unlike most advanced oxidation processes the Fe(III)-oxalate/H_2O_2/photochemical system can initiate to both reductive and oxidative degradation processes. The observed reductive dehalogenation is an attractive remediation strategy for halogenated organic compounds as the process can dramatically reduce the formation of the problematic disinfection by-products often associated with oxidative treatment processes.

3.2 Introduction

The presence of pharmaceutical compounds in aquatic environments is a serious concern due to their extensive use and incomplete removal during wastewater treatment processes(Doll and Frimmel 2003, Seitz et al. 2008). Iodinated x-ray contrast media (ICM), composed of water-soluble iodinated aromatic compounds, are widely used to enhance the imaging of organs or blood vessels during diagnostic tests. Approximately 3.5×10^6 kg per year of ICM are consumed worldwide (Perez and Barcelo 2007). ICM is administered in high daily doses (up to 200 g/day) and excreted primarily non-metabolized (> 95 %) (Mutschler 1996). ICM is frequently detected in wastewater, groundwater, rivers, creeks and even drinking water supplies at elevated concentrations (at µg/L levels for wastewater and surface water) (Schulz et al. 2008, Ternes and Hirsch 2000). The presence of ICM is responsible for the high concentration of adsorbable organic halogen material (AOX) present in hospital wastewater (Kummerer et al. 1998) with the potential for adverse health impacts on humans. Conventional wastewater treatment processes generally do not effectively remediate ICM due to their resistance to biodegradation and high solubility in aqueous environments.

Although specific negative health effects of ICM on humans have not been identified, their extensive use and persistence in the environment are causes for concern. A number of reports have appeared on the treatment of ICM contaminated wastewater and drinking water including treatment by filtration, biotransformation (Kormos et al. 2010) and direct photolysis (Doll and Frimmel 2003, Sichel et al. 2011). These methods however are often not viable for ICM remediation because of extended treatment times, high cost and/or low efficiency. Ozonation treatment of ICM contaminated drinking

water only led to partial removal of non-ionic ICM (30-55 %) and less than 20 % of ionic ICM (Seitz et al. 2008). TiO_2 photocatalytic degradation of ICM has been reported, but there are questions about the efficiency of the process and its application for the mineralization of the contrast agent, iomeprol (Doll and Frimmel 2005). Given the large quantities of ICM released into the environment it is essential to identify effective sustainable water treatment methods. Iopamidol the focus of this study is the most frequently detected ICM in aqueous environments (Duirk et al. 2011, Tian et al. 2014). Shown in **Fig 1.2** iopamidol has molecular weight of 777, and the structure features commonly associated contrast agents, i.e., a central *iodo* substituted aromatic ring. The aromatic ring is substituted with alkyl side chains labeled A and B, which are coupled to the aromatic ring through amide linkages. The chains contain hydroxyl and amide functionalities which make the compound more water soluble.

Advanced oxidation processes (AOPs) such as photo-Fenton or photo-Fenton-like processes have been widely reported to efficiently degrade organic pollutants from wastewater (Tao et al. 2005). These processes involve the generation of hydroxyl radical (•OH) as the primary oxidant. Hydroxyl radical can react rapidly with nearly all organic compounds due to its strong oxidation potential (+2.80V) (Thakur et al. 2010). A variety of iron species and a number of carboxylic acids are abundant in natural environments, their coexistence can establish homogenous photo-Fenton type conditions with the potential to produce reactive species leading to the degradation of organic pollutants under solar irradiation. Oxalic acid, a simple abundant naturally occurring dicarboxylic acid, effectively initiates the degradation of the problematic pollutants, biphenol A and 4-chlorophenol (4-CP), under photo-Fenton conditions (Lee et al. 2014, Li et al. 2006). The

photochemical Fe(III)-oxalate system can be more efficient and catalytic in degrading organic pollutants then Fenton reactions (Fe(III) or Fe(II)/ H_2O_2) because of the rapid redox cycling of iron and faster production of •OH (Jeong and Yoon 2005, Zuo and Zhan 2005). The Fe(III)-oxalate complex exhibits strong ligand-to-metal charge absorption bands in the near UV and visible regions. UV and visible light photoexcitation of Fe(III)-oxalate complex leads to events and species capable of degrading a variety of pollutants as summarized in reactions 1.6 through 1.17.

H_2O_2 has been added as a complementary source for •OH in combination with UV irradiation, ozone and/or photocatalysis to accelerate degradation of organic contaminants (Dionysiou et al. 2004, He et al. 2012). Although the Fe(III)-oxalate complex has been extensively used for photochemical actinometry (Marco Montalti 2006), there are only a limited number of reports on the photochemical applications for water treatment. To date we are unaware of any published reports on the treatment of ICM using a Fe(III)-oxalate photochemical system. We herein report UV and visible light activated Fe(III)-oxalate/ H_2O_2 treatment of iopamidol. In our study, the addition of H_2O_2 significantly increased the degradation of iopamidol. The effects of Fe(III) and oxalate concentrations, and solution pH were studied in the photodegradation of iopamidol. The steady-state concentrations of •OH and $O_2^{-\bullet}$ are reported herein under UV and visible light activated Fe(III)-oxalate/ H_2O_2. Detailed product studies indicate that oxidation and reduction pathways play significant roles in the degradation processes.

3.3 Materials and methods

3.3.1 Materials

Iopamidol was obtained from Ilsung Pharmaceutical Co. (Korea). $FeCl_3 \cdot 6H_2O$, $Na_2C_2O_4$, nitroblue tetrazolium (NBT) and HPLC grade methanol were purchased from Fisher Scientific. Hydrogen peroxide was obtained from Sigma Aldrich (30%). Coumarin was purchased from MP Biomedicals, LLC. 7-hydroxycoumarin was obtained from Acros organics. All reagents were used as received. All aqueous solutions were prepared with Millipore filtered water and volumetric lab equipment.

3.3.2 Sample preparation

The standard photochemical experiments were conducted under the following experimental conditions: initial [iopamidol] = 10 μM, initial [Fe(III)] = 20 μM, initial oxalate concentration [$C_2O_4^{2-}$] = 100 μM and initial [H_2O_2] = 200 μM at the solution pH 3 with 10 mLs solution. Solution pH was adjusted with 0.1 M HNO_3 or 0.1 M NaOH to desired pH values prior to the photochemical reactions. The reaction solution was transferred to a Pyrex cylindrical reactor (12 × 1 in., 150 ml capacity, with a vented Teflon screw top) and gently purged with oxygen for 15 min prior to and during irradiation. A Rayonet photochemical reactor (Southern New England Ultra Violet Company, www.rayonet.org, model RPR-100) equipped with a cooling fan and 4 phosphor-coated inter changeable lamps at λ= 350 nm (0.46 mW/cm^2) and 450 nm (2.25 mW/cm^2) was used for all experiments. The quantum yields for the Fe oxalate dosimeter vary only modestly over the different wavelengths employed in our experiments (Marco Montalti 2006). Aliquots (1 ml) were collected at given time intervals and subjected to high-performance liquid chromatography (HPLC) for analysis. All the experiments were

conducted in triplicate with the mean value representing the data point and reproducibility expressed as error bars (based on the standard deviation among the trials) in the graphs.

3.3.3 Analysis

HPLC analysis of iopamidol

The concentration of the iopamidol was monitored by HPLC, Varian ProStar equipped with a ProStar 410 autosampler and a ProStar 335 photodiode array detector under the following conditions: a Luna RP C18 column (5 μm, 250 × 4.6 mm); 30 μl injection volume and 1 ml/min flow rate. The mobile phase consisted of a linear gradient starting at 5 % methanol, 95 % water increased to 30 % methanol in 5 min and then held constant for an additional 5 min; the detection wavelength was 242 nm.

LC-QTOF/MS analysis of iopamidol and its photoproducts

The analyses of iopamidol and the degradation products were carried out using an Agilent 6530 high resolution accurate-mass quadrupole time-of-flight (Q-TOF) liquid chromatography / mass spectrometer (LC-QTOF/MS). The samples were separated on an Agilent Zobrax eclipse plus C-18 (rapid resolution HD 3.0 × 100 mm, 1.8-Micron) equipped with a guard column (3.0 × 5 mm) of same packing material. The mobile phase consisted of A: 5mM ammonia formate + 0.1% formic acid in H_2O and B: CH_3CN, with a gradient elution of 5 % B for 1 min, followed by a linear increase to 95 % B in 10 min, back to 5 % B over 3 min. The flow rate was 0.4 ml/min and injection volume was 5 μl. The mass spectra (m/z 100-1000) were obtained in positive ion mode with electrospray ionization technology (ESI). Data acquisition and analysis were performed using the Agilent Mass Hunter software (Version B.05.0).

3.3.4 Measurement of steady-state concentration of •OH under UV and visible light

Hydroxyl radical is a powerful oxidant and the basis for the degradation of an extensive number of organic compounds during the application of advanced oxidative treatments for water purification. Hydroxyl radical plays a critical role in the Fenton and photo-Fenton oxidative transformation of organic compounds. With this in mind we employed coumarin as a selective trap for $[\bullet OH]_{ss}$ quantitation. Coumarin reacts with •OH to produce highly fluorescent 7-hydroxycoumarin (7-HOC) ($\lambda_{excitation}$ = 332 nm; $\lambda_{emission}$ = 455 nm), the concentration of •OH can be directly correlated to the 7-HOC fluorescence (Horiba FluoroMax 3 spectrofluorometer). The reaction yield of 7-HOC is 28.6 % (Louit et al. 2005).The trapping experiments were conducted under the same conditions used for degradation of the target compound as follows [Fe(III)] = 20 μM, $[C_2O_4^{2-}]$ = 100 μM, $[H_2O_2]$ = 200 μM, and [coumarin] = 0.1 mM at the solution pH 3. The calibration curve was obtained over a range of initial 7-HOC concentrations (0.5 ~ 10 μM) and [Fe(III)] = 20 μM, $[C_2O_4^{2-}]$ = 100 μM, $[H_2O_2]$ = 200 μM at pH 3. The fluorescence intensity was converted to the concentration of 7-HOC by calculation from the calibration curve normalized for percent yield.

3.3.5 Measurement of steady-state concentration of $O_2^{-\bullet}$ under UV and visible light

Superoxide anion radical is also produced during a number of advanced oxidation processes and we employed nitroblue tetrazolium dichloride (NBT) for the determination of superoxide anion radicals ($O_2^{-\bullet}$). NBT undergoes stepwise reduction via electron transfer upon reaction with $O_2^{-\bullet}$ to form the monoformazan (MF) and diformazan (DF). Both MF and DF are stable organic compounds but insoluble under aqueous solution. Therefore, the formation of $O_2^{-\bullet}$ in the Fe(III)-oxalate photochemical system was

monitored by determining the decomposition of NBT over the initial 30 min irradiation time. Since NBT can react with $O_2^{-\bullet}$ and •OH, 5 % *t*-butanol was added to scavenge all the •OH and thus minimize non-superoxide anion radical initiated degradation of NBT. Experimental conditions for measurement of $[O_2^{-\bullet}]_{ss}$ were as follow: [Fe(III)] = 20 μM, $[C_2O_4^{2-}]$ = 100 μM, $[H_2O_2]$ = 200 μM, [NBT] = 0.1 mM at the solution pH 7. The reactions were performed under UV (350 nm) and visible light (450 nm) irradiation. Aqueous samples (2 ml) were collected at given time intervals and the decomposition of NBT was monitored at wavelength 258 nm by UV-Vis spectrometer.

3.4 Results and discussion

3.4.1 Removal of iopamidol under different oxidant systems

The production of reactive oxygen species and degradation of the target compound is significantly more effective under UV irradiation compared to visible light and thus our focus shifts to the UV process. Photodegradations of iopamidol were carried out under H_2O_2/UV, Fe(III)-oxalate/UV and Fe(III)-oxalate/H_2O_2/UV, to probe the roles of the different components on the photodegradation efficiency. The degradations of iopamidol are nicely fit to pseudo first-order kinetics with the rate constants of 0.004, 0.046 and 0.097 min^{-1} for H_2O_2/UV, Fe(III)-oxalate/UV and Fe(III)-oxalate/H_2O_2/UV conditions, respectively. The H_2O_2/UV photochemical conditions establish the level degradation initiated by direct photolysis and production of •OH from the photochemical degradation of H_2O_2 to •OH. These pathways lead to less than 10 % degradation of iopamidol after 30 mins of treatment. The Fe(III)-oxalate/UV system results in ~ 70 % reduction of the iopamidol concentration while Fe(III)-oxalate/H_2O_2/UV system results in ~ 95 % destruction after 30 mins of UV irradiation

(Fig. 3.1). The enhanced degradation upon addition of H_2O_2 is assigned to redox cycling of Fe(III)/Fe(II) and the generation of additional •OH through Fenton type processes.

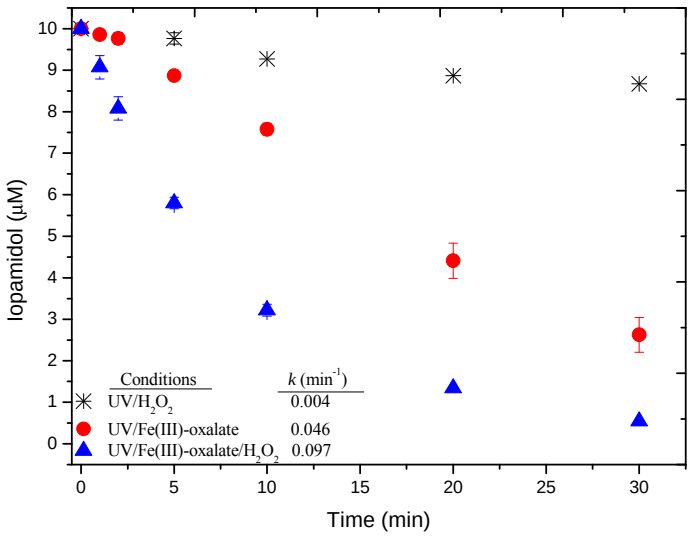

Fig. 3.1. Degradation of iopamidol upon UV (350 nm) treatment in the presence of different chemical additives H_2O_2, Fe(III) and oxalate. ([iopamidol]= 10 μM, [Fe(III)]= 20 μM, [oxalate]= 100 μM and [H_2O_2]= 200 μM at pH 3)

3.4.2 Effect of Fe(III) concentration

The photoactivity of the Fe(III)-oxalate system is influenced by chemical equilibrium and the light adsorption properties of the Fe-oxalate complex. With this in mind the concentration of Fe(III) was varied at constant oxalate and H_2O_2 concentrations **(Fig. 3.2.)** Oxalate concentration was used in excess since a single Fe(III) atom can complex a number of oxalate substrates. The degradation of iopamidol was measured at Fe(III) concentrations of 0, 10, 20 and 50 μM and an oxalate concentration of 100 μM to achieve oxalate: Fe(III) ratios from zero to two. The observed degradation was slowest in the absence of Fe(III) increasing with Fe(III) concentration, consistent with Fenton based

•OH production in the presence of H_2O_2. The rate constants increased from 0.004 to 0.158 min^{-1} with increasing Fe(III) concentration. This result is consistent with previous studies on the degradation of alkylphenol by the Fe(III)-oxalate/sunlight system (Liu et al. 2010). Under the conditions employed 50 µM Fe(III) was the optimal condition among the studied quantities for the remediation of iopamidol. While higher Fe(III) concentrations could result in the formation of more ROS, high concentrations can also lead to competing processes and inhibition.

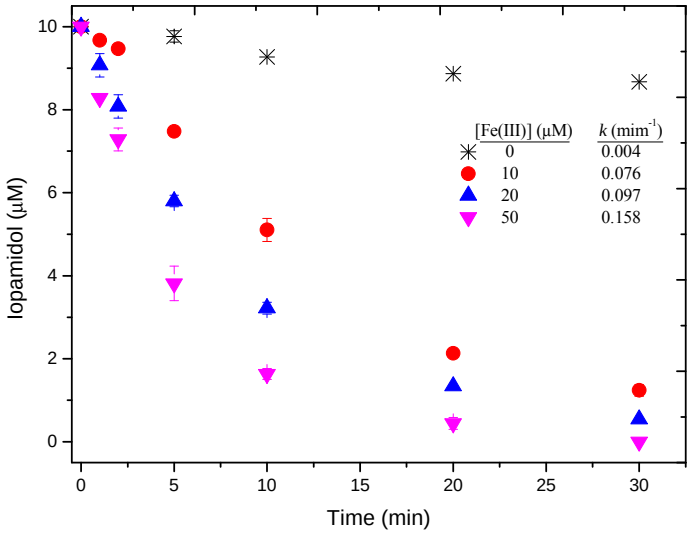

Fig. 3.2. Effect of Fe(III) concentration on the Fe(III)-oxalate/H_2O_2/UV photodegradation of iopamidol. ([iopamidol]= 10 µM, [oxalate]=100 µM and [H_2O_2]= 200 µM at pH 3)

3.4.3 Effect of oxalate concentration

The effect oxalate concentration on the degradation of iopamidol was investigated from 20 to 400 µM at a constant Fe(III) concentration of 20 µM in the presence of H_2O_2 with UV irradiation (350 nm). The degradation of iopamidol at different oxalate concentration is shown in **Fig. 3.3** as a function of UV irradiation time. The influence of

the oxalate had a less pronounced effect on the degradation than varying the Fe(III) concentration. The observed degradations follow pseudo first order kinetics with similar rate constants 0.122 ± 0.025 min^{-1} at oxalate concentrations above 100 µM with a smaller rate constant 0.071 min^{-1} for the lowest oxalate concentration of 20 µM. The most effective degradation was observed at an oxalate concentration of 200 µM under our experimental conditions. Balmer and Sulzberger (Balmer and Sulzberger 1999) reported at oxalate concentrations above 180 µM, the predominant Fe-oxalate complexes are $[Fe(III)(C_2O_4)_2]^-$ and $[Fe(III)(C_2O_4)_3]^{3-}$, which exhibit higher photo-activity than other Fe(III) oxalate complexes, thus leading to faster degradation processes. The slower degradation observed under excess oxalate conditions may be due to the competition for and quenching of the reactive oxygen species.

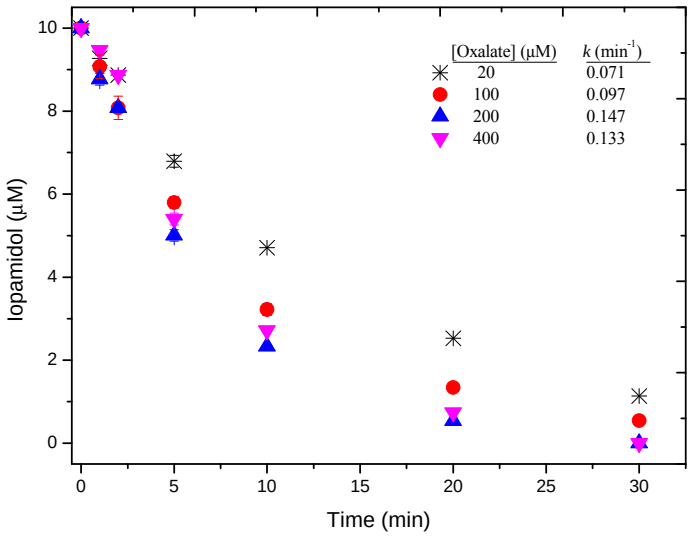

Fig. 3.3. Effect of oxalate concentration on the Fe(III)-oxalate/H_2O_2/UV photodegradation of iopamidol. ([iopamidol]= 10 µM, [Fe(III)]=20 µM and [H_2O_2]= 200 µM at pH 3)

3.4.4 Effect of initial pH values

The solution pH can also have a pronounced effect on the speciation and reactivity of Fe mediated oxidative processes as well as the protonation of organic function groups. Practical water treatments must be applicable over a range of solution pH. The effects of solution pH on the Fe(III)-oxalate/H_2O_2 initiated photodegradation of 10 μM iopamidol were investigated at 20 μM Fe(III), 100 μM oxalate and 200 μM H_2O_2 under UV (350 nm) irradiation. The solubility of these iron complexes drop off significantly under alkaline conditions and thus limit the range of solution pH to acid and neutral conditions. The solution pH was adjusted from 2 to 7 by addition of 0.1 M HNO_3 or 0.1 M NaOH. The degradation of iopamidol as a function of irradiation time at different solution pH is illustrated in **Fig. 3.4**. The observed first-order rate constants are 0.081 min^{-1} for pH 2, 0.097 min^{-1} for pH 3, 0.102 min^{-1} for pH 4, 0.055 min^{-1} for pH 5, 0.002 min^{-1} for pH 6 and 0.001 min^{-1} for pH 7. The observed degradation of iopamidol is strongly dependent on pH in Fe(III)-oxalate/H_2O_2 system. The largest rate constants are observed under strongly acidic conditions with a pronounced decreased in the degradation of 50 % at pH 5, further decreasing to less than 10 % degradation under neutral conditions. The observed pH effect has been attributed to the speciation of the more photoactive Fe(III) complexes $[Fe(III)(C_2O_4)_2]^-$ and $[Fe(III)(C_2O_4)_3]^{3-}$. As the solution pH increases to 5, the complex speciation shifts to the less photoactive species $Fe(III)(C_2O_4)^+$. At higher solution pH, the solubility of Fe(III) and Fe(II) strongly decreased and the main species are Fe(III)-OH and Fe(II)-OH which precipitate and are not appreciatively photoactive. Although $O_2^{-\bullet}$ is predominant relative to $HO_2\bullet$ at solution pH above the pKa (pKa = 4.8) and reduction of Fe(III) to Fe(II) by $O_2^{-\bullet}$ (reactions 1.10

and 1.12) are much faster than those by HO_2• (reactions 1.11 and 1.13), less photoactive Fe(III)/Fe(II) species are available (at pH > 5) for generation of •OH. Our results further demonstrate the photodegradation of iopamidol under Fe(III)-oxalate/H_2O_2/UV treatment is accelerated under acidic conditions.

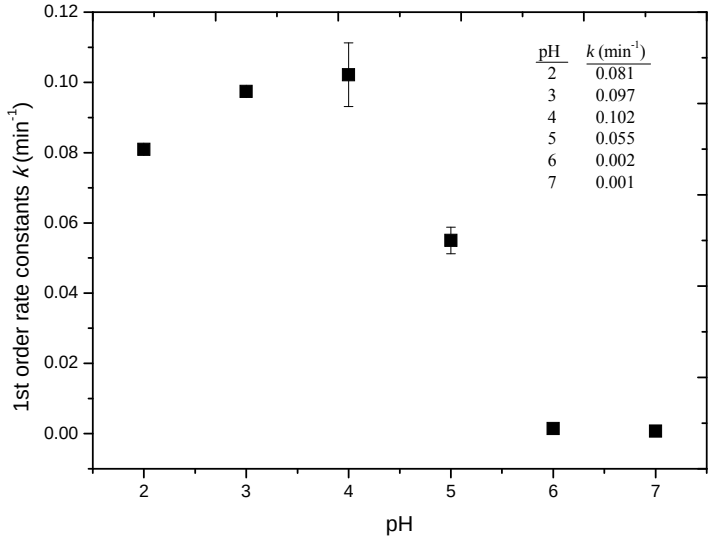

Fig. 3.4. Effect of pH on degradation of iopamidol. ([iopamidol]= 10 μM, [Fe(III)]=20 μM, [oxalate]=100 μM and [H_2O_2]= 200 μM under UV irradiation)

3.4.5 Effect of UV and Visible light irradiation

The Fe(III)-oxalate complex exhibits strong ligand-to-metal charge absorption bands in the UV and visible light regions up to 450 nm (Gulshan et al. 2010). Although UV water treatment processes can be effective, the generation of UV can be costly and solar illumination only contains a small fraction (~5 %) of UV light. The Fe(III)-oxalate/H_2O_2 initiated photodegradations were carried under UV (350 nm) and visible (450 nm) as a function of irradiation time shown in **Fig. 3.5**. The first order rate constants were 0.097 and 0.023 min^{-1}, for UV and visible light treatment, respectively. Although

the degradation was slower under visible light compared with under UV, effective degradation was observed after 30 min of visible light treatment. Visible and UV light sources can effectively initiate Fe(III)-oxalate/H_2O_2 mediated degradation of iopamidol. The combination of both UV and visible portions of the solar spectrum could be a major economical advantage for practical applications of the Fe(III)-oxalate/ H_2O_2 system.

Table 3.1 Pseudo-first-order rate constants under different conditions at pH 3 and UV irradiation

[Fe(III)](μM)	[Oxalate](μM)	[H_2O_2](μM)	k (min^{-1})
0	0	200	0.004
20	100	0	0.046
20	100	200	0.097
0	100	200	0.004
10	100	200	0.076
20	100	200	0.097
50	100	200	0.158
20	20	200	0.071
20	100	200	0.097
20	200	200	0.147
20	400	200	0.133

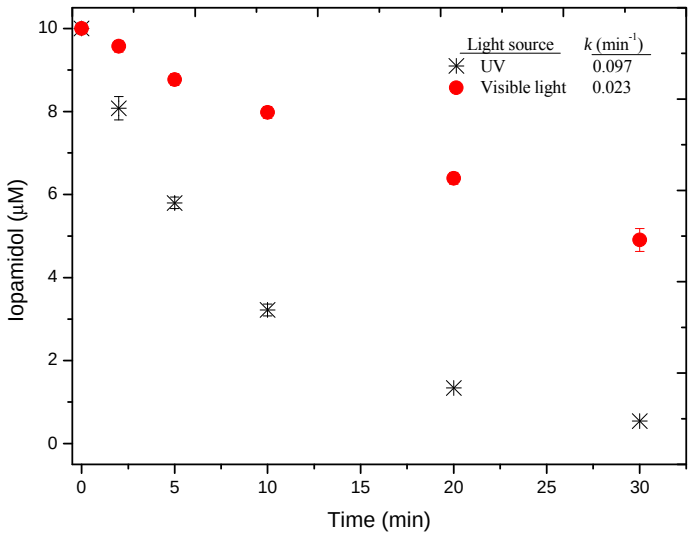

Fig. 3.5. Effects of UV and visible light. ([iopamidol]= 10 μM, [Fe(III)]=20 μM, [oxalate]= 100 μM and [H_2O_2]= 200 μM at pH 3)

3.4.6 Determination of steady state concentration of $[\bullet OH]_{ss}$ and $[O_2^{-\bullet}]_{ss}$ under UV and visible light

The production of •OH during advanced oxidation water treatment is directly correlated to the degradation efficiency. To determine the role of •OH in the photodegradation of iopamidol by Fe(III)-oxalate/H_2O_2/photochemical treatment, the steady-state concentration of •OH, $[\bullet OH]_{ss}$, was measured employing coumarin as a •OH trap. The concentration of the characteristic •OH trap, 7-hydroxycoumarin (7-HOC), was measured using fluorescence (Louit et al. 2005). The fluorescence was converted to concentration employing a calibration curve developed from quantitative concentrations of 7-HOC. The formation rate of •OH is proportional to the formation rate of 7-HOC which can be converted to $[\bullet OH]_{ss}$ by the following equation:

$$\text{Formation rate of } \bullet OH = 0.286 \cdot k_{\text{coumarin} + HO\bullet}\,[\text{coumarin}][HO\bullet] \quad (1)$$

where $k_{\text{coumarin} + HO\bullet} = 6.4 \times 10^9\ M^{-1}\ s^{-1}$ (Singh et al. 2002)

The monitoring of the fluorescence of 7-HOC demonstrates significant production of •OH in the Fe-oxalate/H_2O_2 system under UV and visible irradiation. The production of •OH is ~ four times greater under UV irradiation compared to visible light irradiation, analogous to the observed first order degradation rate constants under UV (0.097 min^{-1}) and visible light irradiation (0.023 min^{-1}). The formation of 7-HOC under UV (350 nm) and visible (450 nm) irradiation was monitored as a function of the irradiation time. Since 6.1 % of •OH can be detected as 7-HOC by using 0.1 mM coumarin (Zhang and Nosaka

2012), the slope of the line in **Fig. 3.6** was divided by 6.1 % to calculate the formation rate of •OH. The rates of formation for •OH under UV (350 nm) and visible light (450 nm) irradiation were 1.19 ± 0.124 and 0.30 ± 0.013 μM/min, respectively under our experimental conditions. The $[•OH]_{ss}$ were 10.88 ± 1.13 $\times 10^{-14}$ M and 2.73 ± 0.12 $\times$ 10^{-14} M under UV (350 nm) and visible light (450 nm) irradiation, respectively. Moreover, $[•OH]_{ss}$ from our experiments is the same order of magnitude as previously reported value 8.33 $\times$ 10^{-14} M using nitrobenzene as a probe under simulated sunlight irradiation (Liu et al. 2010).

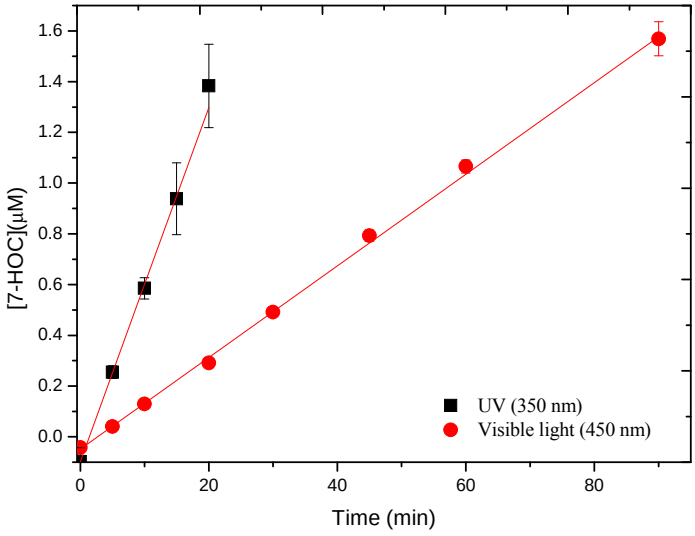

Fig. 3.6. The formation of 7-HOC under UV (350 nm) and visible light (450 nm) irradiation ([coumarin]= 0.1 mM)

Carbon dioxide anion radical is generated during photolysis of the Fe(III)-oxalate complex from the collapse of oxalate anion radical ($C_2O_4^{-\bullet}$) (Zuo and Hoigne 1992). Carbon dioxide anion radical reduces O_2 to $O_2^{-\bullet}$ at a nearly diffusion controlled rate. Superoxide anion radical can also lead to the degradation of the target compound through

direct or indirect chemical reactions. While the generation of $O_2^{-\bullet}$ during photolysis of the Fe(III)-oxalate complex has been reported under simulated solar irradiation (Liu et al. 2010), the quantitative detection of $O_2^{-\bullet}$ has yet to be reported. We monitored the production of $O_2^{-\bullet}$ generated in Fe(III)-oxalate/H_2O_2 system under UV and visible light irradiation using NBT as the probe. The limited solubility of the NBT superoxide anion radical products prohibits their direct detection as a method for determination of the number of superoxide anion radical equivalents. However, the formation rate of $O_2^{-\bullet}$can be assessed based on the degradation rate of NBT as a function of irradiation time by adding *t*-BuOH, as a selective •OH quencher. The observed degradation of NBT in the presence of *t*-BuOH follows pseudo-first-order kinetics. The initial degradation rate was determined from the slope of the reduction in NBT concentration as a function of irradiation time (**Fig. 3.7**) and the concentration of $O_2^{-\bullet}$ estimated using the relationship expressed below:

$$\text{Rate} = k_{\text{NBT} + \text{O2}^{-\bullet}} \cdot [\text{NBT}][\text{O}_2^{-\bullet}] \quad (2)$$

where $k_{\text{NBT} + \text{O2}^{-\bullet}} = 5.88 \times 10^4\ \text{M}^{-1}\text{s}^{-1}$ (Bielski et al. 1980)

Control experiments established minimal or no conversion of NBT is observed under visible light irradiation and direct photolysis may interfere with the ability to detect superoxide anion radical under visible light irradiation. Based on these results and the complications associated with light adsorption and direct photolysis of the probe we are unable to quantify the formation of $O_2^{-\bullet}$ under visible light initiated conditions. Under UV irradiation the initial NBT degradation rate was 0.197 ± 0.017 μM/min. The initial

degradation rate of NBT were used to calculate $[O_2^{-\bullet}]_{ss}$ employing Eq 2, leading to $[O_2^{-\bullet}]_{ss}$ of $5.43 \pm 0.47 \times 10^{-10}$ M under UV irradiation.

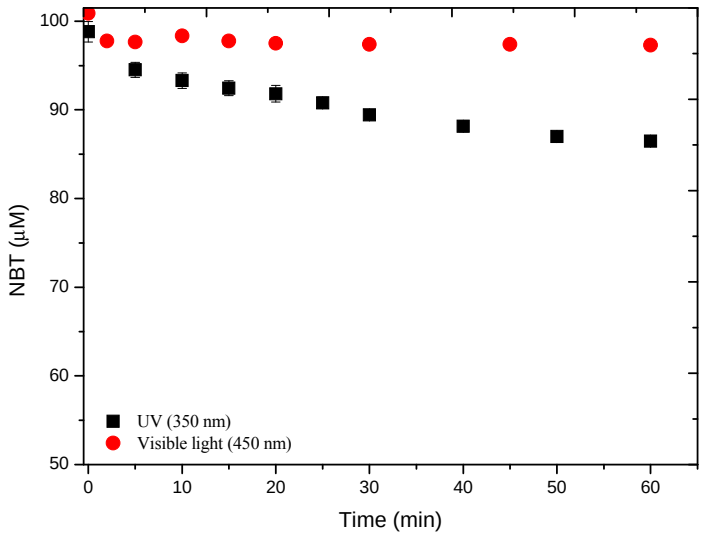

Fig. 3.7. The degradation of NBT under UV (350 nm) and visible light (450 nm) irradiation.

3.4.7 Degradation pathways of iopamidol by oxidation and reduction processes

Product studies were carried out to elucidate the reaction mechanisms in degradation of iopamidol by Fe(III)-oxalate/H_2O_2/UV process. The identification of intermediates was achieved by using positive ESI high resolution LC-MS based on the analysis of extract ion chromatography (EIC) and the corresponding mass spectrum. As demonstrated above •OH plays an important role in the oxidation of iopamidol by Fe(III)-oxalate/H_2O_2/UV process. Based on the MS data and •OH reactivities, degradation pathways were proposed for •OH reactions with iopamidol. In general, •OH reacts with organic compounds via three pathways: electrophilic addition, hydrogen atom abstraction and electron transfer. The hydroxyl radical addition to aromatic rings is generally faster

than H-abstraction and electron transfer, via a resonance-stabilized carbon centered radical. H-abstraction pathways are typically slower and electron transfer is a less common pathway, requiring very electron rich substrates (Buxton et al. 1988).

Hydroxyl radical addition to the aromatic ring *ipso* to an iodine atom is expected to be fast with the subsequent elimination of I• yielding substitution product with observed MW 667, shown in **scheme 3.1**. While two isomers are possible for the substitution product we were unable to distinguish or resolve them. Analogous substitution pathways via •OH addition has also been reported with the treatment of iomeprol by pulse and γ-radiolysis (Jeong et al. 2010) and iopamidol by UV irradiation (Tian et al. 2014). Although H-abstraction pathways are generally slower than •OH addition to aromatic rings or double bonds, there are a number of reactive C_{sp3}-H sites available for H-abstraction in the iopamidol alkyl side chains. The hydrogens alpha to the oxygen atoms (the alcohol functionality) are highly activated towards H-abstraction with the production of stabilized carbon-centered radicals. Such carbon centered radicals can add molecular oxygen and rapidly eliminate hydroperoxyl radical to form ketone a product as represented in the equation below.

$RCH_2OH + HO\bullet \Rightarrow RCH(\bullet)OH + O_2 \Rightarrow RH(OO\bullet)OH \Rightarrow RH(=O) + HO_2\bullet$

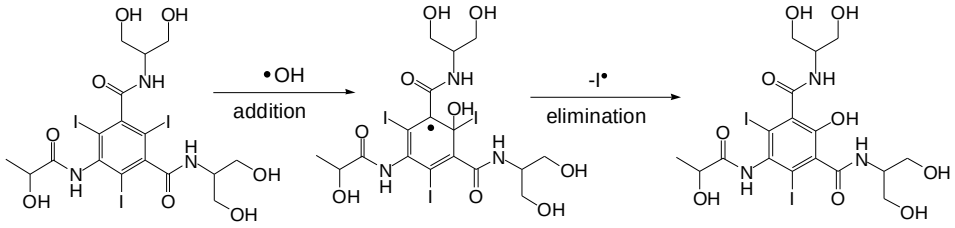

Scheme 3.1. The product with MW of 667 degradation pathways.

The result is the oxidation of an alcohol to the corresponding carbonyl group and MW = 775 as represented in **scheme 3.2**. Analogous oxidation of a second alcohol group yields a product with MW =773 observed in our study. These oxidation pathways are in agreement with the recent study of iopromide transformation in wastewater treatment via H-abstraction and further oxidation of secondary alcohol (Schulz et al. 2008). Two products with MW 741 were also observed in our study. These products correspond to M-36 from iopamidol and are assigned to the loss of two water molecules (dehydration) from side chains (**scheme 3.4**).

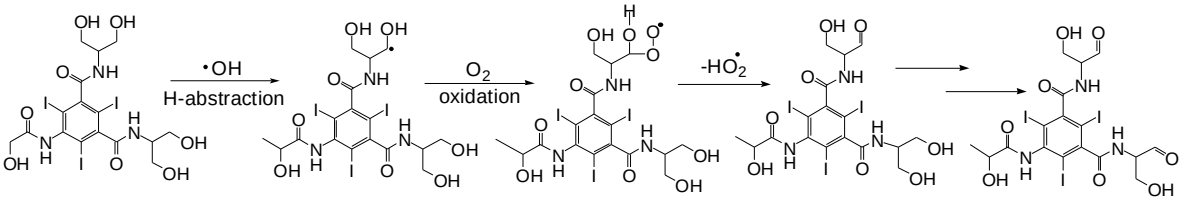

Scheme 3.2. The products with MW of 775 and 773 degradation pathways.

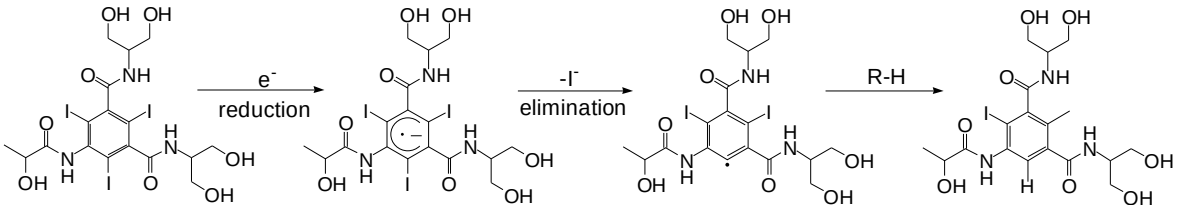

Scheme 3.3. The product with MW of 651 degradation pathways. The same reaction mechanisms for the products with MW of 525 and 399.

The observed degradation pathways of iopamidol by reduction processes appear to be initiated by carbon dioxide anion radical ($CO_2^{-\bullet}$) in the absence of oxygen (purged

with argon). Carbon dioxide anion radical ($CO_2^{-\bullet}$) is a powerful reducing agent and can reduce dissolved oxygen. Reduction of the aromatic ring of iopamidol produces a radical anion. Subsequent loss of I• and H atom via a reductive elimination process yields a by-product with MW of 651 (M-I) (**scheme 3.3**). Sequential reductive elimination yields MW = 525 (M-2I) and MW = 399 (M-3I). The two by-products observed with MW = 651 corresponding to the loss of one I atom are assigned as constitutional isomers represented in **scheme 3.4**. Loss of a second iodine atom leads to two products MW of 525 also assigned to constitutional isomers. The observed product with MW of 399 is attributed to loss of the third and final I atom from iopamidol. Reduction pathways have been reported with the treatment of contrast agent, iomeprol under high energy pulse and γ–radiolysis (Jeong et al. 2010), however such reduction processes had not been previously reported during photochemical treatment of iopamidol.

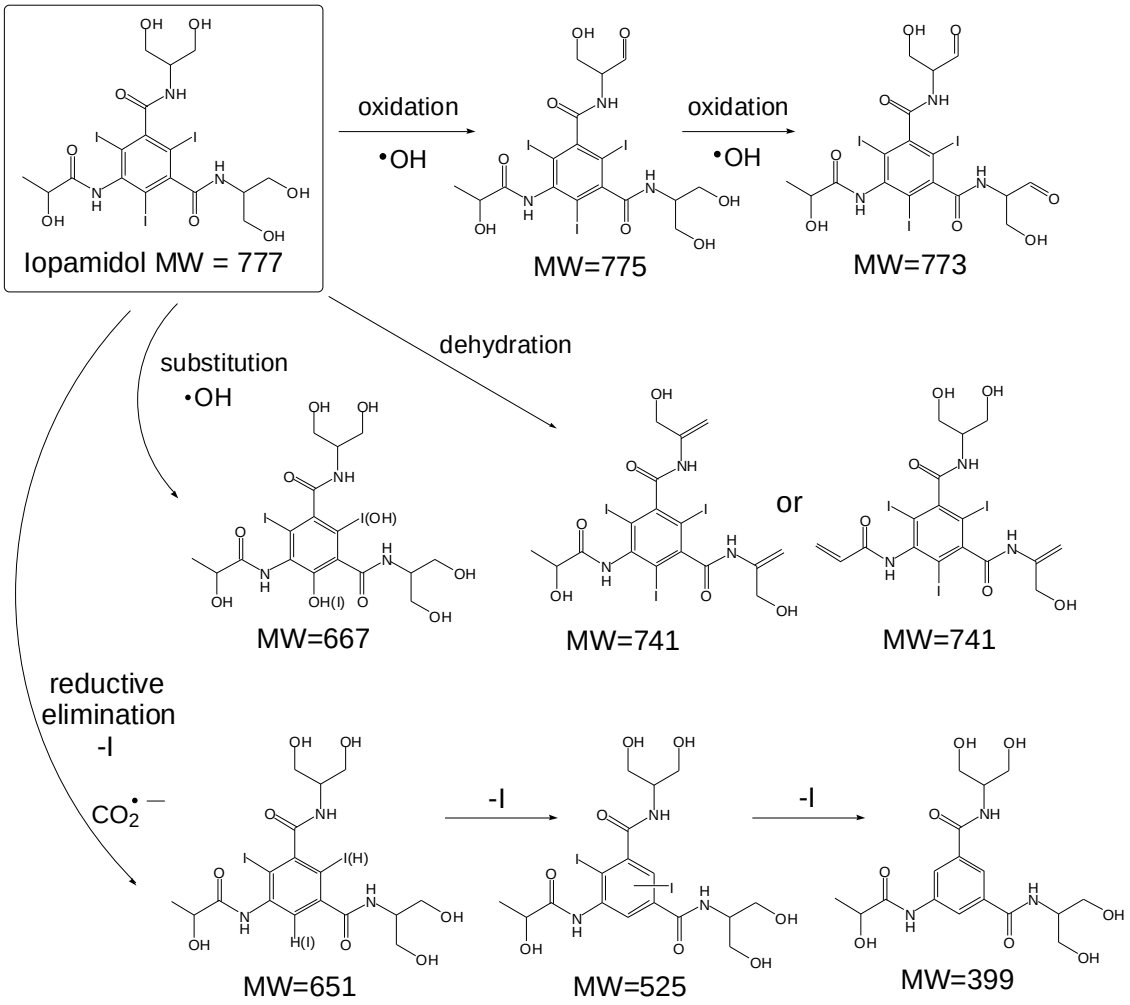

Scheme 3.4. The proposed degradation pathways of iopamidol.

3.5 Conclusions

The ICM model compound, iopamidol is effectively degraded by Fe(III)-oxalate/H_2O_2 photochemical system under UV irradiation and visible light irradiation. The degradation processes follow pseudo-first-order kinetics. Fe(III) concentration was critical and correlates to the formation of photoactive Fe-oxalate complexes and the •OH production during photochemical treatment. The process is most effective under strong acidic pH with the target compound, iopamidol degraded by 95 % within 30 min under

UV irradiation. The formation rates and steady concentrations of •OH and $O_2^{-\bullet}$ were determined under UV (350 nm) and visible light (450 nm) irradiation. The product studies establish oxidative and reductive processes are critical to the observed degradation. The reaction products and reaction pathways were elucidated based on high resolution MS data. The predominant oxidation processes are the oxidation of aromatic ring and side chains by •OH. The reduction processes initiated by the carbon dioxide anion radical ($CO_2^{-\bullet}$) lead to multiple dehalogenations from aromatic ring. The results demonstrate the Fe(III)-oxalate/H_2O_2 photochemical system has promise as an effective method for treatment of ICM contaminated aqueous media.

CHAPTER 4

Radiolysis studies on the degradation of 4-methyl cyclohexane methanol (MCHM) and propylene glycol phenyl ether (PPh) by hydroxyl radical

4.1 Abstract

4-methyl cyclohexane methanol (MCHM) and propylene glycol phenyl ether (PPh) are commonly used as coal processing agents. A large spill of MCHM and PPh into the Elk River near Charleston, West Virginia, led to serious water contamination and concern about the human health consequences and appropriate remediation. We choose to conduct detailed studies on their reactions with hydroxyl radical (•OH), critical to the environmental fate and assessing potential remediation by advanced oxidation processes (AOPs). Time-resolved and steady-state radiolysis methods were employed to conduct detailed kinetic studies and probe the reaction mechanisms of •OH with MCHM and PPh. The bimolecular rate constants using time-resolved competition kinetics with thiocyanate (SCN^-) for reaction of •OH with MCHM and PPh are $5.04 \pm 0.09 \times 10^9$ M^{-1} s^{-1} and $9.15 \pm 0.08 \times 10^9$ M^{-1} s^{-1}, respectively. The formation of the hydroxycyclohexadienyl radical resulting from •OH addition to the aromatic ring in PPh was measured using transient absorption spectroscopy (250 ~ 380 nm) with a maximum absorption at 330 nm. The rate constant for the specific addition of •OH to the aromatic ring in PPh is $8.98 \pm 0.26 \times 10^9$ M^{-1} s^{-1}, indicating •OH reacts primarily by addition to the aromatic ring. Detailed product studies using SPME-GC/MS for MCHM suggest •OH mediated oxidation of MCHM primarily involves H-abstraction followed by radical oxidation pathways. LC-QTOF/MS analysis of •OH reactions with PPh indicate •OH attack to *ortho* and *para* positions of the benzene ring are the predominant reaction pathways. The fundamental kinetic parameters and detailed product studies using pulse and gamma radiolysis provide fundamental mechanistic understanding of •OH initiated reactions, essential to assessing the

remediation of these problematic pollutants in drinking water by AOP and anticipating the biological and environmental fate of MCHM and PPh.

4.2. Introduction

An estimated 10,000 gallons of crude 4-methyl cyclohexane methanol (MCHM) leaked into the Elk River near Charleston, West Virginia contaminating the local drinking water and threatening the human health of 300,000 residents (Tullo et al. 2014). Nearly 1,400 residents in nine counties experienced nausea, rashes, mild burns, and/or stomach disorders after contamination of their water supply. The leaking tank contained 88.5 % MCHM, 7.3 % proprietary mixture of propylene glycol phenyl ether (PPh) and dipropylene glycol phenyl ether (DiPPh), and 4.2 % water by weight (Tullo et al. 2014).

MCHM and PPh are chemical foaming agents used to wash coal and remove impurities that contribute to pollution during combustion. The process using chemicals to wash coal is known as “froth flotation”, which involves the purification of residual coal materials formed during coal processing. MCHM and PPh are used to reduce the surface tension of water in order to stabilize and moderate the size of the air bubbles, then further assist “froth flotation” process (Tullo et al. 2014).

Concentrations of MCHM between 1.04 ~ 3.35 ppm were reported at the West Virginia American Water intake on the Elk River and 1.02 ~ 1.56 ppm in the treated drinking water following the spill (Tullo et al. 2014).The Center for Disease Control & Prevention (CDC) set a screening level of 1 ppm for MCHM (2014a) and 1.2 ppm for PPh in drinking water (2014b). The 28-day study of oral toxicity of pure MCHM indicates 400 mg/kg/day dose were associated with erythropietic, liver and kidney problems (1/20/2014). MCHM has been studied as a dermal irritant resulting in focal

necrosis and eschar at the application sites (Bernard 1998). The regulatory standards of the Occupational Safety and Health Administration consider MCHM as “hazardous” (Jr. Januray 10, 2014). Mammalian studies identified MCHM as a skin and eye irritant (Bernard 1997). A recent study has demonstrated PPh is absorbed by rats, metabolized and excreted via urine and faeces rapidly after oral exposure (Saghir et al. 2003). PPh exhibits low oral and inhalation toxicities with oral LD_{50} in male and female Fischer 344 rats of 2,830 and 3730 mg/kg, respectively (Saghir et al. 2003). PPh is also an eye irritant in rabbits (2004).

Given the reports of negative health consequences and the absence of detailed toxicological studies on the impact of MCHM and PPh on human health, water works were closed and alternative water sources required for 300,000 people in Charleston, West Virginia. Little information on MCHM and PPh has been reported, and effective and efficient removals from contaminated water are unexplored. Among limited reports, West Virginia American Water’s engineers used carbon filtration in an attempt to purify to the contaminated water before distribution (Howard January 10, 2014). However, because of the large volume of contaminated water, carbon filtration was not practical or viable. A biodegradability study demonstrated that crude MCHM was not “readily biodegradable” using microorganisms extracted from wastewater treatment sludge (Beglinger 1997). Although PPh is considered biodegradable more than 60 % degradation after 28 days incubation under aerobic conditions (2004). Biodegradation for treatment of MCHM and PPh is time-consuming and not efficient, thus limiting its application for water purification.

Advanced oxidation processes (AOPs) are effective for the treatment of water contaminated with a wide variety of pollutants (Cooper et al. 1998, Zhao et al. 2014a, Zhao et al. 2014b). AOPs generally employ the formation of hydroxyl radical (•OH) as the primary oxidant. Hydroxyl radical is a very powerful oxidant and can react rapidly with nearly all organic compounds due to its strong oxidation potential (+2.80V). A fundamental kinetic and mechanistic understanding of the reactions for •OH with MCHM and PPh are critical to assessing the potential application of AOP for their remediation. Determination of the bimolecular rate constants for •OH with MCHM and PPh, and the corresponding degradation pathways are critical to effectively assess the application of AOPs on water purification. To our best knowledge, this is the first detailed studies of •OH mediated oxidation of MCHM and PPh. We herein report the kinetic studies focusing on the determination of bimolecular rate constants for •OH with MCHM and PPh using transient absorbance spectroscopy (TAS) and competition methods. at different treatment doses. Detailed product studies were accomplished employing steady-state γ-radiolysis and liquid chromatography coupled to Q-TOF/MS for PPh and solid phase microextraction (SPME) gas chromatography/MS for MCHM to identify the intermediates and determine the degradation pathways.

4.3 Materials and methods

4.3.1 Materials

PPh was purchased from Sigma Aldrich. A mixture of *trans* and *cis* isomeric MCHM were obtained from TCI America. HPLC grade acetonitrile and potassium thiocyanate were purchased from Fisher Scientific. All reagents were used as received.

All aqueous solutions were prepared with Millipore filtered water and volumetric lab equipment.

4.3.2 Pulse radiolysis and γ-radiolysis

Electron pulse radiolysis experiments were conducted at the US Department of Energy, Notre Dame Radiation Laboratory using the 8-MeV Titan Beta model TBS-8/16-1S linear accelerator. Detailed irradiation and transient absorption detection system has been described previously (Song et al. 2009b). Dosimetry was performed using N_2O-saturated of 10 mM potassium thiocyanate (KSCN) solution at wavelength of 472 nm. All experimental data were obtained by averaging 8-12 replicate pulses using continuous flow mode instrument.

The radiolysis of water is described in Eq. 4.1.

$$H_2O \text{ /\/\/\} \rightarrow e_{aq}^- (0.27) + \cdot H (0.06) + \cdot OH (0.28) + H_2 (0.05) + H_2O_2 (0.07) + H_3O^+ (0.27) \quad (4.1)$$

(where the numbers in brackets are the radiation chemical yields of these species (G-values) per 100 eV absorbed energy).

In addition to ·OH, hydrated electron (e_{aq}^-) and hydrogen atom (·H) are also generated with relatively high yields. To study the reactions with ·OH, the solutions are saturated with nitrous oxide (N_2O), which quantitatively converts hydrated electron (e_{aq}^-) and hydrogen atom (·H) to ·OH (Eq. 4.2 and 4.3) (Buxton et al. 1988).

$$e_{aq}^- + N_2O + H_2O \rightarrow N_2 + {}^-OH + \cdot OH \qquad k_1 = 9.1\times 10^9\ M^{-1}s^{-1} \qquad (4.2)$$

$$\cdot H + N_2O \rightarrow \cdot OH + N_2 \qquad k_3 = 2.1\times 10^6\ M^{-1}s^{-1} \qquad (4.3)$$

A Shepherd 109-86 Cobalt-60 (^{60}Co) γ source was employed for steady-state γ-radiolysis experiments with a dose rate of 0.0325 kGy/min, as measured by Fricke dosimetry. All the aqueous solutions were presaturated with N_2O before γ-irradiation.

4.3.3 LC/MS analysis of PPh and its products

The analysis of PPh and the degradation products were carried out using a Bruker micro high resolution accurate-mass quadrupole time-of-flight (Q-TOF) ultra-high pressure liquid chromatography/mass spectrometer (UPLC-QTOF/MS). The samples were separated on a Waters XBrigde plus C-18 (3.0 × 50 mm, 5-Micron). The mobile phase consisted of A: H_2O and B: CH_3CN, with a gradient elution of 5 % B for 1 min, followed by a linear increase to 100 % B in 10 min, holding 100 % B for 5 min and back to 5 % B in 3 min. The flow rate was 0.4 ml/min and injection volume was 20 µl. The mass spectra (m/z 100-1000) were obtained in positive ion mode with electrospray ionization technology (ESI).

4.3.4 SPME GC/MS analysis of MCHM and its products

Thermo scientific ISQ gas chromatography/mass spectrometer (GC/MS) was used for analysis of MCHM and the degradation products. The autosampler fitted with a solid phase microextraction (SPME) sampling system (Supelco, Bellefonte, PA) was used to extract and inject all the samples. The SPME system consisted of a SPME fiber holder and a stableflex fiber with the coating materials of 24 Ga 50/30 µm divinylbenzene/carboxen/polydimethylsiloxane (DVB/CAR/PDMS). A waters column was used for separation with a helium carrier gas at flow rate of 1 mL/min. The column temperature was programmed at 35º C for 5 min, followed by a linear increase to 300º C

at 8º C/min, holding at 300º C for 3 min. The mass spectra (m/z 10-500) were obtained with electron impact ionization technology (EI).

4.4 Results and discussion

4.4.1 Kinetic studies of PPh with hydroxyl radical

Hydroxyl radical is selectively generated by pulse radiation of a N_2O saturated aqueous solution, immediately following the pulse transient absorption spectra (TAS) is used to monitor the formation of transients. The intermediate resulting from the reaction of PPh with •OH generated by pulse radiolysis was monitored by TAS in the range of 250 ~ 380 nm shown in **Fig. 4.1**. The observed transient absorption in the 300 ~ 350 nm range is characteristic of the hydroxycyclohexadienyl radical formed by •OH addition to the aromatic ring (Song et al. 2009a). Measurement of the bimolecular rate constant for addition of •OH to PPh can be obtained by monitoring the growth kinetics of a characteristic absorption at 330 nm (PPh hydroxycyclohexadienyl species) as a function of PPh concentration (**Fig. 4.2a**). The •OH concentrtaion remains constant while PPh concentration was varied from 42 ~ 200 μM. The bimolecular rate constant for the addition of •OH to the aromatic ring in PPh was determined by fitting exponential curves to the pseudo-first-order growth kinetics and plotting these values as a function of PPh concentration to give the linear plot shown in **Fig. 4.2b**. The slope of this line yields a bimolecular rate constant of $8.98 \pm 0.26 \times 10^9$ M^{-1} s^{-1} for the specific addition of •OH to the aromatic ring in PPh.

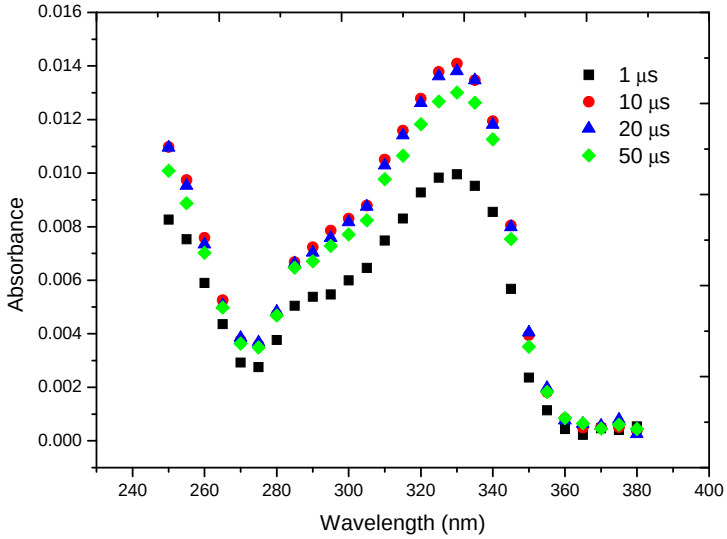

Fig. 4.1. Time-resolved transient absorption spectra obtained from the reaction of hydroxyl radical and PPh.

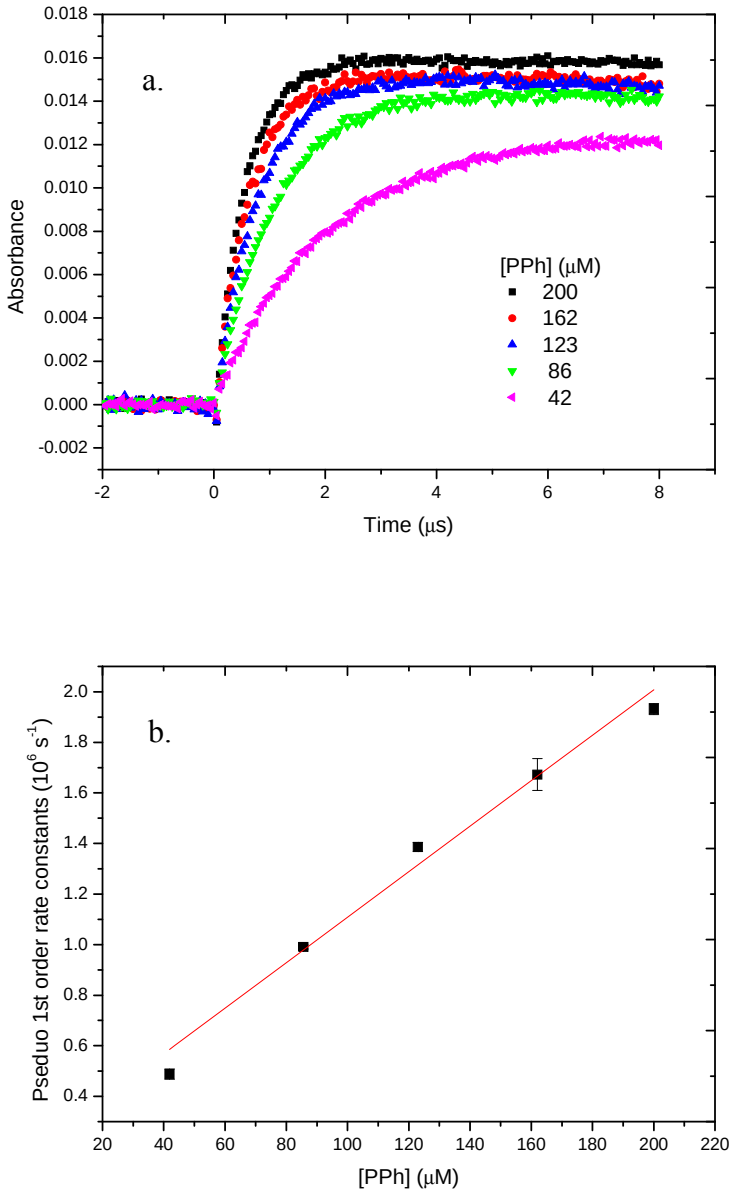

Fig. 4.2. Transient absorption kinetics for determination of bimolecular rate constant for PPh and •OH. **a**. Growth kinetics of the transient absorption at 330 nm in the pulse radiolysis solution of 200, 162, 123, 86 and 42 μM PPh. **b**. Bimolecular rate constant determined for the reaction of hydroxyl radical and PPh at 330 nm. The slope from the line represents the specific rate constant of $8.98 \pm 0.26 \times 10^9$ M^{-1} s^{-1}.

The result from direct monitoring of transient absorption spectra at 330 nm only represents the reaction pathways for •OH addition to the aromatic ring. Other possible

reaction sites specifically hydrogen abstraction of aliphatic hydrogens from the side chain in PPh can also lead to the degradation of PPh. A number of these six aliphatic reaction sites are activated by an adjacent oxygen atom. While H-abstraction pathways are well established, the resulting stabilized carbon-centered radical products absorb at short wavelengths, below the range of our detection system. With this in mind the competition kinetics were used to determine the overall bimolecular rate constant for the reaction of PPh with •OH. The competition kinetic experiments were carried out using SCN^- as the competitor and monitoring the product $(SCN)_2^{-\bullet}$ of SCN^- and hydroxyl radical at 470 nm. Eq. (4.4) and (4.5) are the reactions of SCN^- with PPh and with hydroxyl radical, respectively.

$$\bullet OH + PPh \xrightarrow{k_1} \text{Products} \tag{4.4}$$

$$\bullet OH + 2SCN^- \xrightarrow{k_2} OH^- + (SCN)_2^{\bullet-} \tag{4.5}$$

This competition can be described by the following equation (4.6):

$$\frac{[(SCN)_2^{\bullet-}]_0}{[(SCN)_2^{\bullet-}]} = 1 + \frac{k_1[PPh]}{k_2[SCN^-]} \tag{4.6}$$

Where $[(SCN)_2^{-\bullet}]_0$ is initial amount of $(SCN)_2^{-\bullet}$ without PPh in the solution, $[(SCN)_2^{-\bullet}]$ is the corresponding amount of this transient in the presence of PPh (0 ~ 198 μM). $[(SCN)_2^{-\bullet}]_0/[(SCN)_2^{-\bullet}]$ is determined from A_0/A_{SCN^-} shown in **Fig. 4.3** (directly proportional to A_0/A_{SCN^-}). A plot of $[(SCN)_2^{-\bullet}]_0/[(SCN)_2^{-\bullet}]$ as a function of concentration ratio [PPh]/[SCN^-] yields a straight line with the slope of k_1/k_2 and "y" intercept of 1. The rate constant for the reaction of SCN^- with •OH is well established: $k_2 = 1.1 \times 10^{10}$ M^{-1} s^{-1}, the overall bimolecular rate constant for PPh and •OH can be calculated (Buxton et al. 1988). The absorbance of $(SCN)_2^{-\bullet}$ at 472 nm decreases with the increasing of PPh

concentration shown in **Fig. 4.3 insert**. The overall bimolecular rate constant for PPh and •OH calculated from the slope of straight line in **Fig. 4.3** is $9.15 \pm 0.08 \times 10^9$ M^{-1} s^{-1}. Comparison of the overall bimolecular rate constants of PPh with ·OH and the specific rate constants for addition to aromatic ring suggests ~ 94 % of ·OH initiated reactions occur at the aromatic ring in PPh; thus H-abstractions account for 5 ~ 10 % of overall ·OH initiated reactions pathways. There are six aliphatic H atoms and one OH in the side chain of PPh available for H-abstraction. The H atom in hydroxyl group (-OH) is generally much less reactive than aliphatic H atoms (sp^3-H) due to the stronger O-H bond compared to C-H bond. The three primary H atoms (1º) in the methyl group have reduced reactivity compared to secondary (2º) and tertiary (3º) aliphatic H atoms. The two equivalent 2º hydrogens in PPh will have enhanced the reactivity from the adjacent oxygen atom. The single tertiary hydrogen (3º) also influenced by the presence of adjacent oxygen atom is considered the most reactive among the aliphatic hydrogens. The different electronic effects and statistically factors will determine the partitioning of these competing reaction pathways. Rate constants for ·OH addition to aromatic ring and H-abstraction are generally on the order of 10^9-10^{10} and 10^8 M^{-1} s^{-1}, respectively. H-abstraction is generally slower by 1 or 2 orders of magnitude than ·OH addition, consistent with our observation that the addition of •OH to the aromatic ring in PPh is the predominant reaction pathway.

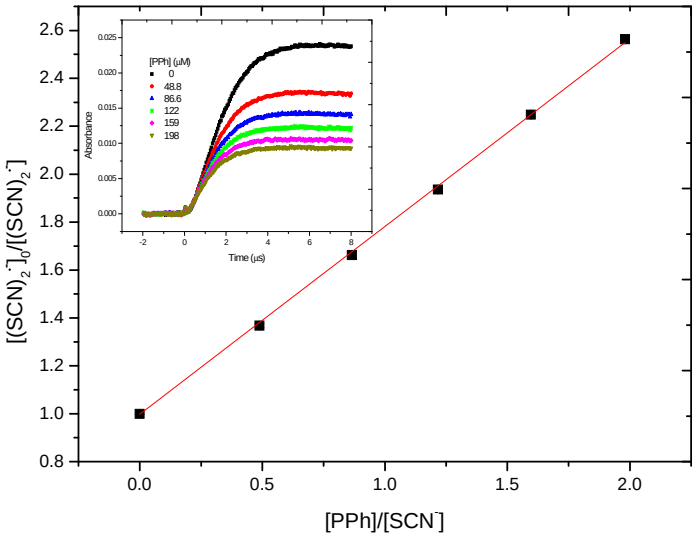

Fig. 4.3. Thiocyanate competition kinetics for determination of overall bimolecular rate constant for PPh and •OH. The straight line gives the slope of 0.7903 ± 0.0075, corresponding the overall bimolecular rate constant of $9.15 \pm 0.08 \times 10^9$ M^{-1} s^{-1}.(Insert graph: kinetics of $(SCN)_2^{-\bullet}$ formation at 472 nm with 100 μM SCN^- changing the PPh concentration with 0 μM, 48.8 μM, 86.6 μM, 122 μM, 159 μM and 198 μM.)

4.4.2 Kinetic studies of MCHM with hydroxyl radical

MCHM does not possess double bonds or π systems for •OH addition. The reaction pathways for •OH with MCHM will involve H-abstraction with the formation of a localized carbon centered radicals. Direct measurement of the rate constant for H-abstraction is not feasible because localized carbon centered radicals do not absorb wavelength within the range of our detection system. With this in mind, SCN^- competition kinetics were employed for determination of the overall bimolecular rate constant for •OH and MCHM. The competition kinetics was obtained by monitoring a characteristic absorption of $(SCN)_2^{-\bullet}$ at 470 nm as described earlier. A decrease in the absorbance of $(SCN)_2^{-\bullet}$ at 472 nm is observed with increasing MCHM added in the

solution shown in **Fig. 4.4 insert**. The slope of the straight line in **Fig. 4.4** yields the corresponding overall bimolecular rate constant for MCHM and •OH of $5.04 \pm 0.09 \times 10^9$ M^{-1} s^{-1}. While H-abstraction accounts for the major reaction pathways of •OH reaction with MCHM, several reaction sites are possible and their anticipated relative reactivities are discussed. The H atom in hydroxyl group (-OH) typically is the least reactivity due to the stronger O-H bond compared to C-H bond. The relative reactivities of hydrogens decrease in the order of 3º > 2º > 1º in Csp^3-H positions. Two 2º H atoms in CH_2-OH have enhanced reactivity due to the adjacent electron-donating oxygen atom. Therefore, 3º H atoms and 2º CH_2-OH are expected to be the most reactive sites for H-abstraction based on the electronic factors.

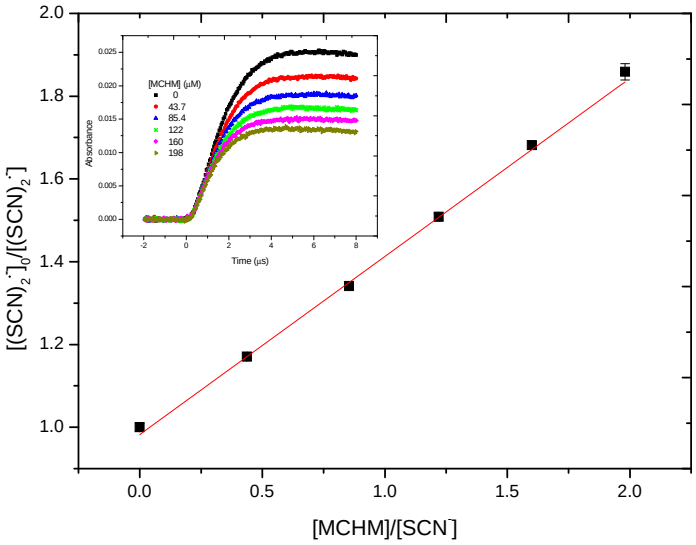

Fig. 4.4. Thiocyanate competition kinetics for determination of overall bimolecular rate constant for MCHM and •OH. The straight line gives the slope of 0.4353 ± 0.0079, corresponding the overall bimolecular rate constant of $5.04 \pm 0.09 \times 10^9$ M^{-1} s^{-1}. (Insert graph: Kinetics of $(SCN)_2^{-\bullet}$ formation at 472 nm with 100 µM SCN^- changing the MCHM concentration with 0 µM, 43.7 µM, 85.4 µM, 122 µM, 160 µM and 198 µM.)

4.4.3 Degradation Pathway for hydroxyl radical mediated oxidation of PPh and MCHM

In addition to the kinetic studies for •OH with PPh and MCHM, product studies were carried out to elucidate the reaction mechanisms in degradation of PPh and MCHM by hydroxyl radical. The experiments of product studies were conducted using ^{60}Co steady-state radiolysis under N_2O saturated condition with initial concentration of 100 μM for PPh and MCHM. The identification of PPh degradation intermediates was achieved by using positive ESI high resolution LC-MS based on the analysis of total ion chromatography (TIC) and the corresponding mass spectrum. The identification of MCHM degradation intermediates was obtained using solid phase microextraction (SPME)-GC/MS. Hydroxyl radical typically reacts with organic compounds via three pathways: electrophilic addition, hydrogen atom abstraction and electron transfer. The hydroxyl radical addition to aromatic rings is generally faster than H-abstraction and electron transfer, via a resonance-stabilized carbon centered radical. H-abstraction pathways are typically slower and electron transfer is a less common pathway, requiring very electron rich substrates (Buxton et al. 1988).

4.4.3.1 PPh degradation pathway

As discussed in the kinetic studies, the electron rich 2º Hs have the enhanced the reactivity from the adjacent oxygen atom and are readily abstracted by ·OH to form stabilized carbon-centered radical. Hydroxyl radical can attack such stabilized carbon-centered radical to yield product with MW 168, and then further oxidation by ·OH leads to the keto product with MW of 166. We observed the product with MW of 166 as a minor product, which is consistent with our proposed reaction pathway.

Kinetic studies indicate the majority of ·OH-mediated oxidation occurs at the aromatic ring of PPh by ·OH electrophilic addition. Two products with MW of 190 (M+ Na^+) were observed, corresponding to the addition of 16 mass units to PPh (M+ Na^+). Hydroxyl radical is an electrophile and thus addition to an aromatic ring can be directed by the electronic influence of the substituent. In the case of PPh the substituent is an alkyl group and electron donating which enhances the electron density and reactivity for addition of electrophilic ·OH at the *ortho* and *para* positions relative to the *meta* position. Following this logic we propose the two products with MW 190 are the *ortho* and *para* products. Oxidation of ROH to the corresponding carbonyl ketone product (MW=166) was observed in our studies, which can form the steric hindrance with the ortho position, leading to less ·OH attack to the *ortho* position. According to **Fig. 4.5**, the amount of product (MW= 190) at RT 4.9 min was much higher than the product (MW= 191) at RT 3.8 min. Therefore, we propose the higher amount product is hydroxyl *para* product and the lower amount of product is the hydroxyl *ortho* product.

We also observe the product with MW 94, possibly from the hydrolysis of ketone product (MW=166) or results from ·OH addition to ipso position. Similar ·OH addition to *ipso* position has been reported for the degradation of nonylphenol by involving *ipso*-hydroxylation at the first step and proceeding via *ipso* substitution (Kolvenbach et al. 2007). We spiked phenol (MW=94) in the treated sample and the RT for phenol and product with MW 94 are the same (RT=4.2 min), which is consistent with our proposed product (**Scheme 4.1**). A recent study has also been reported that PPh was predominantly metabolized to phenol (~ 60 % administrated dose) in rats, which agrees with our determination of phenol as one of the oxidation products (Saghir et al. 2003). The

reaction profile as a function of γ-radiation dose is shown in **Fig. 4.6**. All these three products reach the maximum levels at approximately 0.3 kGy.

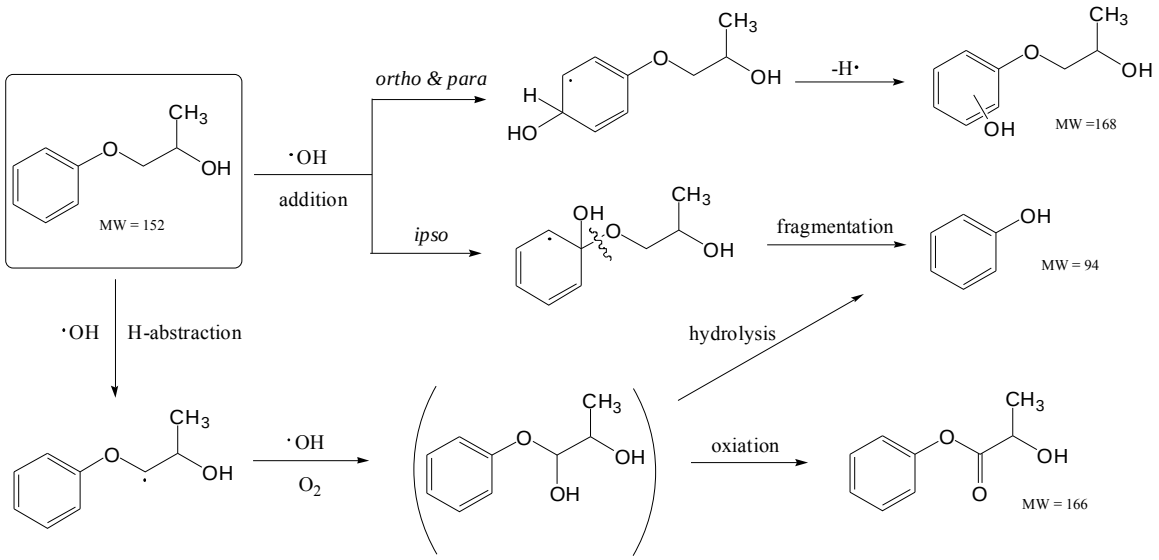

Scheme 4.1. The proposed reaction pathways for ·OH with PPh.

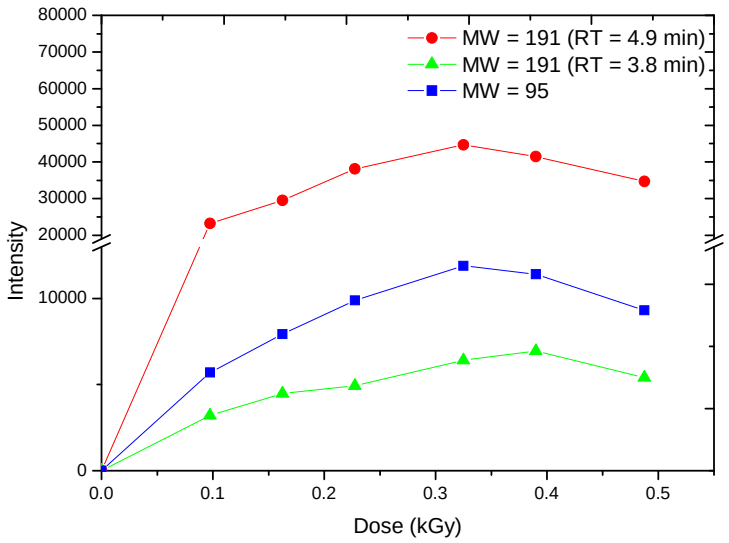

Fig. 4.5. The reaction profile of PPh degradation products as a function of radiation under N_2O saturated conditions.

4.4.3.2 MCHM degradation pathways

Hydroxyl radical mediated oxidation of MCHM involves H-abstraction (**Scheme 4.2**). Hydrogen atoms attached to CH_2-OH are highly reactive towards abstraction due to its adjacent hydroxyl group. As a result, H-abstraction at C1 leads to the generation of stabilized carbon-centered radical. Such stabilized carbon-centered radicals can add a molecular oxygen and subsequently eliminate a hydroperoxyl radical to yield the corresponding aldehyde products with MW 126 (RT = 11.88 min)(P1). Elimination of -CHO and addition of a molecular oxygen to C2 result in the formation of peroxyl radical intermediate, which can collapse to keto product with MW 112 (P2) or yield a double bond product (MW = 96) (P3) in the ring by elimination of a hydroperoxyl radical (Cooper et al. 2009).

Tertiary H atoms at C2 and C5 are also expected to be readily abstracted, yielding the stabilized carbon-centered radicals. Addition of molecular oxygen to these stabilized carbon-centered radicals and subsequent elimination of hydroperoxyl radicals can form double bond products with the same MW 126. Similar formation of double bond in the ring by elimination of a hydroperoxyl radical has been reported for gas-phase oxidation of cyclohexane (Buda et al. 2006). We assign the retention times for C2-C3 (P4) and C4-C5 (P5) double bond products are 14.06 min and 14.43 min, respectively, based on the analysis of NIST GC database. Further oxidation of double bond products results in the formation of corresponding aldehyde products with MW 124. The short chain carboxylic acids, including acetate, formate and oxalate are produced by multiple steps oxidation of intermediates. Such short chain carboxylic acids were detected using ion chromatography and also quantified to obtain the maximum formed concentration of 129 ppb for formate,

854 ppb for oxalate and < LOD for acetate ([MCHM]$_0$ = 200 μM). The reaction profile of MCHM degradation products as a function of γ-radiation dose is shown in **Fig. 4.6**.

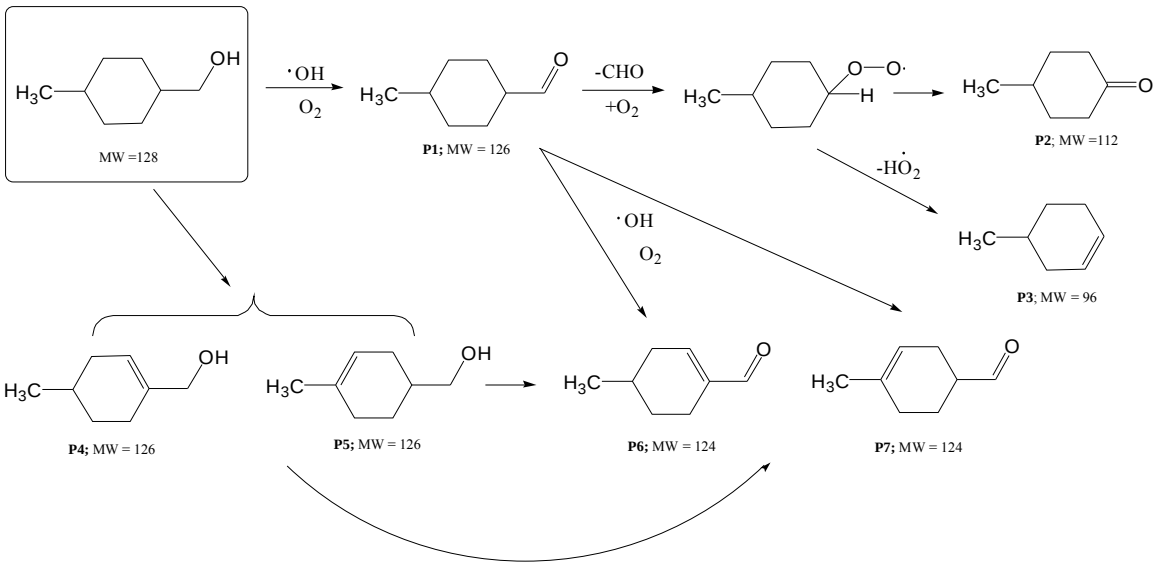

Scheme 4.2. The proposed reaction pathways for ·OH with MCHM.

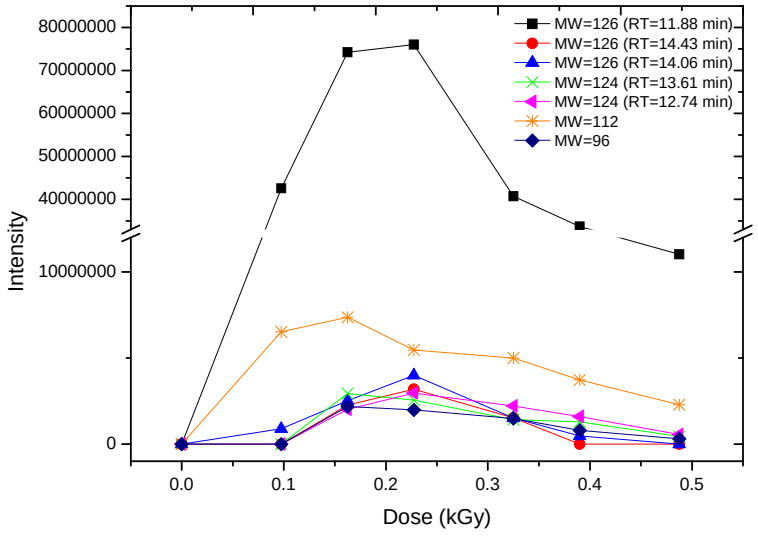

Fig. 4.6. The reaction profile of MCHM degradation products as a function of radiation under N_2O saturated conditions.

4.5 Conclusions

The bimolecular rate constants of ·OH with MCHM and PPh were evaluated as $5.04 \pm 0.09 \times 10^9$ M^{-1} s^{-1} and $9.15 \pm 0.08 \times 10^9$ M^{-1} s^{-1}, respectively, by pulse radiolysis. Detailed product studies were determined to elucidate ·OH mediated oxidation reaction pathways by gamma radiolysis. The results demonstrate that •OH addition to ortho and *para* positions in PPh are the predominant reaction pathways; H-abstraction are primary reaction mechanisms for ·OH mediated oxidation of MCHM. Our results indicate hydroxyl radical based advanced oxidation processes (AOPs) can effectively destroy pollutants from drinking water and radiolysis technique is an attractive remediation strategy for the application of oxidative water treatments.

CHPATER 5

Ferrate (VI) mediated degradation and detoxification of the potent cyanotoxin, cylindrospermopsin

5.1 Abstract

Cylindrospermopsin (CYN), a potent cyanotoxin mainly produced by *cylindrospermopsis raciborskii*, regularly exists in drinking water sources and poses a serious risk to humans and the environment. Ferrate (VI) mediated degradation kinetics of CYN and the model compound 6-hydroxymethyl uracil (6-HOMU) are reported as a function of solution pH. Fe(VI) oxidation of CYN followed second-order kinetics with the bimolecular rate constant decreasing from 38.8 ± 0.07 $M^{-1}s^{-1}$ at pH 7 to 5.0 ± 0.1 $M^{-1}s^{-1}$ at pH 9.5. Detailed product studies using liquid chromatography coupled to Q-TOF/MS indicated Fe(VI) mediated reactions primarily occur via oxidation of the uracil ring in CYN. Electrophilic attack at the unsaturated double bond C5-C6 in the uracil ring leads to the oxidation cleavage with the formation of corresponding carbonyl product with *m/z* 448. Subsequent amide hydrolysis of the ring opened product yields a new product with *m/z* 350. Sequential loss carbonyl groups yields products with *m/z* 320, 292 and 290. Hydrolysis of the amide functional groups in the uracil ring in CYN is assigned to a product with *m/z* 375. ELISA results demonstrate Fe(VI) treatment of CYN leads to detoxification and the oxidation products did not exhibit significant biological activity. Our results provide a better understanding of the fundamental kinetic parameters and the reaction pathways of CYN oxidation by Fe(VI), which are critical to evaluate the Fe(VI) treatment technology for the remediation of CYN and uracil based problematic cyanotoxins in drinking water.

5.2 Introduction

The significant increase in the occurrences of cyanobacterial blooms (harmful algae blooms HABs) in industrial and potable water is an emerging environmental issue.

Seventy percent of HABs can produce potent toxins, which pose a tremendous risk to humans and the environment (de la Cruz et al. 2013, Liu et al. 2015). Cyanobacteria can produce a range of cyanotoxins, one of the most problematic cyanotoxins in drinking water is cylindrospermopsin (CYN), an alkaloid hepatotoxin with uracil ring, tricyclic guanidine and sulfate group (**Fig. 5.1**). CYN has been showed to be genotoxic (Humpage et al. 2005) and carcinogenic (Falconer and Humpage 2001) and is reported to cause the damage of main target organs, including the liver, kidney, thymus, lungs and adrenal glands (Harada et al. 1994).The toxic activity of CYN partly results from the uracil moiety which inhibits protein translation or it bands to DNA to cause strand breakage (Banker et al. 2001). Human positioning incident by CYN was first discovered on Palm Island, Australia in 1979, which led to hepatoenteritis in 138 children and 10 adults (Griffiths and Saker 2003, Zhao et al. 2014b).The presence of CYN has been primarily limited to warm regions, recent reports confirm the occurrences of CYN extend to more temperate regions in Europe, such as Italy, Germany and France (de la Cruz et al. 2013).

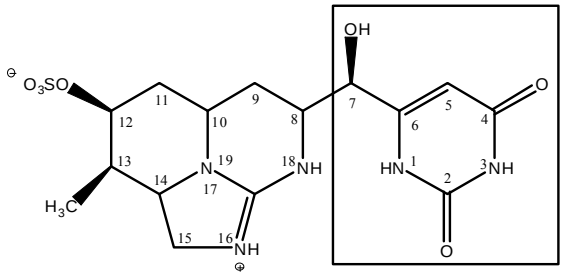

Fig. 5.1. The structure of cylindrospermopsin (CYN)

A number of factors such as global warming and eutrophication have contributed to more frequent HABs events. With the increasing pressure and global need for clean water, it is desirable to identify a sustainable treatment process for the elimination of naturally occurring cyanotoxins from drinking water. Conventional water treatment

methods such as coagulation, flocculation, sedimentation and filtration only lead to minimal removal of cyanotoxins. Activated carbon has shown effectively removal of cyanotoxins, however, treatments of large volumes of contaminated water are time-consuming and not economically applicable. Although a variety of chemical oxidants have been reported for removal of cyanotoxins, such as chlorine, ozone and permanganate, by-products like trihalomethanes (THMs) (by chlorination) and bromate (by ozonation) are a serious environmental issue (Rodríguez et al. 2007a, Rodríguez et al. 2007b).The permanganate dose required for CYN oxidation is very high and not applicable in waterworks. Advanced oxidation processes (AOPs) have also been studied for degradation of pollutants and cyanotoxins based on hydroxyl radical oxidation (Song et al. 2012, Zhao et al. 2014a). A few studies have reported for the removal of CYN and 6-HOMU, the CYN model compound, by UV and visible light activated (VLA) TiO_2 photocatalysis (Zhang et al. 2015, Zhao et al. 2014b).

Ferrate ($Fe^{VI}O_4^{2-}$, Fe(VI)) treatment as an environmentally friendly method has received considerable attention for the remediation of a wide variety of pollutants and toxins (Jiang et al. 2014, Lee et al. 2009) due to the reagent's selective oxidizing properties. Fe(VI) is a powerful oxidant with large reduction potential (+2.20V) (Sharma 2002).and undergoes the reactions (1) and (2) in acidic and alkaline solution, respectively (Wood 1958).Fe(VI) has triprotonated, diprotonated, monoprotonated and deprotonated species present in acidic and basic pH range with three pKa shown in reactions (4-6). The decomposition of Fe(VI) in water leads to the formation of Fe(III) and molecular oxygen by reaction (3). The reduction of Fe(VI) leads to non-toxic by-product Fe(III), indicating Fe(VI) as an environmentally friendly oxidant can be applied for water purification.

$$FeO_4^{2-} + 8H^+ + 3e^- \leftrightarrow Fe^{3+} + 4H_2O \quad (1)$$

$$FeO_4^{2-} + 4H_2O + 3e^- \leftrightarrow Fe(OH)_3 + 5OH^- \quad (2)$$

$$2FeO_4^{2-} + 10H_2O \rightarrow 2Fe^{3+} + 20OH^- \quad (3)$$

$$H_3FeO_4^+ \leftrightarrow H^+ + H_2FeO_4 \qquad pK_{a1} = 1.6 \pm 0.2 \quad (4)$$

$$H_2FeO_4 \leftrightarrow H^+ + HFeO_4^- \qquad pK_{a2} = 3.5 \quad (5)$$

$$HFeO_4^- \leftrightarrow H^+ + FeO_4^{2-} \qquad pK_{a3} = 7.3 \pm 0.1 \quad (6)$$

The oxidation of CYN by Fe(VI) has not yet been reported. To the best of our knowledge this is the first detailed study of Fe(VI) mediated oxidation of CYN. We report herein the kinetic studies of Fe(VI) with CYN and model compound 6-HOMU over a range of solution pH (7 ~ 9.5). Detailed product studies were performed using liquid chromatography coupled to Q-TOF/MS to identify the oxidation intermediates and determine the degradation pathways. The biological activities of CYN oxidation products during Fe(VI) treatment were evaluated using ELISA. Our results indicate the Fe(VI) as a promising water-treatment method can be applied for the remediation of uracil based problematic cyanotoxins in drinking water.

5.3 Material and methods

5.3.1 Materials

Sodium phosphate, sodium borate and HPLC grade methanol were purchased from Fisher Scientific. The humic acid was obtained from Fluka. All reagents were used as received. The model compound (6-hydroxymethyl uracil) was synthesized according to standard organic functional group transformations (Zhao et al. 2014b). Potassium ferrate (K_2FeO_4) of high purity (~ 98 %) was obtained from Dr. Sharma's group. Fe(VI)

solutions were prepared by adding to 5 mM Na_2HPO_4 / 1 mM $Na_2B_4O_7 \cdot 10\ H_2O$ buffer at pH 9.0. All aqueous solutions were prepared with Millipore filtered water.

5.3.2 Kinetic studies

Kinetic experiments were conducted at the room temperature using pseudo-first-order conditions with [Fe(VI)] >> [6-HOMU] and [CYN]. Aliquots were collected at given time intervals and then quenched with hydroxylamine before analyzing with high-performance liquid chromatography (HPLC). The hydroxylamine concentration was used at least 20 times higher than Fe(VI) concentration so that the reaction was stopped right after adding the quencher. Fe(VI) concentration was measured by colorimetric method (Lee et al. 2005).at the same time intervals with 6-HOMU concentration. The second order rate constants of Fe(VI) with CYN and 6-HOMU were determined using the method described by (Hu et al. 2008)(details in results section) in the pH range of 7 ~ 9.5.

5.3.3 Biological activity using ELISA

Enzyme-linked immunosorbent assay (ELISA) was used to assess the biological activity of the treated sample as a function of irradiation time using colorimetric procedures described in Abraxis (Abraxis). CYN samples were diluted 500 times with Milli-Q water for ELISA. The microtiter plate was measured at 450 nm on an *i*Quant reader within 15 min after stopping the reaction. The inhibition of enzyme activity was measured at known CYN concentrations to establish the standard curve.

5.3.4 Analysis

HPLC analysis of CYN and 6-HOMU

The concentration of CYN was monitored by HPLC, Varian ProStar equipped with a ProStar 410 autosampler and a ProStar 335 photodiode array detector under the

following conditions: a Luna RP C18 column (5 μm, 250 × 4.6 mm); 50 μl injection volume and 1 ml/min flow rate; The mobile phase consisted of a linear gradient starting at 5 % methanol, 95 % water increased to 60 % methanol in 6 min and then held constant for an additional 5 min; the detection wavelength was at 262 nm. 6-HOMU concentration was monitored using a modified HPLC analytical method described by Zhao (Zhao et al. 2014b).

LC-QTOF/MS analysis of iopamidol and its photoproducts

The analyses of CYN and the degradation products were carried out using an Agilent 6530 high resolution accurate-mass quadrupole time-of-flight (Q-TOF) liquid chromatography / mass spectrometer (LC-QTOF/MS). The samples were separated on an Agilent Zobrax eclipse plus C-18 (rapid resolution HD 3.0 × 100 mm, 1.8-Micron) equipped with a guard column (3.0 × 5 mm) of same packing material. The mobile phase consisted of A: 2 % acetonitrile + 0.2% acetic acid in H_2O and B: 2 % H_2O + 0.2% acetic acid in acetonitrile, with a gradient elution of 5 % B for 1 min, followed by a linear increase to 95 % B in 10 min, back to 5 % B over 3 min. The flow rate was 0.4 ml/min and injection volume was 5 μl. The mass spectra (m/z 100-1000) were obtained in positive ion mode with electrospray ionization technology (ESI). Data acquisition and analysis were performed using the Agilent Mass Hunter software (Version B.05.0).

5.4. Results and discussion

5.4.1 Kinetics

Since the reaction of CYN and Fe(VI) is pH dependent, the degradation of CYN by Fe(VI) was conducted in pH range 7 - 9.5 to evaluate the degradation efficiency with different pH values. The concentration of CYN was monitored by HPLC as a function of

treatment time. The degradation of CYN follows pseudo-first-order kinetics. The reaction kinetic of CYN and Fe(VI) can be described in Eq. (7). The second-order-rate constants for the reaction of CYN and Fe(VI) were determined using the equation (8) converted from Eq. (7),where [CYN] << [Fe(VI)].

$$\frac{\mathrm{d[CYN]}}{\mathrm{d}t} = -k_2\,[\mathrm{Fe(VI)}][\mathrm{CYN}] \tag{7}$$

$$\ln([\mathrm{CYN}]_0/[\mathrm{CYN}]_t) = k_2 \int_0^t [\mathrm{Fe(VI)}]\mathrm{d}t \tag{8}$$

The $\int_0^t [\mathrm{Fe(VI)}]\mathrm{d}t$ represents the Fe(VI) exposure which is integrated of Fe(VI) concentration over the time (in Fig. 2). The second-order-rate constant (the slope) was obtained by plotting the natural logarithm of CYN concentration versus the Fe(VI) exposure, yielding k = (38.91 ± 0.99) $M^{-1}s^{-1}$ at pH 7 shown in **Fig. 5.2a** (inserted fig). The second-order-rate constant of 6-HOMU and Fe(VI) was obtained by Eq. (8), giving the k = (112.112 ± 8) $M^{-1}s^{-1}$ at pH 7 shown in **Fig. 5.2b** (inserted fig).

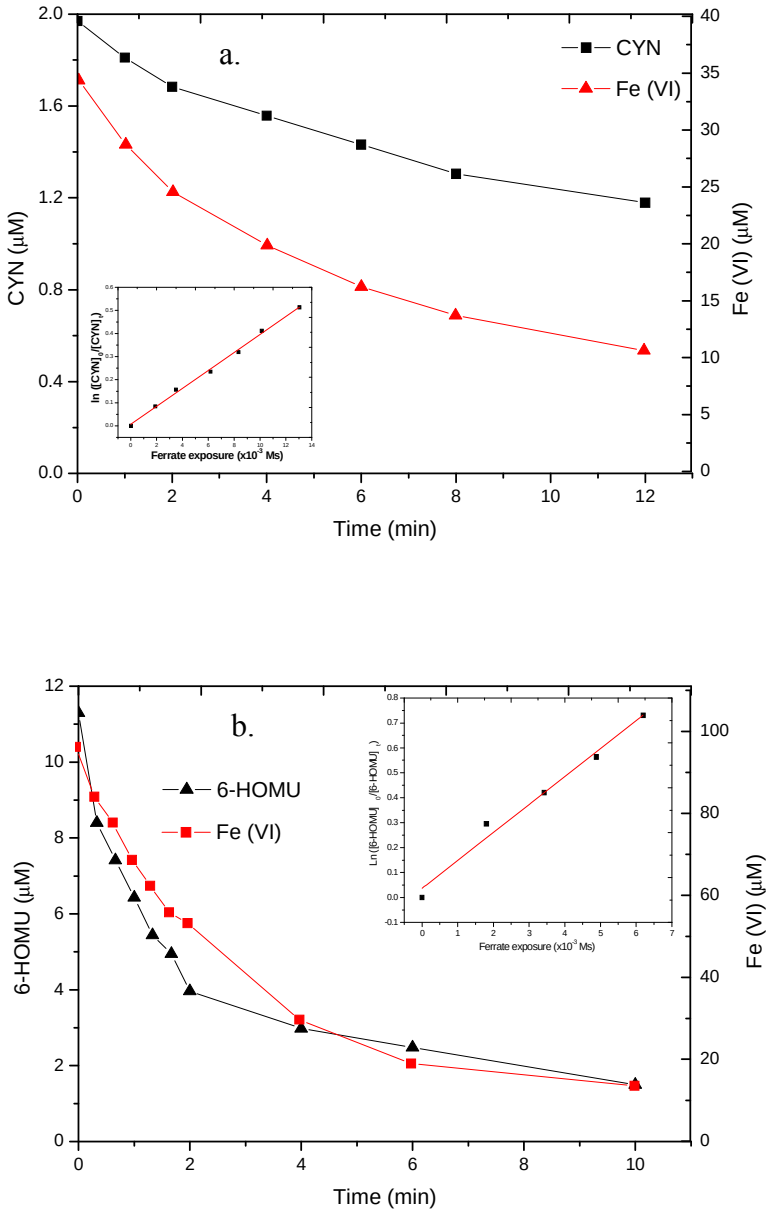

Fig. 5.2. Kinetics of CYN and 6-HOMU with Fe(VI). a). CYN and Fe(VI) degradation at pH 7 ([CYN]$_0$ = 2 μM, Fe(VI) = 40 μM). Insert shows the second order rate constant for CYN and Fe(VI) reaction using Eq. 7. b). 6-HOMU and Fe(VI) degradation at ph 7 ([6-HOMU]0 = 10 μM, Fe(VI) = 100 μM). Insert shows the second order rate constant for 6-HOMU and Fe(VI) reaction using Eq. 7

The second order rate constants (k) for the reactions of Fe(VI) with CYN and 6-HOMU as a function of pH is shown in **Fig. 5.3**. The reactivity of Fe(VI) with CYN decreases with the increase of pH; the similar trend was also observed for the reaction of Fe(VI) with 6-HOMU. The k were similar for Fe(VI) with 6-HOMU and CYN at pH 8 ~ 9.5, indicating Fe(VI) mediated reaction primary occur via oxidation of the uracil ring in CYN. Fe(VI) has a tendency to react with electron-rich organic moieties, such as amines, oldfin and aniline (Lee et al. 2009, Sharma 2013). Therefore, the unsaturated double bond C5-C6 and amines N1 and N3 in the uracil ring are expected to be the primary sites for Fe(VI) oxidation.

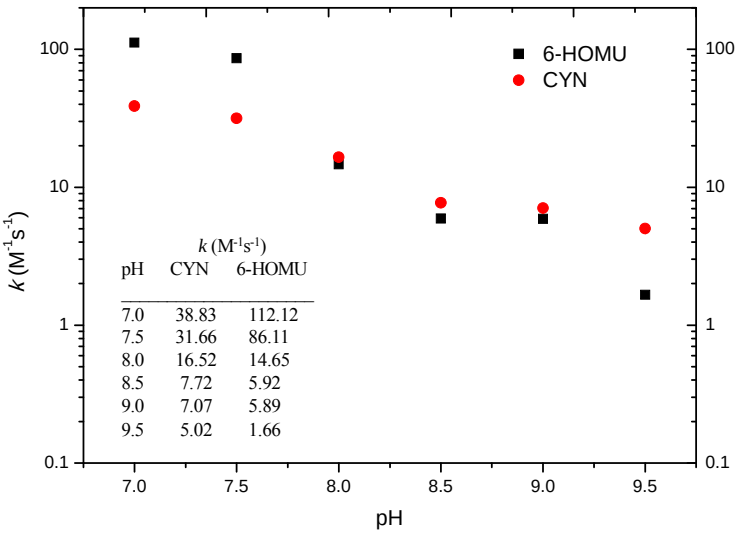

Fig. 5.3. The second order rate constants (k) for the reactions of Fe(VI) with CYN and 6-HOMU as a function of pH in range of 7 ~ 9.5.

Selective oxidants such as ozone (O_3), chlorine, permanganate (MnO_4^-) and chlorine dioxide (ClO_2), and non-selective oxidant hydroxyl radical (•OH) have been reported for mediated oxidation of CYN (Rodríguez et al. 2007a, Song et al. 2012).The

kinetics of second order rate constants and/or apparent rate constants (k_{app}) of different oxidants with CYN is summarized in **Table 5.1**. The non-selective oxidant hydroxyl radical (•OH) mediated oxidation of CYN shows the highest reactivity than other oxidants, which can react with CYN via attack the uracil ring (accounting for 84 %) (Song et al. 2012) and hydrolysis of tricyclic guanidine group (He et al. 2014).The reactivity of CYN with selective oxidants O_3, chlorine and ClO_2 is pH dependent: the k_{app} for the reaction of CYN with O_3 and ClO_2 decreased with decreasing pH, while a maximum k_{app} for CYN with chlorine was observed at pH 7. O_3 has orders of magnitude higher reactivity than other selective oxidants at neutral pH conditions. O_3 can rapidly react with the deprotonated amine moieties in CYN. Followed by O_3, chlorine also exhibits higher reactivity with CYN by reacting with the uracil ring in CYN to form non-toxic 5-chloro-CYN and cylindrospermic acid (Rodríguez et al. 2007b).Based on the results from the present study and previous studies (Rodríguez et al. 2007a, Song et al. 2012),the reactivity order with CYN was •OH > O_3 > chlorine > Fe(VI) > MnO_4^- > ClO_2. In addition, •OH, O_3, chlorine and Fe(VI) are suitable options for oxidative removal of CYN in water treatment, while MnO_4^- and ClO_2 are not appropriate oxidants for degradation of CYN due to the low reactivity with CYN.

Table 5.1. The kinetics of second order rate constants and/or apparent rate constants (k_{app}) of different oxidants with CYN

Oxidants	Hydroxyl radical (•OH)	ozone (O_3)	chlorine	ferrate (VI)	permanganate (MnO_4^-)	chlorine dioxide (ClO_2)
CYN (k, $M^{-1}s^{-1}$)	5.08×10^9	3.4×10^5	490	16.52	0.3	0.9

5.4.2 Product Identification

Since there are no previous reports addressing the product identification of CYN oxidation by Fe (VI), it's becoming critical to determine the reaction pathways and mechanisms to develop the fundamental understanding of Fe(VI) mediated oxidation of CYN. Detailed product studies were conducted at $[CYN]_0$ = 15 μM and [Fe(VI)] = 50 μM to make sure the initial intermediates were observed under our experimental conditions. The identification of intermediates was achieved by using positive ESI high resolution LC-MS based on the analysis of molecular ion masses and the target MS/MS spectrum. The tandem MS/MS spectrum of a CYN standard showed the product ion and its fragmentation pattern of m/z 416 > 336 > 318 > 274 > 194 > 176 as previously reported by Guzmán-Guillén (Guzmán-Guillén et al. 2012). The fragments ions at m/z 336 and 318 resulted from the loss of sulfate group (- 80 Da) with a subsequent lost of H_2O (- 18 Da); the fragment ion at m/z 274 was assigned to the loss of hydroxymethyl uracil group (- 142 Da); the fragments ions at m/z 194 and 176 corresponded to the loss of sulfate group (- 80 Da) and H_2O (- 18 Da) from the fragment ion at m/z 274. Determination of intermediates was achieved using these characteristic fragmentation patterns in order to confirm the presence of specific functional groups.

In generally, Fe(VI) has a tendency to react with electron-rich organic moieties, such as amines, oldfin and aniline. The reactivity of Fe(VI) with amines has been reported following the order of primary (1º) amine > secondary (2º) amine >> tertiary (3º) amine (negligible) (Lee and von Gunten 2010).Therefore, the unsaturated double bond C5-C6 and secondary amines N1 and N3 in the uracil ring are expected to be the primary sites for Fe(VI) oxidation attack. The proposed intermediates and reaction pathways are

shown in **Scheme 5.1**. The reaction of Fe(VI) with CYN is initiated by electrophilic attack at the unsaturated double bond C5-C6. Two possible pathways have been proposed: a) formation of a cyclic ester from a 3 + 2 electrocyclic addition of Fe(VI) to the double bond; or b) formation of a four-centered organometallic complex from a 2 + 2 addition to the double bond (Hu et al. 2008).Both of these two possible pathways lead to the formation of product m/z 448 with the same fragmentation pattern of 368 and 350, which is hard to distinguish between [3 + 2] and [2 + 2] addition. The hydrolysis of –C6ON1H or –C6OHN1H group in the uracil ring formed the product m/z 350, which has been determined as cylindrospermopsic acid (Merel et al. 2010, Song et al. 2012).and reported as nontoxic in mice up to a dose of 10 mg/kg mouse intraperitioneal injection (Banker et al. 2001).

Fe(VI) can undergo electron abstraction at the carboxylate anion in cylindrospermopsic acid (m/z 350), leading to loss of CO_2 and subsequent hydrolysis to product m/z 322. Fe(VI) has been reported to selectively oxidize alcohols to the corresponding aldehydes/ketones (Lee and Gai 1993). In our study, the product m/z 322 can be oxidized to the aldehyde form product m/z 304. There is one proton available on product m/z 304 (R-CHO) for abstraction by Fe(VI), resulting in oxidation to product m/z 320. Although the product m/z 322 and 304 were not observed under our experimental conditions, the detectable product m/z 320 demonstrated the above reaction pathways were reasonable. Such reaction pathways are similar to UV/H_2O_2 initiated hydroxyl radical attack to CYN reported by He et al (He et al. 2014). Decarboxylation and hydroxylation of product m/z 320 led to the formation of product m/z 292 and its further oxidation to ketone product m/z 290. We observed two peaks with m/z 292 and same

mass fragments of 292 > 240 > 194 in our study, which are consistent with recent findings of TiO_2 photocatalytic degradation of CYN by Zhang (Zhang et al. 2015). The ring opening processes lead to a transformation of m/z 292a to m/z 292b (Garrison et al. 1970, Sheu and Foote 1995). The retention time of m/z 292a was slightly longer than m/z 292b, which indicate the polarity of product structure with m/z 292a was less than that of m/z 292b. This probably resulted from the contribution of hydroxyl group on C8 to the well distribution of electron density in molecule, leading to less polarity of product m/z 292a, as previously reported by Zhang (Zhang et al. 2015).

Another product with m/z 375 was observed involving hydrolysis of the urea functional group (-NHCONH-) in the uracil moiety, leading to the ring opening, which can also be transformed to product with m/z 320 by several steps. Such hydrolysis of the urea groups has been observed for Fe(VI) oxidation of carbamazepine (Hu et al. 2008) and acid hydrolysis of phenylurea in previous studies (O'Connor and Barnett 1973).Similar reaction pathways have also been reported in the •OH mediated degradation of CYN by Song et al (Song et al. 2012).

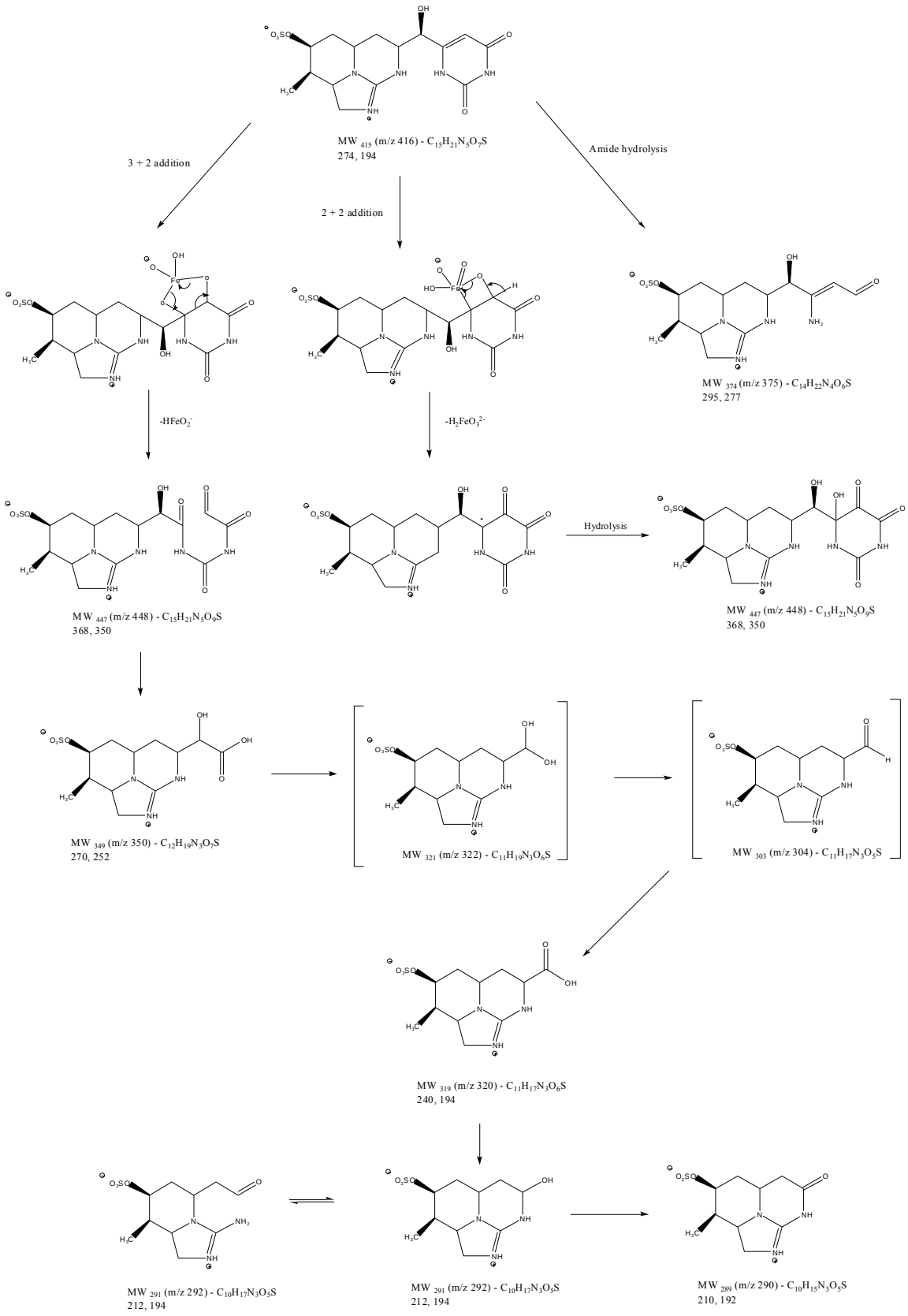
MW 415 (m/z 416) - C15H21N5O7S
274, 194
3 + 2 addition
2 + 2 addition
Amide hydrolysis
MW 374 (m/z 375) - C14H22N4O6S
295, 277
-HFeO2-
-H2FeO32-
MW 447 (m/z 448) - C15H21N5O9S
368, 350
Hydrolysis
MW 447 (m/z 448) - C15H21N5O9S
368, 350
MW 349 (m/z 350) - C12H19N3O7S
270, 252
MW 321 (m/z 322) - C11H19N3O6S
MW 303 (m/z 304) - C11H17N3O5S
MW 319 (m/z 320) - C11H17N3O6S
240, 194
MW 291 (m/z 292) - C10H17N3O5S
212, 194
MW 291 (m/z 292) - C10H17N3O5S
212, 194
MW 289 (m/z 290) - C10H15N3O5S
210, 192

Scheme 5.1. The proposed reaction pathways for Fe(VI) with CYN.

5.4.3 Detoxification analysis of CYN oxidation products

A limited number of studies have been reported on the assessment of biological activity of CYN oxidation products (Chen et al. , Zhang et al. 2015). The toxic activity of CYN results from the uracil moiety as mentioned above (Banker et al. 2001). Our product studies demonstrate the Fe(VI) mediated oxidation of CYN primary occur on the uracil moiety, leading to the open ring products. It is important to assess the biological activity of product-mixture during the Fe(VI) treatment in order to evaluate the environmental risks of degradation products. The biological activities of CYN following Fe(VI) treatment are determined using ELISA measurements. The CYN ELISA is an immunoassay for the quantitative and sensitive detection of CYN in water samples at ng/mL levels. This process involves CYN antibodies binding with second specific antibodies to generate color signal measured at 450 nm. A calibration curve for $\%B/B_0$ as a function of the CYN standards is shown in **Fig. 5.4.** The $\%B/B_0$ for each standard was calculated by dividing the mean absorbance value for each standard by the Zero Standard (Standard 0) mean absorbance. The calibration curve was from 0.05 to 2 ppb CYN with IC_{50} concentration of 0.17 ppb. Samples showing a lower concentration than 0.05 ppb of CYN are considered to be negative.

The samples were diluted 500 times to make sure the residual CYN concentration within the range of the calibration curve for ELISA measurements. As shown in **Fig. 5.5**, Fe(VI) treatment significantly decreases the biological activities of CYN product-mixture, which parallel the CYN concentration determined by HPLC. The biological activity concentration from ELISA decreased slower than the CYN concentration from HPLC,

which indicates the by-products formed during Fe(VI) treatment may have analogous biological activity. Up to 97 % of the biological activities were removed following Fe(VI) treatment for 120 min. The small portion at the end of treatment from ELISA reached the detection limit of the calibration curve and was considered to be insignificant. Our observations suggest that Fe(VI) treatment can readily degrade CYN, and its oxidation products did not exhibit the significant biological activity after the treatment.

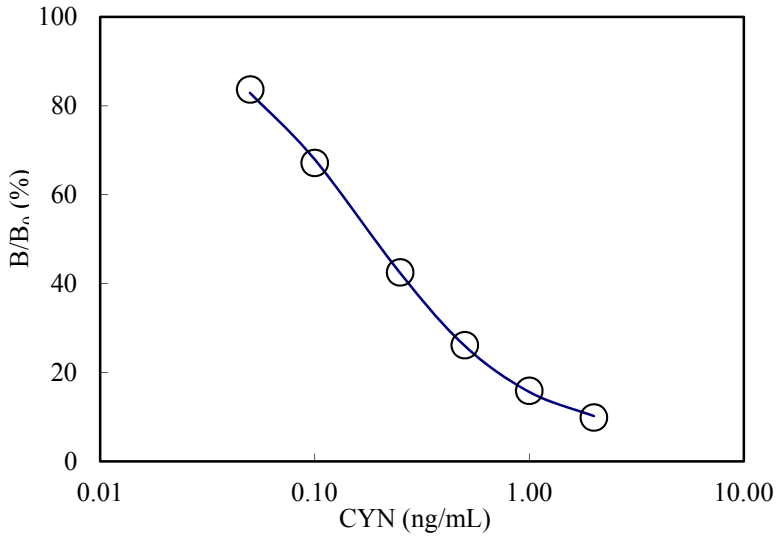

Fig. 5.4. The calibration curve for %B/B$_0$ as a function of CYN concentration. IC$_{50}$ = 0.17 ppb.

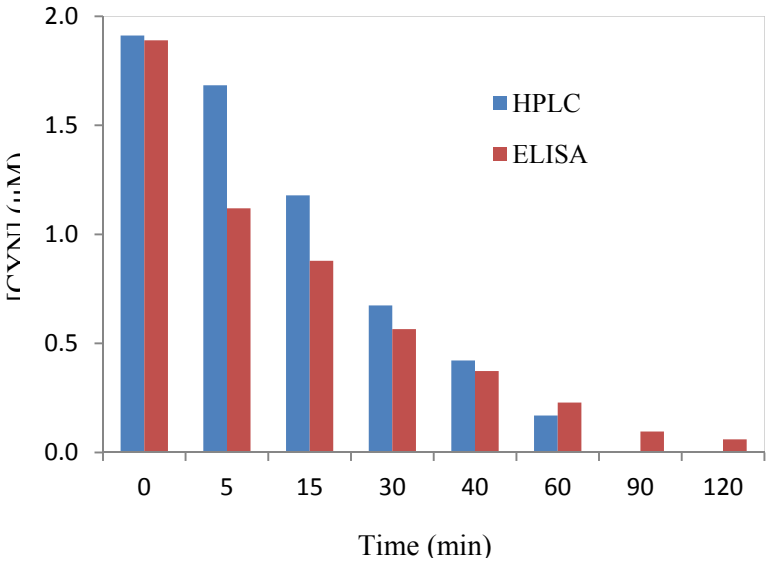

Fig. 5.5. Fe(VI) oxidation of CYN. The concentrations of CYN were measured by HPLC and ELISA.([CYN] = 2 μM, Fe(VI) = 50 μM at pH = 8)

5.5 Conclusions

Ferrate (VI) treatment can lead to the effective degradation of CYN and the model compound 6-hydroxymethyl uracil (6-HOMU) under neutral pH condition. The kinetic studies were reported to determine the reactivity of Fe(VI) with CYN and 6-HOMU as a function of solution pH. Fe(VI) oxidation of CYN followed second-order kinetics with the bimolecular rate constant decreasing from 38.83 ± 0.07 $M^{-1}s^{-1}$ at pH 7 to 5.02 ± 0.04 $M^{-1}s^{-1}$ at pH 9.5. Product studies demonstrated Fe(VI) oxidation of uracil ring in CYN are the predominant reaction pathways, which are critical to the biological activity. The biological activities of CYN product-mixture decreased as a function of Fe(VI) treatment. The oxidation products did not pose the significant biological activity after 120 min treatment. Our results indicate the Fe(VI) as a promising water-treatment method can be applied for the remediation of uracil based problematic cyanotoxins in drinking water.

CHAPTER 6
General Conclusions

Cyanobacteria have become the focus of extensive research studies because of their increased prevalence and the diverse toxic compounds they can produce. Of particular concern is *cylindrospermopsis raciborskii* (Nostocales) which has spread from the tropics to more temperate climates and become a worldwide concern. The powerful biological activity has a significant environmental impact and threatens the health and lives of human beings. UV and visible light activated (VLA) TiO_2 photocatalysts as the promising solar-driven TiO_2 materials were employed for the degradation of CYN model compound, 6-hydroxymethyl uracil (6-HOMU). The degradation of 6-HOMU follows a pseudo-first-order kinetic model using nitrogen and fluorine-TiO_2 (NF-TiO_2), phosphorus and fluorine-TiO_2 (PF-TiO_2) and sulfur-TiO_2 (S-TiO_2) under UV irradiation. NF-TiO_2 performs the most photoactive, followed by marginally active PF-TiO_2 and inactive S-TiO_2 under visible light irradiation. The pseudo-first-order constants increase as pH increase from 3 ~ 9 under VLA NF-TiO_2. The dissolved metals Fe^{3+}, Cu^{2+} and up to 10 ppm humic acid can enhance the degradation of 6-HOMU. The roles of reactive species, •OH, $^1O_2$, $O_2^{-\bullet}$ and h^+_{vb} were studied by adding the specific scavengers and the results indicate that $O_2^{-\bullet}$ plays a critical role in VLA NF-TiO_2 photocatalysis of 6-HOMU.

Fe (VI) as an environmentally friendly oxidant was employed for the degradation of CYN and its model compound 6-hydroxymethyl uracil (6-HOMU) due to its large reduction potential (+ 2.2 V). Kinetic studies of Fe(VI) degradation of CYN and 6-HOMU were conducted to determine second order rate constants over a range of pH (6.5 ~ 9.5). Fe(VI) degradation of CYN indicate that second order rate constants decrease from 38.83 ± 0.07 $M^{-1}s^{-1}$ at pH 7 to 5.02 ± 0.04 $M^{-1}s^{-1}$ at pH 9.5 due to changing acid-base speciation of Fe(VI). Product studies indicate Fe(VI) mediated degradation

pathways predominantly occur via oxidation of the uracil ring in CYN, leading to oxidation and ring opened products. ELISA results demonstrate Fe(VI) oxidation process leads to a significant decrease in the biological activity of CYN as a function of treatment time.

Iodinated X-ray contrast media (ICM) compounds are widely used pharmaceuticals for intravascular administration to enhance the imaging of organs or blood vessels during diagnostic tests. Although ICM compounds have not shown any specific health effects on humans, precautionary and prediction are necessary because of their contribution to adsorbable organically halogen (AOX). Iron based treatments and oxidative processes have received considerable attention for the remediation of a wide variety of pollutants. We report the investigation of Fe(III)-oxalate/H_2O_2/UV process for the remediation of iopamidol a model for ICM. The observed degradation follows first order and can be achieved at solution pH from 2 to 7. Kinetic studies were used to optimize reaction conditions, reactant ratios, wavelength of irradiation and solution pH. Under our optimal conditions, the rates of hydroxyl radical (•OH) and superoxide anion radical ($O_2^{-\bullet}$) production were 1.19 ± 0.12 and 0.19 ± 0.02 μM/min under UV (350 nm) irradiation, respectively. Detailed product studies using liquid chromatography couple to Q-TOF-MS demonstrate both reduction (multiple dehalogenations) and oxidation (oxidation of the aromatic ring and side chains) contribute to the degradation pathways. The reduction processes appear to be initiated by the carbonate radical anion ($CO_2^{-\bullet}$) while oxidation processes are consistent with •OH initiated reaction pathways.

4-methylcyclohexanemethanol (MCHM) and propylene glycol phenyl ether (PPh) are related to the contamination of local drinking water in Charleston, West Virginia, on

Jan 9, 2014. Hydroxyl radical (·OH) mediated oxidation of MCHM and PPh were studied to obtain the bimolecular rate constants using transient absorption spectrum and competition kinetics. The bimolecular rate constants of ·OH with MCHM and PPh were $5.04 \pm 0.09 \times 10^9$ M^{-1} s^{-1} and $9.15 \pm 0.08 \times 10^9$ M^{-1} s^{-1}, respectively, by pulse radiolysis. Product studies indicate •OH addition to *ortho* and *para* positions in PPh are the predominant reaction pathways; H-abstraction are primary reaction mechanisms for ·OH mediated oxidation of MCHM. The fundamental kinetic parameters and proposed reaction pathways using pulse and gamma radiolysis are important to evaluate the reactive species (·OH) initialized reactions for the remediation of these problematic pollutants in drinking water and also critical to assess the radiolysis techniques as a potential water treatment for organic pollutants.

REFERENCE

(1/20/2014) Summary Report of Short-term Screening Level Calculation and Analysis of Available Animal Studies for MCHM (http://emergency.cdc.gov/chemical/MCHM/westvirginia2014/pdf/MCHM-Summary-Report.pdf), The Centers for Disease Control & Prevention

(2004) Propylene glycol phenyl ether (http://www.chem.unep.ch/irptc/sids/OECDSIDS/770354.pdf). The Organization for Economic Cooperation and Development/Screening Information Data Set (OECD SIDS).

(2014a) Information about MCHM - 2014 West Virginia Chemical Release (http://emergency.cdc.gov/chemical/MCHM/westvirginia2014/mchm.asp). The Center for Disease Control & Prevention (CDC).

(2014b) Information about PPh - 2014 West Virginia Chemical Release (http://emergency.cdc.gov/chemical/MCHM/westvirginia2014/pph.asp). The Center for Disease Control & Prevention (CDC).

Abdelmelek, S.B., Greaves, J., Ishida, K.P., Cooper, W.J. and Song, W. (2011) Removal of Pharmaceutical and Personal Care Products from Reverse Osmosis Retentate Using Advanced Oxidation Processes. Environmental Science & Technology 45(8), 3665-3671.

Abraxis Cylindrospermopsin ELISA (Microtiter Plate). Technical Note Product No. 522011.

ADEL AL-KDASI, A.I., KATAYON SAED, CHUAH TEONG GUAN (2004) TREATMENT OF TEXTILE WASTEWATER BY ADVANCED OXIDATION PROCESSES – A REVIEW. Global Nest: the Int. J. 6(3), 222-230.

Albinet, A., Minero, C. and Vione, D. (2010) Photochemical generation of reactive species upon irradiation of rainwater: Negligible photoactivity of dissolved organic matter. Science of the Total Environment 408(16), 3367-3373.

Balmer, M.E. and Sulzberger, B. (1999) Atrazine Degradation in Irradiated Iron/Oxalate Systems: Effects of pH and Oxalate. Environmental Science & Technology 33(14), 2418-2424.

Banker, R., Carmeli, S., Werman, M., Teltsch, B., Porat, R. and Sukenik, A. (2001) Uracil moiety is required for toxicity of the cyanobacterial hepatotoxin cylindrospermopsin. Journal of Toxicology and Environmental Health-Part A 62(4), 281-288.

Beglinger, J.M. (1997) Determination of ready biodegradability (Biotic degradation) using CO_2 evolution test modified sturm

(http://www.eastman.com/Literature_Center/Misc/Crude_MCHM_Ready_Biodegradation_Study.pdf). Eastman Kodak Company ES-97-112.

Beranek, R., Neumann, B., Sakthivel, S., Janczarek, M., Dittrich, T., Tributsch, H. and Kisch, H. (2007) Exploring the electronic structure of nitrogen-modified TiO_2 photocatalysts through photocurrent and surface photovoltage studies. Chemical Physics 339(1–3), 11-19.

Bernard, L.G. (1997) Acute Dermal Irritation Study in the Rabbit (http://www.eastman.com/Literature_Center/Misc/Crude_MCHM-Skin_Irritation_Study). eastman Kodak Company TX-97-256.

Bernard, L.G. (1998) Acute dermal toxicity study in the rat (http://www.eastman.com/Literature_Center/Misc/Crude_MCHM-Acute_Dermal_Toxicity_Study.pdf). Eastman Kodak Company TX-97-308.

Bielski, B.H.J., Shiue, G.G. and Bajuk, S. (1980) Reduction of nitro blue tetrazolium by CO_2^- and O_2^- radicals. The Journal of Physical Chemistry 84(8), 830-833.

Bourke, A.T.C., Hawes, R.B., Neilson, A. and Stallman, N.D. (1983) An outbreak of hepato-enteritis (the Palm Island mystery disease) possibly caused by algal intoxication. Toxicon 21(Supplement 3), 45-48.

Bourke, A.T.C., Hawes, R.B., Neilson, A. and Stallman, N.D. (1986) PALM ISLAND MYSTERY DISEASE. Medical Journal of Australia 145(9), 486-486.

Buda, F., Heyberger, B., Fournet, R., Glaude, P.-A., Warth, V. and Battin-Leclerc, F. (2006) Modeling of the Gas-Phase Oxidation of Cyclohexane. Energy Fuels 20, 1450-1459.

Buxton, G.V., Greenstock, C.L., Helman, W.P. and Ross, A.B. (1988) CRITICAL-REVIEW OF RATE CONSTANTS FOR REACTIONS OF HYDRATED ELECTRONS, HYDROGEN-ATOMS AND HYDROXYL RADICALS (.OH/.O-) IN AQUEOUS-SOLUTION. Journal of Physical and Chemical Reference Data 17(2), 513-886.

Canonica, S., von Gunten, U. and Wenk, J. (2011) Reply to Comment on "Effect of Dissolved Organic Matter on the Transformation of Contaminants Induced by Excited Triplet States and the Hydroxyl Radical". Environmental Science & Technology 45(18), 7947-7948.

Chatterjee, D. and Dasgupta, S. (2005) Visible light induced photocatalytic degradation of organic pollutants. Journal of Photochemistry and Photobiology C: Photochemistry Reviews 6(2-3), 186-205.

Chen, L., Zhao, C., Dionysiou, D.D. and O'Shea, K.E. TiO_2 photocatalytic degradation and detoxification of cylindrospermopsin. Journal of Photochemistry and Photobiology A: Chemistry 307–308(0), 115-122.

Chen, Y., Hu, C., Hu, X.X. and Qu, J.H. (2009) Indirect Photodegradation of Amine Drugs in Aqueous Solution under Simulated Sunlight. Environmental Science & Technology 43(8), 2760-2765.

Chiswell, R.K., Shaw, G.R., Eaglesham, G., Smith, M.J., Norris, R.L., Seawright, A.A. and Moore, M.R. (1999) Stability of cylindrospermopsin, the toxin from the cyanobacterium, Cylindrospermopsis raciborskii: Effect of pH, temperature, and sunlight on decomposition. Environmental Toxicology 14(1), 155-161.

Chow, C.W.K., Drikas, M., House, J., Burch, M.D. and Velzeboer, R.M.A. (1999) The impact of conventional water treatment processes on cells of the cyanobacterium Microcystis aeruginosa. Water Research 33(15), 3253-3262.

Codd, G., Bell, S., Kaya, K., Ward, C., Beattie, K. and Metcalf, J. (1999) Cyanobacterial toxins, exposure routes and human health. European Journal of Phycology 34(4), 405-415.

Codd, G.A. (1995) Cyanobacterial toxins: Occurrence, properties and biological significance. Water Science and Technology 32(4), 149-156.

Cooper, W.J., Cramer, C.J., Martin, N.H., Mezyk, S.P., O'Shea, K.E. and Sonntag, C.v. (2009) Free Radical Mechanisms for the Treatment of Methyl tert-Butyl Ether (MTBE) via Advanced Oxidation/Reductive Processes in Aqueous Solutions. Chemical Reviews 109(3), 1302-1345.

Cooper, W.J., Curry, R.D. and O'Shea, K.E. (1998) Environmental applications of ionizing radiation, John Wiley & Sons.

de la Cruz, A.A., Hiskia, A., Kaloudis, T., Chernoff, N., Hill, D., Antoniou, M.G., He, X., Loftin, K., O'Shea, K., Zhao, C., Pelaez, M., Han, C., Lynch, T.J. and Dionysiou, D.D. (2013) A review on cylindrospermopsin: the global occurrence, detection, toxicity and degradation of a potent cyanotoxin. Environmental Science: Processes & Impacts 15(11), 1979-2003.

Dionysiou, D.D., Suidan, M.T., Baudin, I. and Laîné, J.-M. (2004) Effect of hydrogen peroxide on the destruction of organic contaminants-synergism and inhibition in a continuous-mode photocatalytic reactor. Applied Catalysis B: Environmental 50(4), 259-269.

Doll, T.E. and Frimmel, F.H. (2003) Fate of pharmaceuticals—photodegradation by simulated solar UV-light. Chemosphere 52(10), 1757-1769.

Doll, T.E. and Frimmel, F.H. (2005) Cross-flow microfiltration with periodical back-washing for photocatalytic degradation of pharmaceutical and diagnostic residues–evaluation of the long-term stability of the photocatalytic activity of TiO_2. Water Research 39(5), 847-854.

Duirk, S.E., Lindell, C., Cornelison, C.C., Kormos, J., Ternes, T.A., Attene-Ramos, M., Osiol, J., Wagner, E.D., Plewa, M.J. and Richardson, S.D. (2011) Formation of Toxic Iodinated Disinfection By-Products from Compounds Used in Medical Imaging. Environmental Science & Technology 45(16), 6845-6854.

Falconer, I.R. (1998) Algal toxins and human health, pp. 53-82, Springer.

Falconer, I.R. (2005) Cyanobacterial Toxins of Drinking Water Supplies: Cylindrospermopsins and Microcystins, CPC Press, Boca Raton.

Falconer, I.R. and Humpage, A.R. (2001) Preliminary evidence for in vivo tumour initiation by oral administration of extracts of the blue-green alga Cylindrospermopsis raciborskii containing the toxin cylindrospermopsin. Environmental Toxicology 16(2), 192-195.

Fox, M.A. and Dulay, M.T. (1993) Heterogeneous photocatalysis. Chemical Reviews 93(1), 341-357.

Garrison, W.M., Kland-English, M.J., Sokol, H.A. and Jayko, M.E. (1970) Radiolytic degradation of the peptide main chain in dilute aqueous solution containing oxygen. The Journal of Physical Chemistry 74(26), 4506-4509.

Griffiths, D.J. and Saker, M.L. (2003) The palm island mystery disease 20 years on: A review of research on the cyanotoxin cylindrospermopsin. Environmental Toxicology 18(2), 78-93.

Guerard, J.J., Chin, Y.P., Mash, H. and Hadad, C.M. (2009) Photochemical Fate of Sulfadimethoxine in Aquaculture Waters. Environmental Science & Technology 43(22), 8587-8592.

Gulshan, F., Yanagida, S., Kameshima, Y., Isobe, T., Nakajima, A. and Okada, K. (2010) Various factors affecting photodecomposition of methylene blue by iron-oxides in an oxalate solution. Water Research 44(9), 2876-2884.

Guzmán-Guillén, R., Prieto, A.I., González, A.G., Soria-Díaz, M.E. and Cameán, A.M. (2012) Cylindrospermopsin determination in water by LC-MS/MS: Optimization and validation of the method and application to real samples. Environmental Toxicology and Chemistry 31(10), 2233-2238.

Haag, W.R., Hoigne´, J.r., Gassman, E. and Braun, A.M. (1984) Singlet oxygen in surface waters — Part I: Furfuryl alcohol as a trapping agent. Chemosphere 13(5–6), 631-640.

Halling-Sorensen, B., Nielsen, S.N., Lanzky, P.F., Ingerslev, F., Lutzhoft, H.C.H. and Jorgensen, S.E. (1998) Occurrence, fate and effects of pharmaceutical substances in the environment - A review. Chemosphere 36(2), 357-394.

Han, C., Pelaez, M., Likodimos, V., Kontos, A.G., Falaras, P., O'Shea, K. and Dionysiou, D.D. (2011) Innovative visible light-activated sulfur doped TiO_2 films for water treatment. Applied Catalysis B: Environmental 107(1–2), 77-87.

Harada, K., Ohtani, I., Iwamoto, K., Suzuki, M., Watanabe, M.F., Watanabe, M. and Terao, K. (1994) Isolation of cylindrospermopsin from a cyanobacterium Umezakia natans and its screening method. Toxicon 32, 73-84.

He, X., Pelaez, M., Westrick, J.A., O'Shea, K.E., Hiskia, A., Triantis, T., Kaloudis, T., Stefan, M.I., de la Cruz, A.A. and Dionysiou, D.D. (2012) Efficient removal of microcystin-LR by UV-C/H2O2 in synthetic and natural water samples. Water Research 46(5), 1501-1510.

He, X., Zhang, G., de la Cruz, A.A., O'Shea, K.E. and Dionysiou, D.D. (2014) Degradation Mechanism of Cyanobacterial Toxin Cylindrospermopsin by Hydroxyl Radicals in Homogeneous UV/H_2O_2 Process. Environmental Science & Technology 48(8), 4495-4504.

Ho, L., Meyn, T., Keegan, A., Hoefel, D., Brookes, J., Saint, C.P. and Newcombe, G. (2006) Bacterial degradation of microcystin toxins within a biologically active sand filter. Water Research 40(4), 768-774.

Howard, B.C. (January 10, 2014) What's the chemical behind West Virginia's River spill ? - Spill in the Elk River brings a "do not drink" advisory.

Hu, L., Martin, H.M., Arce-Bulted, O., Sugihara, M.N., Keating, K.A. and Strathmann, T.J. (2008) Oxidation of Carbamazepine by Mn(VII) and Fe(VI): Reaction Kinetics and Mechanism. Environmental Science & Technology 43(2), 509-515.

Humpage, A.R., Fenech, M., Thomas, P. and Falconer, I.R. (2000) Micronucleus induction and chromosome loss in transformed human white cells indicate clastogenic and aneugenic action of the cyanobacterial toxin, cylindrospermopsin. Mutation Research/Genetic Toxicology and Environmental Mutagenesis 472(1–2), 155-161.

Humpage, A.R., Fontaine, F., Froscio, S., Burcham, P. and Falconer, I.R. (2005) Cylindrospermopsin Genotoxicity and Cytotoxicity: Role Of Cytochrome P-450 and

Oxidative Stress. Journal of Toxicology and Environmental Health, Part A 68(9), 739-753.

Jeong, J., Jung, J., Cooper, W.J. and Song, W. (2010) Degradation mechanisms and kinetic studies for the treatment of X-ray contrast media compounds by advanced oxidation/reduction processes. Water Research 44(15), 4391-4398.

Jeong, J. and Yoon, J. (2005) pH effect on OH radical production in photo/ferrioxalate system. Water Research 39(13), 2893-2900.

Jercinovic, D.E. (1985) Petroleum-Product Contamination of Soil and Water in New Mexico, Environmental Improvement Division, Ground Water/Hazardous Waste Bureau.

Jiang, W., Chen, L., Batchu, S.R., Gardinali, P.R., Jasa, L., Marsalek, B., Zboril, R., Dionysiou, D.D., O'Shea, K.E. and Sharma, V.K. (2014) Oxidation of Microcystin-LR by Ferrate(VI): Kinetics, Degradation Pathways, and Toxicity Assessments. Environmental Science & Technology 48(20), 12164-12172.

Jr., K.W. (Januray 10, 2014) What is 'Crude MCHM'? Few know.

Kolpin, D.W., Furlong, E.T., Meyer, M.T., Thurman, E.M., Zaugg, S.D., Barber, L.B. and Buxton, H.T. (2002) Pharmaceuticals, hormones, and other organic wastewater contaminants in US streams, 1999-2000: A national reconnaissance. Environmental Science & Technology 36(6), 1202-1211.

Kolvenbach, B., Schlaich, N., Raoui, Z., Prell, J., Zühlke, S., Schäffer, A., Guengerich, F.P. and Corvini, P.F.X. (2007) Degradation Pathway of Bisphenol A: Does ipso Substitution Apply to Phenols Containing a Quaternary α-Carbon Structure in the para Position? Applied and Environmental Microbiology 73(15), 4776-4784.

Kormos, J.L., Schulz, M., Kohler, H.-P.E. and Ternes, T.A. (2010) Biotransformation of Selected Iodinated X-ray Contrast Media and Characterization of Microbial Transformation Pathways. Environmental Science & Technology 44(13), 4998-5007.

Kummerer, K., Erbe, T., Gartiser, S. and Brinker, L. (1998) AOX-emissions from hospitals into municipal waste water. Chemosphere 36(11), 2437-2445.

Lee, D.G. and Gai, H. (1993) Kinetics and mechanism of the oxidation of alcohols by ferrate ion. Canadian Journal of Chemistry 71(9), 1394-1400.

Lee, J., Kim, J. and Choi, W. (2014) Oxidation of aquatic pollutants by ferrous–oxalate complexes under dark aerobic conditions. Journal of Hazardous Materials 274(0), 79-86.

Lee, Y. and von Gunten, U. (2010) Oxidative transformation of micropollutants during municipal wastewater treatment: Comparison of kinetic aspects of selective (chlorine,

chlorine dioxide, ferrateVI, and ozone) and non-selective oxidants (hydroxyl radical). Water Research 44(2), 555-566.

Lee, Y., Yoon, J. and von Gunten, U. (2005) Spectrophotometric determination of ferrate (Fe(VI)) in water by ABTS. Water Research 39(10), 1946-1953.

Lee, Y., Zimmermann, S.G., Kieu, A.T. and von Gunten, U. (2009) Ferrate (Fe(VI)) Application for Municipal Wastewater Treatment: A Novel Process for Simultaneous Micropollutant Oxidation and Phosphate Removal. Environmental Science & Technology 43(10), 3831-3838.

Li, F.B., Chen, J.J., Liu, C.S., Dong, J. and Liu, T.X. (2006) Effect of iron oxides and carboxylic acids on photochemical degradation of bisphenol A. Biology and Fertility of Soils 42(5), 409-417.

Li, X.H., Zhang, H.D., Zheng, X.X., Yin, Z.Y. and Wei, L. (2011) Visible light responsive N-F-codoped TiO2 photocatalysts for the degradation of 4-chlorophenol. Journal of Environmental Sciences-China 23(11), 1919-1924.

Liu, G., Zheng, S., Xing, X., Li, Y., Yin, D., Ding, Y. and Pang, W. (2010) Fe(III)–oxalate complexes mediated photolysis of aqueous alkylphenol ethoxylates under simulated sunlight conditions. Chemosphere 78(4), 402-408.

Liu, S., Zhao, Y., Ma, F., Ma, L., O'Shea, K., Zhao, C., Hu, X. and Wu, M. (2015) Control of Microcystis aeruginosa growth and associated microcystin cyanotoxin remediation by electron beam irradiation (EBI). Rsc Advances 5(40), 31292-31297.

Louit, G., Foley, S., Cabillic, J., Coffigny, H., Taran, F., Valleix, A., Renault, J.P. and Pin, S. (2005) The reaction of coumarin with the OH radical revisited: hydroxylation product analysis determined by fluorescence and chromatography. Radiation Physics and Chemistry 72(2-3), 119-124.

Ma, J. and Liu, W. (2002) Effectiveness of ferrate (VI) preoxidation in enhancing the coagulation of surface waters. Water Research 36(20), 4959-4962.

Marco Montalti, A.C., Luca Prodi, M. Teresa Gandolfi (2006) Handbook of Photochemistry, CRC Press, Boca Raton.

Merel, S., Clément, M., Mourot, A., Fessard, V. and Thomas, O. (2010) Characterization of cylindrospermopsin chlorination. Science of the Total Environment 408(16), 3433-3442.

Mulazzani, Q.G., Dangelantonio, M., Venturi, M., Hoffman, M.Z. and Rodgers, M.A.J. (1986) INTERACTION OF FORMATE AND OXALATE IONS WITH RADIATION-

GENERATED RADICALS IN AQUEOUS-SOLUTION - METHYLVIOLOGEN AS A MECHANISTIC PROBE. Journal of Physical Chemistry 90(21), 5347-5352.

Munter, R. (2001) Advanced oxidation processes - current status and prospects. Proc. Est. Acad. Sci., Chem. 50, 59-80.

Mutschler, E. (1996) Arzneimittelwirkungen, 7th Ed. Wissenschaftliche Verlagsgesellschaft, Stuttgart, .

Newcombe, G., Morrison, J., Hepplewhite, C. and Knappe, D.R.U. (2002) Simultaneous adsorption of MIB and NOM onto activated carbon: II. Competitive effects. Carbon 40(12), 2147-2156.

Newcombe, G. and Nicholson, B. (2004) Water treatment options for dissolved cyanotoxins. Journal of Water Supply Research and Technology-Aqua 53(4), 227-239.

O'Connor, C.J. and Barnett, J.W. (1973) Acid hydrolysis of phenylurea, 4-fluorophenylurea, and 3-methylphenylurea. Journal of the Chemical Society, Perkin Transactions 2 (10), 1457-1461.

Ohtani, I., Moore, R.E. and Runnegar, M.T.C. (1992) Cylindrospermopsin: a potent hepatotoxin from the blue-green alga Cylindrospermopsis raciborskii. Journal of the American Chemical Society 114(20), 7941-7942.

Ollis, D.F. (2005) Kinetics of liquid phase photocatalyzed reactions: An illuminating approach. Journal of Physical Chemistry B 109(6), 2439-2444.

Pelaez, M., de la Cruz, A.A., Stathatos, E., Falaras, P. and Dionysiou, D.D. (2009) Visible light-activated N-F-codoped TiO2 nanoparticles for the photocatalytic degradation of microcystin-LR in water. Catalysis Today 144(1–2), 19-25.

Pelaez, M., Falaras, P., Kontos, A.G., de la Cruz, A.A., O'Shea, K., Dunlop, P.S.M., Byrne, J.A. and Dionysiou, D.D. (2012a) A comparative study on the removal of cylindrospermopsin and microcystins from water with NF-TiO_2-P25 composite films with visible and UV-vis light photocatalytic activity. Applied Catalysis B-Environmental 121, 30-39.

Pelaez, M., Nolan, N.T., Pillai, S.C., Seery, M.K., Falaras, P., Kontos, A.G., Dunlop, P.S.M., Hamilton, J.W.J., Byrne, J.A., O'Shea, K., Entezari, M.H. and Dionysiou, D.D. (2012b) A review on the visible light active titanium dioxide photocatalysts for environmental applications. Applied Catalysis B-Environmental 125, 331-349.

Perez, S. and Barcelo, D. (2007) Fate and occurrence of X-ray contrast media in the environment. Analytical and Bioanalytical Chemistry 387(4), 1235-1246.

Privat, E.J. and Sowers, L.C. (1996) A proposed mechanism for the mutagenicity of 5-formyluracil. Mutation Research/Fundamental and Molecular Mechanisms of Mutagenesis 354(2), 151-156.

Rodríguez, E., Onstad, G.D., Kull, T.P.J., Metcalf, J.S., Acero, J.L. and von Gunten, U. (2007a) Oxidative elimination of cyanotoxins: Comparison of ozone, chlorine, chlorine dioxide and permanganate. Water Research 41(15), 3381-3393.

Rodríguez, E., Sordo, A., Metcalf, J.S. and Acero, J.L. (2007b) Kinetics of the oxidation of cylindrospermopsin and anatoxin-a with chlorine, monochloramine and permanganate. Water Research 41(9), 2048-2056.

Saghir, S.A., Brzak, K.A. and Bartels, M.J. (2003) Oral absorption, metabolism and excretion of 1-phenoxy-2-propanol in rats. Xenobiotica 33, 1059-1071.

Saker, M.L., Thomas, A.D. and Norton, J.H. (1999) Cattle mortality attributed to the toxic cyanobacterium Cylindrospermopsis raciborskii in an outback region of north Queensland. Environmental Toxicology 14(1), 179-182.

Santoke, H., Song, W.H., Cooper, W.J. and Peake, B.M. (2012) Advanced oxidation treatment and photochemical fate of selected antidepressant pharmaceuticals in solutions of Suwannee River humic acid. Journal of Hazardous Materials 217, 382-390.

Schulz, M., Loffler, D., Wagner, M. and Ternes, T.A. (2008) Transformation of the X-ray contrast medium lopromide in soil and biological wastewater treatment. Environmental Science & Technology 42(19), 7207-7217.

Seitz, W., Jiang, J.-Q., Schulz, W., Weber, W.H., Maier, D. and Maier, M. (2008) Formation of oxidation by-products of the iodinated X-ray contrast medium iomeprol during ozonation. Chemosphere 70(7), 1238-1246.

Sharma, V.K. (2002) Potassium ferrate(VI): an environmentally friendly oxidant. Advances in Environmental Research 6(2), 143-156.

Sharma, V.K. (2011) Oxidation of inorganic contaminants by ferrates (VI, V, and IV)–kinetics and mechanisms: A review. Journal of Environmental Management 92(4), 1051-1073.

Sharma, V.K. (2013) Ferrate(VI) and ferrate(V) oxidation of organic compounds: Kinetics and mechanism. Coordination Chemistry Reviews 257(2), 495-510.

Sheu, C. and Foote, C.S. (1995) Photosensitized Oxygenation of a 7,8-Dihydro-8-oxoguanosine Derivative. Formation of Dioxetane and Hydroperoxide Intermediates. [Erratum to document cited in CA122:106358]. Journal of the American Chemical Society 117(16), 4726-4726.

Sichel, C., Garcia, C. and Andre, K. (2011) Feasibility studies: UV/chlorine advanced oxidation treatment for the removal of emerging contaminants. Water Research 45(19), 6371-6380.

Singh, T.S., Madhava Rao, B.S., Mohan, H. and Mittal, J.P. (2002) A pulse radiolysis study of coumarin and its derivatives. Journal of Photochemistry and Photobiology A: Chemistry 153(1–3), 163-171.

Song, W.H., Cooper, W.J., Peake, B.M., Mezyk, S.P., Nickelsen, M.G. and O'Shea, K.E. (2009a) Free-radical-induced oxidative and reductive degradation of N,N '-diethyl-m-toluamide (DEET): Kinetic studies and degradation pathway. Water Research 43(3), 635-642.

Song, W.H., Xu, T.L., Cooper, W.J., Dionysiou, D.D., De La Cruz, A.A. and O'Shea, K.E. (2009b) Radiolysis Studies on the Destruction of Microcystin-LR in Aqueous Solution by Hydroxyl Radicals. Environmental Science & Technology 43(5), 1487-1492.

Song, W.H., Yan, S.W., Cooper, W.J., Dionysiou, D.D. and O'Shea, K.E. (2012) Hydroxyl Radical Oxidation of Cylindrospermopsin (Cyanobacterial Toxin) and Its Role in the Photochemical Transformation. Environmental Science & Technology 46(22), 12608-12615.

Stewart, I., Webb, P., Schluter, P. and Shaw, G. (2006) Recreational and occupational field exposure to freshwater cyanobacteria – a review of anecdotal and case reports, epidemiological studies and the challenges for epidemiologic assessment. Environmental Health: A Global Access Science Source 5(1), 1-13.

Stylidi, M., Kondarides, D.I. and Verykios, X.E. (2004) Visible light-induced photocatalytic degradation of Acid Orange 7 in aqueous TiO_2 suspensions. Applied Catalysis B-Environmental 47(3), 189-201.

Tao, X., Su, J.M., Chen, J.F. and Zhao, J.C. (2005) A novel route for waste water treatment: photo-assisted Fenton degradation of dye pollutants accumulated in natural polyelectrolyte microshells. Chemical Communications (36), 4607-4609.

Ternes, T.A. and Hirsch, R. (2000) Occurrence and behavior of X-ray contrast media in sewage facilities and the aquatic environment. Environmental Science & Technology 34(13), 2741-2748.

Thakur, R.S., Chaudhary, R. and Singh, C. (2010) Fundamentals and applications of the photocatalytic treatment for the removal of industrial organic pollutants and effects of operational parameters: A review. Journal of Renewable and Sustainable Energy 2(4).

Thomas, A., Saker, M.L., Norton, J.H. and Olsen, R.D. (1998) Cyanobacterium Cylindrospermopsis raciborskii as a probable cause of death in cattle in northern Queensland. Australian Veterinary Journal 76(9), 592-594.

Tian, F.-X., Xu, B., Lin, Y.-L., Hu, C.-Y., Zhang, T.-Y. and Gao, N.-Y. (2014) Photodegradation kinetics of iopamidol by UV irradiation and enhanced formation of iodinated disinfection by-products in sequential oxidation processes. Water Research 58(0), 198-208.

Tong, A.Y.C., Braund, R., Warren, D.S. and Peake, B.M. (2012) TiO_2-assisted photodegradation of pharmaceuticals - a review. Central European Journal of Chemistry 10(4), 989-1027.

Tullo, A.H., Kemsley, J., Hogue, C. and Morrissey, S.P. (2014) OBSCURE CHEMICAL TAINTS WATER SUPPLY. Chemical & Engineering News 92(7), 10-15.

Turner, P.C., Gammie, A.J., Hollinrake, K. and Codd, G.A. (1990) Pneumonia associated with contact with cyanobacteria.

Wood, R.H. (1958) The Heat, Free Energy and Entropy of the Ferrate(VI) Ion. Journal of the American Chemical Society 80(9), 2038-2041.

Wu, G.S., Wen, J.L., Nigro, S. and Chen, A.C. (2010) One-step synthesis of N- and F-codoped mesoporous TiO_2 photocatalysts with high visible light activity. Nanotechnology 21(8).

Xu, T.L., Cai, Y. and O'Shea, K.E. (2007) Adsorption and photocatalyzed oxidation of methylated arsenic species in TiO_2 suspensions. Environmental Science & Technology 41(15), 5471-5477.

Xu, Z., Jing, C., Li, F. and Meng, X. (2008) Mechanisms of Photocatalytical Degradation of Monomethylarsonic and Dimethylarsinic Acids Using Nanocrystalline Titanium Dioxide. Environmental Science & Technology 42(7), 2349-2354.

Yang, B., Ying, G.-G., Zhao, J.-L., Liu, S., Zhou, L.-J. and Chen, F. (2012) Removal of selected endocrine disrupting chemicals (EDCs) and pharmaceuticals and personal care products (PPCPs) during ferrate(VI) treatment of secondary wastewater effluents. Water Research 46(7), 2194-2204.

Zee-Chen, K.-Y. and Cheng, C.C. (1967) Pyrimidines. XX. A convenient preparation of orotaldehyde and thymine-6-carboxaldehyde. Journal of Heterocyclic Chemistry 4(1), 163-165.

Zhang, G., Wurtzler, E.M., He, X., Nadagouda, M.N., O'Shea, K., El-Sheikh, S.M., Ismail, A.A., Wendell, D. and Dionysiou, D.D. (2015) Identification of TiO_2

photocatalytic destruction byproducts and reaction pathway of cylindrospermopsin. Applied Catalysis B: Environmental 163(0), 591-598.

Zhang, J. and Nosaka, Y. (2012) Quantitative Detection of OH Radicals for Investigating the Reaction Mechanism of Various Visible-Light TiO2 Photocatalysts in Aqueous Suspension. The Journal of Physical Chemistry C 117(3), 1383-1391.

Zhao, C., Arroyo-Mora, L.E., DeCaprio, A.P., Sharma, V.K., Dionysiou, D.D. and O'Shea, K.E. (2014a) Reductive and oxidative degradation of iopamidol, iodinated X-ray contrast media, by Fe(III)-oxalate under UV and visible light treatment. Water Research 67(0), 144-153.

Zhao, C., Pelaez, M., Dionysiou, D.D., Pillai, S.C., Byrne, J.A. and O'Shea, K.E. (2014b) UV and visible light activated TiO_2 photocatalysis of 6-hydroxymethyl uracil, a model compound for the potent cyanotoxin cylindrospermopsin. Catalysis Today 224(0), 70-76.

Zhao, J., Chen, C. and Ma, W. (2005) Photocatalytic Degradation of Organic Pollutants Under Visible Light Irradiation. Topics in Catalysis 35(3-4), 269-278.

Zheng, S., Cai, Y. and O'Shea, K.E. (2010) TiO_2 photocatalytic degradation of phenylarsonic acid. Journal of Photochemistry and Photobiology a-Chemistry 210(1), 61-68.

Zuo, Y. and Hoigne, J. (1992) Formation of hydrogen peroxide and depletion of oxalic acid in atmospheric water by photolysis of iron(III)-oxalato complexes. Environmental Science & Technology 26(5), 1014-1022.

Zuo, Y. and Zhan, J. (2005) Effects of oxalate on Fe-catalyzed photooxidation of dissolved sulfur dioxide in atmospheric water. Atmospheric Environment 39(1), 27-37.

VITA

CEN ZHAO

Born, Fushun, Liaoning, China

2006-2010	Bachelor of Science in Applied Chemistry Shenyang Agricultural University Shenyang, Liaoning, China
2010 -present	Doctoral Candidate Florida International University Miami, Florida, USA

PUBLICATIONS AND PRESENTATIONS

C.A.A. de, A. Hiskia, T. Kaloudis, N. Chernoff, D. Hill, M.G. Antoniou, X. He, K. Loftin, K. O'Shea, C. Zhao, M. Pelaez, C. Han, T.J. Lynch, D.D. Dionysiou, A review on cylindrospermopsin: the global occurrence, detection, toxicity and degradation of a potent cyanotoxin, Environmental Science.: Processes Impacts 15 (2013) 1979-2003.

C. Zhao, M. Pelaez, D.D. Dionysiou, S.C. Pillai, J.A. Byrne, K.E. O'Shea, UV and visible light activated TiO2 photocatalysis of 6-hydroxymethyl uracil, a model compound for the potent cyanotoxin cylindrospermopsin, Catalysis Today 224 (2014) 70-76.

C. Zhao, L.E. Arroyo-Mora, A.P. DeCaprio, V.K. Sharma, D.D. Dionysiou, K.E. O'Shea, Reductive and oxidative degradation of iopamidol, iodinated X-ray contrast media, by Fe(III)-oxalate under UV and visible light treatment, Water Research 67 (2014) 144-153.

L. Chen, C. Zhao, D.D. Dionysiou, K. E. O'Shea, TiO2 photocatalytic degradation and detoxification of cylindrospermopsin, Journal of Photochemistry & Photobiology, A: Chemistry 307-308 (2015) 115-122.

C. Zhao, M. Luzi, M. Pelaez, D. D. Dionysiou and K. E.O'Shea, TiO_2 photocatalysis of 6-hydroxymethyl uracil as a model for the cylindrospermopsin, poster presentation at *the 17th International Conference on Semiconductor Photocatalysis and Solar Energy Conversion*, November 11-15, 2012, Jacksonville, Florida.

C. Zhao, M. Pelaez, D. D. Dionysiou**,** S. C. Pillai, J. A. Byrne and K. E. O'Shea, Visible Light Activated (VLA) TiO_2 photocatalysis of 6-hydroxymethyl uracil as a model compound for the cylindrospermopsin, oral presentation at the *245th American Chemical Society (ACS) National Meeting,Division of Environmental Chemistry,*April 7-11, 2013, New Orleans, Louisiana

K. E. O'Shea, C. Zhao, D. D. Dionysiou, M. Pelaez ,W. Song , J. A. Byrne, S. C. Pillai, Advanced oxidation of cylinderspermopsin (cyanobacterial toxin). Mechanistic and practical considerations, oral presentation at *the 245th American Chemical Society (ACS) National Meeting, Division of Environmental Chemistry*, April 7-11, 2013, New Orleans, Louisiana

C. Zhao, D. D. Dionysiou and K. E. O'Shea, Photodegradation of iodinated x-ray contrast mediam iopamidol by Fe(III)-oxalate system with the composition of H_2O_2, poster presentation at *the 19th International Conference on Advanced Oxidation Technologies for Treatment of Water, Air and Soil*, November 17-21, 2013, San Diego, California.

W. Jiang, C. Zhao, L. Zhu, V. K. Sharma, S. R. Batchu, P. R. Gardinali, D. D. Dionysiou, K. E. O'Shea, Oxidation of Microcystin-LR by Ferrate (VI): Intermediates, Degradation Pathways and Toxicity Assesement, *poster presentation at the 247th American Chemical Society (ACS) National Meeting,Division of Environmental Chemistry*, March 16-20, 2014, Dallas, Texas

C. Zhao, L. E. Arroyo-Mora, A. P. DeCaprio, D. D. Dionysiou, K. E. O'Shea, Photodegradation of iodinated X-ray contrast media iopamidol by Fe(III)-oxalate system with the composition of H_2O_2, *oral presentation at the 248th American Chemical Society (ACS) National Meeting,Division of Environmental Chemistry*, August 10-15, 2014, San Francisco, California.

C. Zhao, V. K. Sharma, D. D. Dionysiou, K. E. O'Shea, Oxidation of cylindrospermopsin and its model compound 6-hydroxymethyl uracil by Ferrate (VI), *poster presentation at the 248th American Chemical Society (ACS) National Meeting,Division of Environmental Chemistry*, August 10-15, 2014, San Francisco, California.